Fluorescent Multiple Chemical Sensing using Time-Domain Fluorescence Lifetime Imaging

Dissertation zur Erlangung des Doktorgrads der Naturwissenschaften
(Dr. rer. nat.)

der Fakultät Chemie und Pharmazie
der Universität Regensburg

vorgelegt von

Stefan Nagl

Regensburg, im Mai 2008

Diese Doktorarbeit entstand in der Zeit vom Juni 2004 bis zum April 2008 am Institut für Analytische Chemie, Chemo- und Biosensorik der Universität Regensburg.

Die Arbeit wurde angeleitet von Prof. Otto S. Wolfbeis

Promotionsgesuch eingereicht am:	27.05.2008	
Kolloquiumstermin:	19.06.2008	
Prüfungsausschuß:	Vorsitzender:	Prof. Hans-Helmut Kohler
	Erstgutachter:	Prof. Otto S. Wolfbeis
	Zweitgutachter:	Prof. Achim Göpferich
	Drittprüfer:	Prof. Bernhard Dick

CONTENTS

CHAPTER 3

A Dual Fluorescence Sensor for Trace Oxygen and Temperature with a Large Temperature Range and Unmatched Oxygen Sensitivity

CHAPTER 4

A Method for Simultaneous Luminescence Sensing and Imaging of Two Species Using Optical Probes of Different Luminescence Decay Time

CHAPTER 1
INTRODUCTION

1.1. Time-resolved Imaging

One of the first people who used time-resolved imaging was the photographer Eadweard Muybridge in 1878, who had been hired by the university founder Leland Stanford to prove a bet that there were moments during horse galloping, when horses have all four hooves off the ground (Fig. 1.1).

Fig 1.1. Horse galopping, imaged with a timing resolution of approx. 50 ms, from Ref. 1.

Those images used fast mechanical shutters. In the early twentieth century a novel technique for fast imaging emerged that was based on repeated exposition of a photographic film with short light pulses ("stroboscopic imaging").[2] The step towards timescales required for most molecular light emission processes was made possible by, among many other developments, the invention of digital charge-coupled device (CCD) technology[3] and the availability of high-energy ultrashort laser pulses.[4]

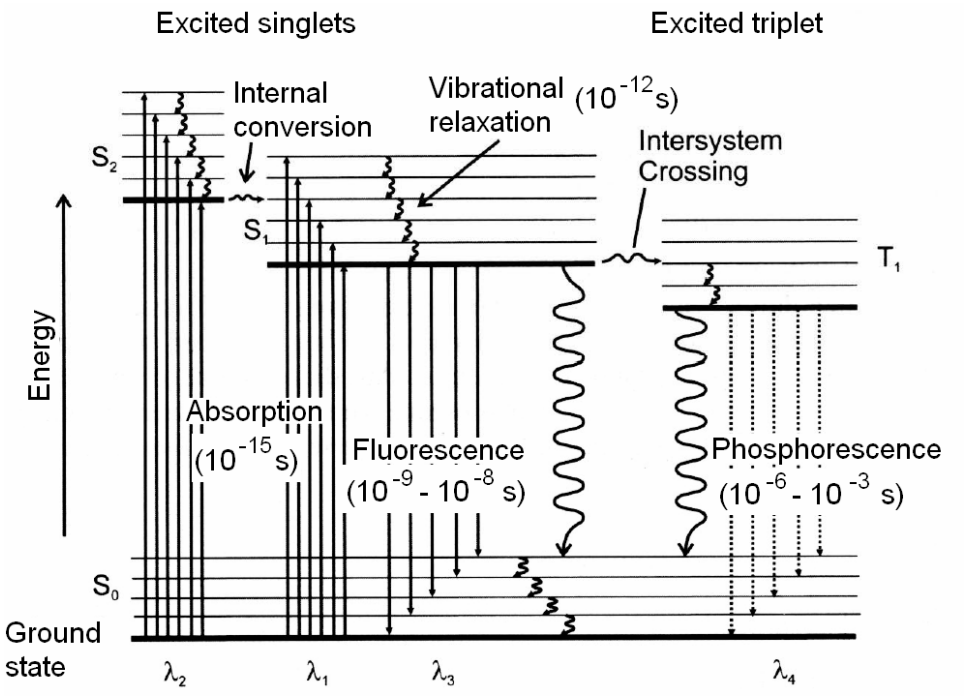

Fig 1.2. The Jablonski diagram showing typical timescales of electronic transitions.

Characteristic timescales of electronic transitions are depicted in Fig. 1.2 (Jablonski diagram). Fluorescence emission in organic molecules follows an exponential decay law and is mostly found in the timescale of hundreds of picoseconds (ps) to a few nanoseconds (ns). Because the transition to the triplet state violates a selection rule in quantum mechanics ($\Delta s \neq 0$), the timescale of phosphorescence is much longer and found to occur in microseconds (μs) to milliseconds (ms).

The fluorescence decay is usually generally described by a multiexponential decay function,[5,6]

$$I(t) = \sum_i a_i \cdot e^{-t/\tau_i} \qquad \text{(Eq. 1.1)}$$

although other approaches such as using a stretched exponential decay exist.[7] The fluorescence lifetime can be measured in the frequency or in the time domain (Fig. 1.3). Both approaches are suitable for imaging.

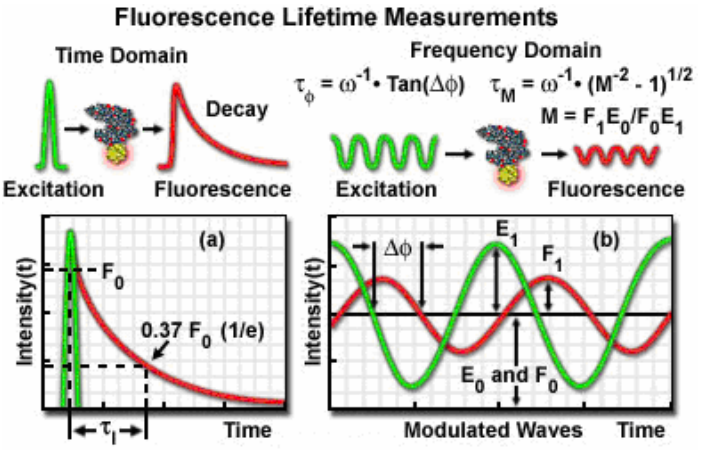

Fig 1.3. Fluorescence lifetime measurement techniques, from Ref. 8.

In a frequency-domain lifetime measurement a sinusoidally modulated light source is employed, and the phase shift of the emission with respect to the excitation light is determined. For time-domain fluorescence lifetime imaging, two main approaches exist. Time correlated single photon counting (TCSPC) is a point scanning method that uses timing information of many individual photons arriving at a photomultiplier to convolute a decay curve. The image is then digitally calculated out of many point measurements (Fig. 1.4.a). It is mainly used along with confocal microscopy. Gated CCD imaging on the other hand records a number of images at different delays with respect to the excitation light pulse and calculates lifetimes from the temporal light intensity behavior of each CCD pixel.

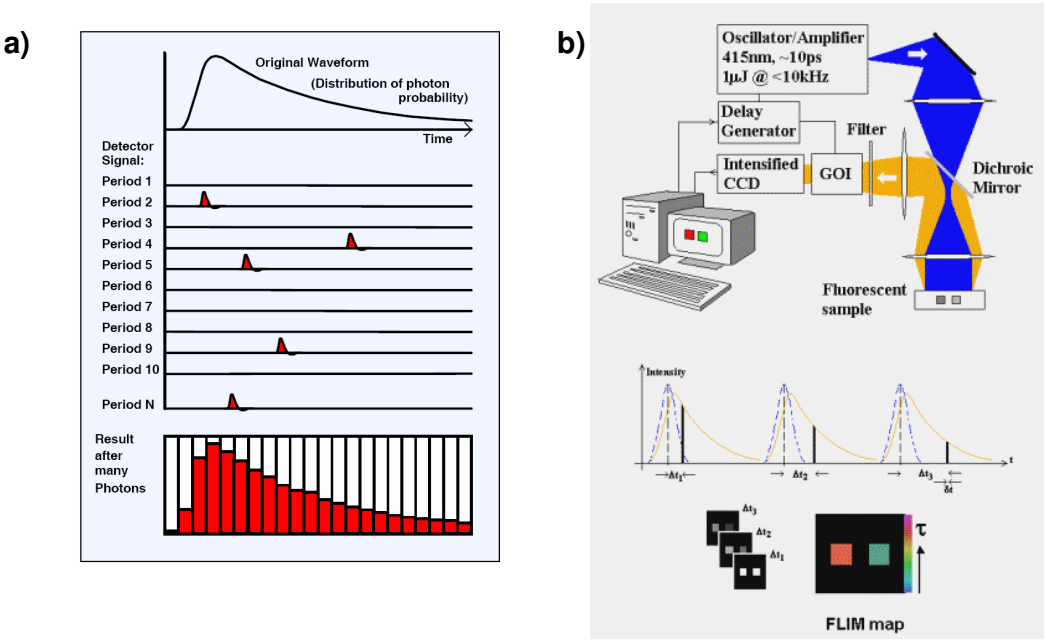

Fig 1.4. Time-domain imaging techniques. a) TCSPC deconstructing the decay curve at each point using single photon arrival times, from Ref. 9, b) gated CCD imaging using fast intensifiers or other modulators from Ref. 10.

1.2. Chemical Sensors and Biosensors

Sensors have become part of our daily life to an extent we are not aware of: temperature sensors turn refrigerators on and off, pressure sensors display oil pressure in cars and elsewhere, and photosensors turn on and off city lights, to mention only a few.

Most chemical sensors are around for only about 30 years only though, with some notable exceptions such as the pH glass electrode reported in 1909 by Haber and Klemensiewicz[11] or Clark's oxygen electrode in 1956.[12] The first biosensor can also be attributed to Clark when he described an experiment in 1962 using his oxygen electrode covered with a dialysis membrane filled with glucose oxidase.[13] Nowadays, the most often produced chemical sensor is the solid-state oxygen sensor (of the conductivity type, used by the millions in catalytic converters, and capable of continuously and reversibly recording

oxygen levels in combustion gases). The literature on chemical sensors increased strongly after the 1970s. Following the success of electrochemical sensors and the invention of ion-selective electrodes, the first optical sensors were reported, in particular plain sensors, based on absorption or fluorescence, using the optical signal of the analyte itself, and indicator-mediated sensors for oxygen and pH using indicator probes. Chemical sensors have experienced a further thrust following the availability of optical fibers, which enabled sensors to be used over large distances or invasively. The 1980s saw the widespread adaption of sensor technology to biochemical reactions. Biochemical interactions, however, often have some degree of irreversibility and are therefore limiting sensor utility. This is not often a problem in enzymatic and cell-based sensors, but more so with biosensors based on immunoreactions and in gene sensors. Main activities in this area involved electrochemical and optical approaches such as evanescent wave absorption and fluorescence. The surface plasmon resonance effect was applied to (mainly biochemical) sensing at about the same time as the first piezo-electric sensors in the 1980s. They are often referred to as quartz micro balances and used for continuous sensing of chemicals such as gases, but mainly for biochemical purposes. The most widely used (and produced) sensors are those for oxygen in the form of the lambda (oxygen) probe in catalytic converters and the glass pH electrode. Several books[14] describe the state of the art in chemical sensing and biosensing, and biannual reviews are available, focusing mainly on fiber-optic sensors.[15]

Material aspects were found to be particularly critical since numerous sensing schemes have been proposed but many of them failed in practice due to limitations in the performance of the chemicals/materials used. It may be stated that there are more sensory schemes than sensors.

There is no authoritative and universally accepted definition of neither of the terms sensor, chemical sensor or biosensor yet, a fact to which much confusion and misperceptions of chemo- and biosensor terminology can be attributed. Part of the problem is the derivation of the word sensor. It is ultimately from the latin words *sensus* and *sensorium,* having a meaning almost completely conserved in the English words sense and sensibility. Used to describe largely emotional rather than rational phenomena, they are ambiguous and individual in their meaning. Some of the proverbial senses of humans in particular and most of the animal kingdom are vision (sight), audition (hearing), gestation (taste), olfaction (smell) and tactition (touch). In all cases a *receptor* responds to a particular stimulus, and this receptor interacts with a *transducer* leading to a *signal* cascade ultimately arriving at the brain.

Simple logic reveals that this architecture can indeed also be used to identify and define any artificial sensor, and it was used by IUPAC in 1991 to identify the main constituents of a chemical sensor.[16] There are also a number of different definitions (e.g. Ref. 17, and ref. therein). The molecular receptor is often embedded into a *matrix* such as a *membrane*, which can also provide some selectivity. Alternative names for the receptor include primary element and recognition element. Much like in biology, where the senses convert the input ultimately into an electrical signal in the brain, the sensor converts the input variable into an *electrical signal* suitable for measurement.[16] Importantly, a sensor works (in the ideal case) *reversibly*, and *continuously*. True sensors (independent of whether physical or chemical) enable a parameter (a chemical species) to be monitored over time. Ideally, a sensor is placed in contact with the sample, and the results are displayed over time. This has been accomplished almost perfectly with numerous physical sensors, but much less so with (bio)-chemical sensors.

The sensor may be self-contained or part of a larger signal processing chain. If using *signal conditioning* such as amplification, filtering, or analog-digital conversion is contained within the sensor, the devices are often called *integrated sensors*. Such sensors, also possessing built-in *signal processing*, are called *intelligent* or *smart sensors*.[18-20]

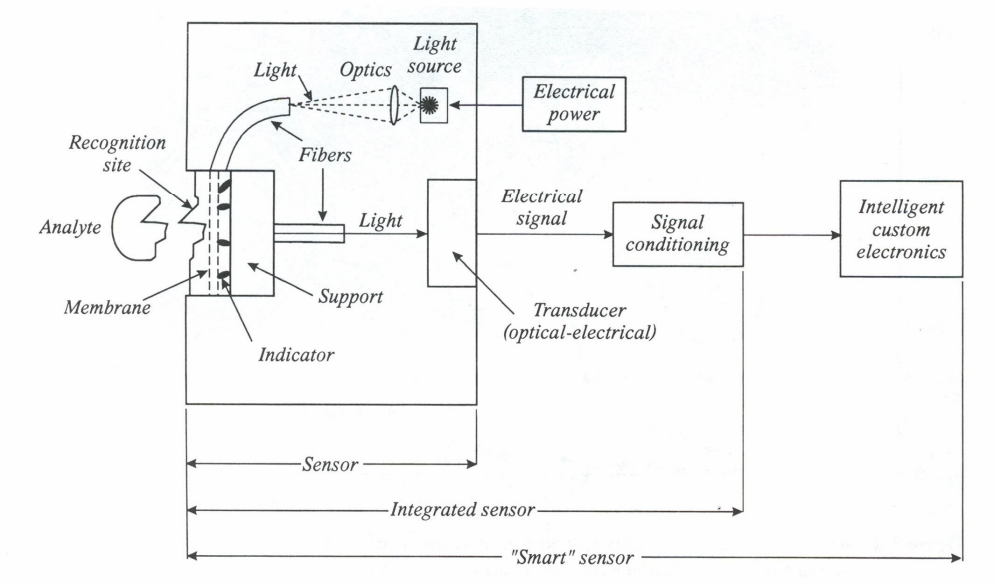

Fig. 1.5. The integral components of a (fiber-optic) chemical sensor or biosensor. Revised from Ref. 20.

It is therefore easy to realize that simple test strips are not sensors, neither are complex analytical instruments, although they may in parts consist of even a multitude of different sensors, e.g. a fluorescence spectrometer may contain photosensors, thermal sensors, humidity sensors etc.

The following definition of a chemical sensor (to which many refer to as the *Cambridge definition*)[21] is one of the most appropriate: *Chemical sensors are miniaturized devices which can deliver real-time and on-line information on the presence of specific compounds or ions in even complex samples.*

Definitions of biosensors are somewhat diverse,[18,22,23] but most of them agree that their distinction from chemical sensors arises from the fact that they use a biological or bioengineered component such as an enzyme, an antibody, a polynucleic acid, or even whole cells or tissue slices as the receptor element for molecular recognition. A biosensor can therefore be regarded as a special type of a chemical sensor. More recently, the definition of biosensors has been extended to systems that can detect and determine biological species, for example by making use of molecularly imprinted polymers (MIPs). Thus, for example, a pH electrode capable of sensing the pH of blood is not a biosensor because it does not use a biological receptor, and neither detects a biological, but a chemical species, the proton. On the other hand, a gene sensor for lead ions in drinking water is a biosensor.

Optical sensors are, by definition, based on the measurement of photons. Therefore, the transducer in optical chemical sensors and biosensors always has to be a configuration involving one or more photodetectors such as a photodiode or a CCD chip.

A classification of fluorescence sensors according to the scheme outlined in Table 1.1 is suggested. The first group (type A) consists of the so-called plain sensors, which in fact are simply based on the measurement of the intrinsic fluorescence of an analyte.

A second class of sensors (type B) is based on the use of a luminescent indicator for a species that either has no useful (= measurable) intrinsic fluorescence, or that cannot be detected specifically in complex samples. Chemical sensors of type C utilize a fluorescent indicator which is involved in a reaction with the analyte such as a pH indicator which is responsive to a reaction in which protons are generated or taken up. Examples include sensors for CO_2, NH_3 and gaseous HCl.

The most direct form of biosensors is represented by class D, in which the emission change of a cofactor of particular enzymatic reaction is recorded. Mostly the NAD^+/NADH pair is employed, although there are also some examples with FAD/$FADH_2$. Most fluorescent biosensors, however, employ an indicator for a substrate or product that reacts with the analyte in an enzymatic reaction (class E). They can therefore be regarded as the biosensor analogs of type C. The most prominent representatives are glucose biosensors employing the generation of protons, oxygen, or hydrogen peroxide by glucose oxidase. The last class F is comprised of the wide area of affinity sensors, although strictly treated most of them do not qualify as sensors because they are based on irreversible, non-covalent high affinity interactions such as between particular proteins and monoclonal antibodies.

Table 1.1. Classification of luminescence-based optical sensors.

Sensor Type	Description	Origin of the analytical signal
A	Plain sensor	Intrinsic fluorescence of an analyte
B	Directly indicator-mediated chemical sensor	Luminescence of an indicator for the species of interest
C	Indirectly indicator-mediated chemical sensor	Emission of an indicator for a species that is formed or consumed in the recognition process of the species of interest
D	Direct enzymatic biosensors	Luminescence of a cofactor which is formed or consumed during a biochemical reaction (analogous to type B)
E	Indicator-mediated biosensors	Fluorescence of an indicator which responds to a species formed or consumed during a biochemical reaction involving the analyte (analogous to type C)
F	Affinity sensors (mostly irreversible)	Fluorescent detection of noncovalent binding events such as antibody-antigen, complementary polynucleotide strands (DNA, RNA, PNA) receptor-ligand, enzyme-inhibitor, aptamers or MIPs and their substrates etc. (by analogy to types B or C)

1.3. Optical Multiple Chemical Sensing

The optical approach is capable of multianalyte monitoring meaning that multiple parameters can be determined simultaneously. Such sensors are called multisensors. A subgroup of these are the so-called compensating sensors, meaning that apart from the analyte itself, the sample is also evaluated for a second species which interferes with the result. This interference is then corrected for. For example, all known fluorescence-based oxygen sensors suffer from

interference by temperature. A second (temperature) sensor is needed to compensate for its effects.[24,25] Several strategies can be employed to achieve optical multisensing.

The most straightforward and easily implemented approach is based on so-called multispot sensors, which are also called sensor arrays if there are more than a few individual sensors. In these, individual sensors are placed in a way that the sample is contacted simultaneously or successively with all of the sensors. The analytical signal is then read out and processed (Fig. 1.6a,b).

Although this approach is attractive and widely used, there are several limitations in it. The presence of a spatial distance between the sensors implies that they are not suitable for microscopic or microfluidic investigations of both parameters at the same site, and that the analytes can never be determined truly simultaneously, as no part of the sample can ever be in contact with both sensors at the same time. Furthermore, the limited volume of a sample that is available in clinical chemistry limits the number of sensors that can be exposed to e.g. a given blood sample. If one can sense n parameters with one sensor spot, the number of sensors can be reduced by n-1.

True multiple sensing is based on the use of a single sensing spot that yields a multitude of optical information that can serve as analytical information for more than one species. So far, dual sensors have been described only, whilst triple sensors await their realization. Two different architectures exist: Single layer dual sensors contain all indicators within a single embedding polymer (Fig. 1.6c). Dual layer dual sensors are composed of two layers superimposed, each with an indicator for one analyte.

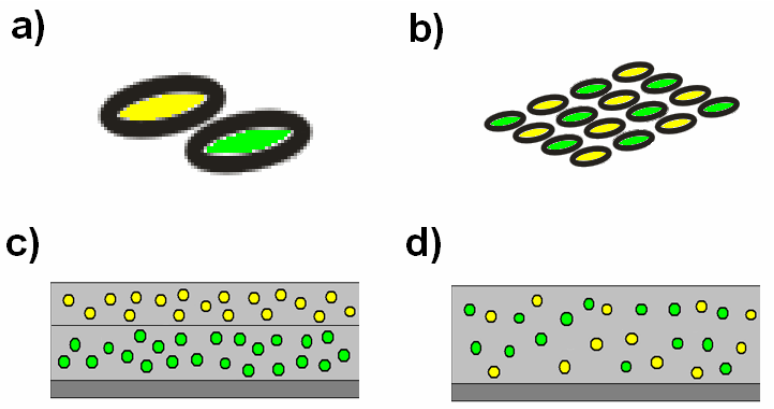

Fig. 1.6. Types of dual sensors: a) two-spot sensors, b) sensor arrays, c) dual layer sensors, d) single layer sensors.

In a true dual or multiple sensor, the information on the parameters of interest is acquired at regularly identical sites, often over a large region of interest, for example when imaging certain areas. What are the challenges and drawbacks of such sensors? Cross-sensitivities with respect to the analyte as well as spectral cross-talk are to be avoided. In the case of dual layer sensors also cross-leaching of the components may occur, particularly when plasticizers are used and response times may be unacceptably long, whereas in the case of single layer sensors suitable indicators and polymers are often incompatible. Layers embedded with multiple indicators are also occasionally displaying increased photodecomposition and signal drifts compared to single sensors, particularly when oxygen sensors (which generate singlet oxygen) are present. One favorable solution to many of the above problems is the use of permeation-selective micro- and nanoparticles, which allow to create a favorable microenvironment for each indicator while being able to apply a biocompatible sensor layer. Hydrogels are particularly attractive matrices in this respect, as they are inherently hydrophilic and therefore allow to disperse hydrophobic indicator-doped particles without significant leaching or decomposition problems.

Since such chemical sensors are based on the use of (fluorescent) indicator dyes, sophisticated spectroscopic methods need to be found in order to separate signals. One way to separate two signals is of course by spectral separation, which however is possible only if the two indicators have well separated bands that do not overlap. Other analytical parameters include fluorescence decay time and anisotropy. This means, in effect, that the optical signals can be multiplexed in various ways. For example, they can be acquired at several wavelengths and after several delay times in parallel. It requires appropriate indicator chemistries and spectroscopic methods, though, to separate the complex signals that originate from such a multiple sensor. On the other hand, the use of multiple sensors leads the way for further miniaturization.

Also, many of the methods so far do work only in single-spot based sensors, but hardly in an imaging format. This is due to the lack of sensor homogeneity and indicator brightness. Improved indicators and more sophisticated methods and instrumentation are needed so to achieve further progress.

It can be stated that multiple sensors have attractive features in that

(a) two or more parameters can be sensed at the very same site and simultaneously;

(b) they enable chemical sensors to be compensated for effects of temperature if combined with a temperature sensor chemistry;

(c) they enable unspecific sensors to be made more specific;

(d) they enable smaller sample volumes to be analyzed for more parameters than with monosensors;

(e) they enable sensing of several parameters in cases where the sample volume is limited (such as in the case of blood), or in the case of microscopy or microfluidic devices.

1.4. Sensor Miniaturization and Microarray Technology

Miniaturized analytical devices, most prominently microarray ("biochip") and microfluidic ("lab-on-a-chip") systems hold great opportunities by incredibly increasing throughput and decreasing consumption and thereby ultimately cost and energy.

The genome projects have yielded previously unknown floods of data.[26] Allowing for maximum multiplexing with minimum PCR propagation, DNA microarrays have rapidly become the tools of choice for gene expression profiling and SNP screening.[27] Although the earliest microarrays studies were done using proteins and peptides,[28,29] other formats were lagging behind DNA chips for long, due to their lower chemical stability and lack of sufficient numbers of probes needed to enable economic use of microarrays. However, within the past few years the efforts towards large-scale characterization of proteomes and other biological interaction networks have increased dramatically,[30] aided by much work in providing suitable analytical methods for these tasks. A number of different bioanalytical microarray formats have been developed and now allow high-throughput interaction screening. Protein microarrays are at the forefront, but arrays based on the use of whole cells, peptides or carbohydrates are increasingly being used.

As it has been since the earliest work,[28,29] fluorescence is the most widely used analytical technique on all microarray formats. It is extremely sensitive, rapid, nontoxic, nondestructive and comparatively inexpensive. On the negative side, it usually requires the use of a label, which may possibly interfere with the binding event on the microarray surface, particularly when the native structure of the analyte molecule has not yet been fully established. However, the label can usually easily be directed onto sites which are not essential for functionality (e.g. outer lysine, serine or cysteine residues of proteins).

Other methods adapted for microarrays include radioactive labeling, which is, in principle, an extremely sensitive and versatile technique.[31] However, it is subject to health and environmental concerns. It has largely been replaced by fluorescent methods in many areas of bioanalysis. Detection of microarray binding can also be done using mass spectrometry (MS).[32a] MS does not require the use of a label, and gives rich information about the structure of the bound analyte, which is particularly useful in protein formats. The backdraws of this technique are the costs and complexity associated with it. In particular it decreases the throughput through its intricate readout and thereby contradicts one of the major advantages of microarrays, the rapid, highly-multiplexed screening. Another technique which has found attention is surface plasmon resonance (SPR) imaging.[32b] This optical phenomenon, which relies on a total internal reflection illumination configuration to excite plasmons on conducting surfaces is capable of highly sensitive real-time bioanalysis without using markers. However, SPR is also associated with disadvantages, e.g. in specificity and efficiency of detecting many analytes. There is an increasing number of microarray publications emerging,[33] and no reason to believe that fluorescence will lose its dominant role in microarray detection in the foreseeable future. Other analytical methods will certainly also continue to be improved and add value to the biochip field.

In the protein microarray field, lots of different detection methods can be found [see Ref. 34-36 for reviews]. Broadly, protein microarrays can be divided into analytical protein arrays, having the goal of quantifying protein content in a specific sample, and protein function arrays, which aim to determine interactions of proteins with proteins or other molecules (Fig. 1.7). The first step in each protein array is the immobilization of a protein recognizing molecule onto the solid substrate. Most typically, this is an antibody or its antigen binding region. After incubation with the antigen-containing sample, detection is performed via direct pre-labeling of the sample, labeled secondary antibodies, or indirect detection via

addition of one or more reagents which ultimately produce emission only if the analyte is present on the chip.

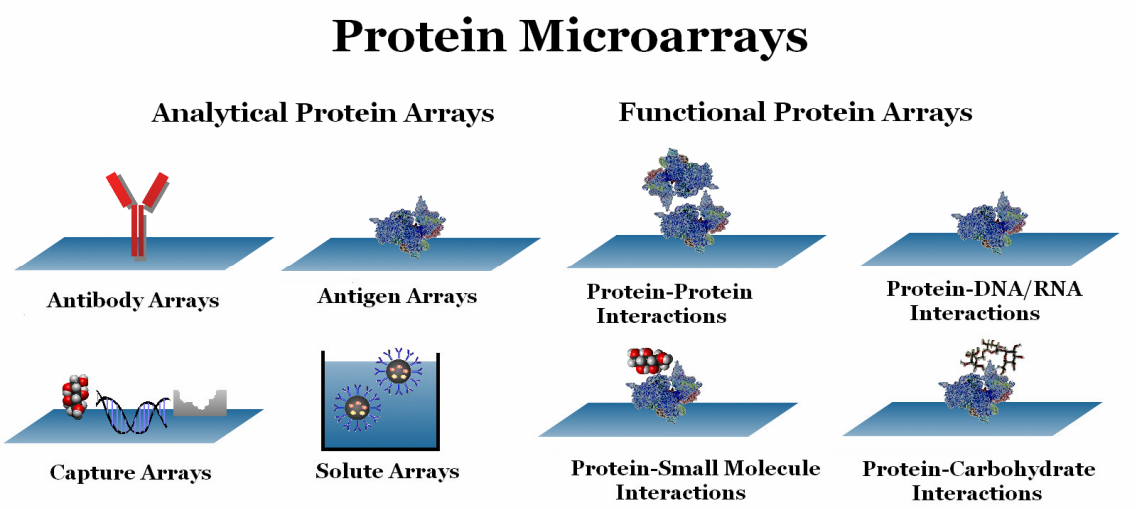

Fig. 1.7. Types of protein microarrays, divided into two subcategories. Analytical protein arrays (left) are used for quantification of target analytes, e.g., antigens using antibody arrays or antibodies using antigen arrays (top). Proteins of interest can also be captured using small molecules, aptamers, or molecularly imprinted polymers. Alternatively, surface-functionalized nanoparticles may be used in solute arrays (bottom). Functional protein arrays (right) can detect interactions of immobilized proteins with virtually any kind of natural or artificial compound, but only the most common are shown.

1.5. Aim of the Research

Most of the materials and detection schemes available so far in optical chemical sensors do only work for a single analyte. In order to progress into multiple analyte sensing, both new materials and detection schemes are necessary that are capable of simultaneous monitoring of more than one analyte. Those areas are not separate, as each detection method puts certain requirements and constraints upon the materials used. This thesis is exclusively concerned with fluorescence lifetime as the analytical parameter, therefore probes had to be found and

developed that produce a large lifetime change in response to species while at the same time maintaining the maximum selectivity possible.

Oxygen is a parameter of paramount importance and materials using the the highly-oxygen sensitive thermally activated delayed fluorescence (TADF) effect of fullerene C_{70} were investigated.[37] Further development of those trace oxygen sensing layers was then focused alongside ruthenium-chelate based probes with a large temperature dependence of their luminescence, to arrive at materials that allow simultaneous sensing of both parameters based on fluorescence lifetime.[38] While the lifetime in these sensors was recorded at separate wavelengths, a novel detection scheme without spectral separation of probes for multiple analytes based on the use of lifetime discrimination only was elaborated.[39] Nanomaterials are very promising in the multiple sensing field as they enable local manipulation of probe environments and polymeric nanoparticles that allow to sense oxygen via their lifetime, as well as ones suitable for temperature detection and inert nanoparticles that allow lifetime-based protein quantification were developed. Lastly, in the microsensing field, a method for protein microarray detection that is based on fluorescence lifetime rather than its intensity was applied.[40]

1.6. References

[1] J. S. Baskin, A. H. Zeweil, *J. Chem. Educ.* **2001**, *78*, 737-751.

[2] E. Jussim, G. Kayafas, *Stopping Time*, Abrams, New York, **1987**.

[3] M. Kikuchi, *Proc. Electrochem. Soc.* **1998**, *98*, 126-133.

[4] D. J. Bradley, *Science Prog.* **1969**, *57*, 301-322.

[5] J.R. Lakowicz, *Principles of Fluorescence Spectroscopy***,** Kluwer, New York, **1999**.

[6] B. Valeur, *Molecular Fluorescence - An Introduction: Principles and Applications*, Wiley-VCH, Weinheim, **2000**.

[7] K. C. Benny Lee, J. Siegel, S. E. D. Webb, S. Lévêque-Fort, M. J. Cole, R. Jones, K. Dowling, M. J. Lever, P. M. W. French, *Biophys. J.*, **2001**, *81*, 1265-1274.

[8] Olympus Microscopy Resource Center, http://www.olympusmicro.com/primer/techniques/fluorescence/fret/images/fretintrofigure10.jpg, **2008**.

[9] W. Becker, *The bh TCSPC Handbook 2nd ed.,* Becker & Hickl, Berlin, **2006**.

[10] Fluorescence Lifetime Imaging, http://www.imperial.ac.uk/research/photonics/research/topics/biomedical_imaging/images/flim1.gif, **2008**.

[11] F. Haber, Z. Klemensiewicz, *Z. Phys. Chem.* **1909**, *67*, 385-427.

[12] L. C. Clark Jnr., R. Wolf, D. Granger, Z. Taylor, *J. Appl. Physiol.* **1953**, *6*, 189-193.

[13] L. C. Clark Jnr., *Ann. NY Acad. Sci.* **1962**, *102*, 29-45.

[14] a) O. S. Wolfbeis (Series Ed.), *Springer Series on Chemical Sensors and Biosensors Vol. 1-4*, Springer, Wien, **2004-2006**, b) B. R. Eggins, *Chemical Sensors and Biosensors,* Chichester, UK, **2002**, c) F. S. Ligler, C. A. Rowe-Taitt (Eds.), *Optical Biosensors: Present and Future*, Elsevier, Amsterdam, **2002**, d) R. P. Thompson, *Fluorescence Sensors and Biosensors*, CRC Press, Boca Raton, **2006**.

[15] O. S. Wolfbeis, *Anal. Chem.* **2006**, *78*, 3859-3873 and references A1-A3 therein.

[16] A. Hulanicki, S. Glab, F. Ingman *Pure Appl. Chem.* **1991**, 63, 1247-1250.

[17] T. Grandke, J. Hesse, *Introduction*, pp.1 in T. Grandke, W. H. Ko (Eds.), *Sensors A Comprehensive Survey*, *Vol. 1*, VCH, Weinheim, **1991**.

[18] W. Goepel, K. D. Schierbaum, *Definitions and Typical Examples*, pp.1 in W. Goepel, J. Hesse, J. N. Zemel (Eds.), *Sensors A Comprehensive Survey*, *Vol. 2*, VCH, Weinheim, **1991**.

[19] P. Hauptmann, *Sensoren - Prinzipien und Anwendungen*, Hanser, Munich, **1990**.

[20] G. Boisdé, A. Harmer, *Chemical and biochemical sensing with optical fibers and waveguides*, Artech House, Norwood, **1996**.

[21] K. Cammann, E. A. Guibault, H. Hall, R. Kellner, O. S. Wolfbeis, *The Cambridge Definition of Chemical Sensors*, In: Proceedings of the Cambridge Workshop on Chemical Sensors and Biosensors Cambridge University Press, New York, **1996**.

[22] A. Brecht, G. Gauglitz, *Biosens. Bioelectron.* **1995**, *10*, 923-926.

[23] D. R. Thévenot, K. Toth, R. A. Durst, G. S. Wilson, *Biosens. Bioelectron.* **2001**, *16*, 121-131.

[24] J. Hradil, C. Davis, K. Mongey, C. McDonagh, B. D. MacCraith, *Meas. Sci. Technol.* **2002**, *13*, 1552-1557.

[25] L. M. Coyle, M. Gouterman, *Sens. Act. B* **1999**, 61, 92-99.

[26] National center for biotechnology information, GenBank, http://www.ncbi.nlm.nih.gov/ Genbank/index.html, **2004**.

[27] A. Schulze, J. Downward, *Nature Cell Biol.* **2001**, *3*, E190-195.

[28] R. Ekins, F. Chu, E. Biggart, *Anal. Chim. Acta* **1989**, *227*, 73-96.

[29] S. P. A. Fodor, J. L. Read, M. C. Pirrung, L. Stryer, A. T. Lu, D. Solas, *Science* **1991**, *251*, 767-773.

[30] N. G. Anderson, A. Matheson, N. L. Anderson, *Proteomics* **2001**, 1, 3-12.

[31] W. Mikulits, H. Dolznig, R. Hofbauer, E. W. Mullner, *BioTechniques* 1999, 26: 846-850.

[32] a) L. O. Lomas, *The Use of Proteinchip® Arrays for Deciphering Biological Pathways* pp. 153 b) G. Franklin, A. McWhirter, *Seein Beneath the Surface of Biomolecular Interactions: Real-time Characterization of Label-free Binding Interactions using Biacore's Optical Biosensors* pp. 57 in D. Kambhampati (Ed.), *Protein Microarray Technology*, Wiley, New York, 2004.

[33] E. Marshall, *Science* **2004**, *306*, 630-631.

[34] G. MacBeath, *Nature Genetics* **2002**, *32*, 526-532.

[35] M. F. Templin, D. Stoll, J. M. Schwenk, O. Pötz, S. Kramer, T. O. Joos, *Proteomics* **2003**, *3*, 2155-2166.

[36] B. B. Haab, *Proteomics* **2003**, *3*, 2116-2122.

[37] S. Nagl, C. Baleizão, S. M. Borisov, M. Schaeferling, M. N. Berberan-Santos, O. S. Wolfbeis, *Angew. Chem. Int. Ed.* **2007**, *46*, 2317-2319.

[38] C. Baleizão, S. Nagl, M. Schaeferling, M. N. Berberan-Santos, O. S. Wolfbeis, *submitted*.

[39] S. Nagl, M. I. J. Stich, M. Schaeferling, O. S. Wolfbeis, *submitted*.

[40] S. Nagl, R. Bauer, U. Sauer, C. Preininger, U. Bogner, M. Schaeferling, *Biosens. Bioelectron.* **2008**, *in press*.

CHAPTER 2
RECORD RESPONSE OPTICAL TRACE OXYGEN SENSING AND IMAGING

2.1. Introduction

Dioxygen is one of the key molecules on Earth. It plays an essential role in the atmosphere, the hydrosphere, the geosphere and not the least the biosphere.[1] Many physiological transformations, chemical reactions and (bio-)technological processes produce or consume O_2, whilst anoxic species, numerous chemical syntheses and manufacturing protocols demand its complete absence. Its extraterrestrial presence is indicative for the presence of life in the form we know.[2] Trace oxygen detection is also important in aerospace research,[3] and from a safety standpoint,[4] as oxygen leaks can cause fires and explosions, and can be harmful in storage chambers and packaged food.[5]

Common trace oxygen sensors are based on amperometry (*Clark* electrodes). These are sensitive and applicable over a wide temperature range but are difficult to miniaturize, invasive, and limited to discrete points.[6]

Optical sensors overcome these limitations. Most are based on the quenching of the long-lived luminescence exhibited by polycyclic aromatic hydrocarbons, transition metal complexes and metalloporphyrins.[7] These are typically placed in inert polymer membranes. Highly permeable matrices are employed in order to sense traces of O_2.[8] Here we show that a so-far unmatched sensitivity combined with an unmatched brightness at high temperatures can be achieved by exploiting the extremely efficient quenching of the delayed fluorescence of the

ellipsoidal fullerene C_{70} embedded into two highly permeable polymer membranes, an organosilica and an ethyl cellulose.

2.2. Results and Discussion

2.2.1. Fluorescence spectra

The electronic states and transitions of C_{70} and other fullerenes, due to the large number of π electrons, lie on the interface between discrete molecular orbitals and band structures.[9] The absorbance of C_{70} displays a peak at 470 nm (ε ≈ 20,000 M^{-1} cm^{-1}). The luminescence of C_{70} is very atypical in several ways. The fluorescence occurs from two excited singlet states. Weak prompt fluorescence (Φ_F: 0.05 %, τ ≈ 650 ps) occurs in the far red (mainly 650-725 nm). Strong energy overlap and many low-lying excited states lead to a quantum yield of triplet formation close to 1 (reported 0.994[9b]). Multiple weak phosphorescence bands are observed between 750 and 950 nm, displaying lifetimes of 20 to 25 ms at room temperature (RT).[9]

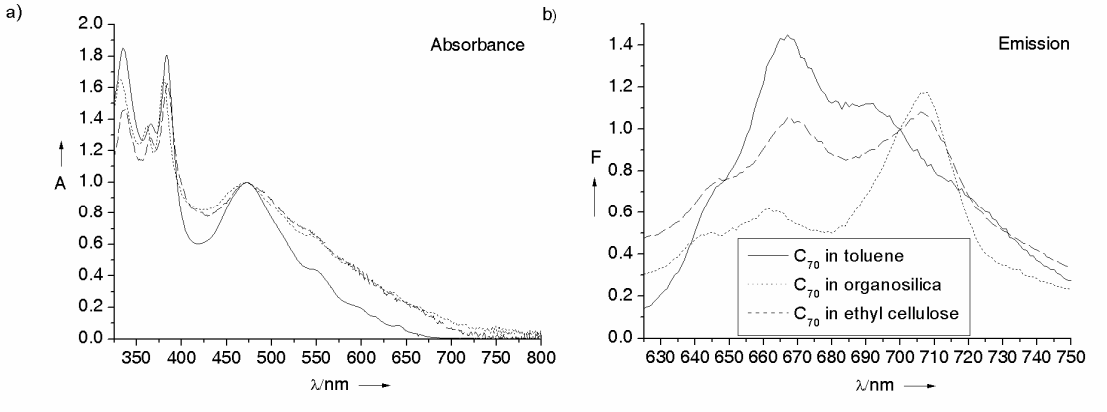

Fig. 2.1. Spectral properties of the fullerene-doped polymer films used in this work and comparison with the spectra of C_{70} in toluene, a) absorbance (normalized to the peak near 470 nm) and b) emission spectra, normalized to the emission at 700 nm (λ_{exc}: 470 nm).

Triplet state lifetimes of this magnitude or even longer are observed for many molecules and are known to be efficiently quenched by molecular oxygen generating excited singlet oxygen. However, all of them are only very weak emitters. C_{70}, in contrast, displays a remarkably strong thermally activated E-type delayed fluorescence (DF). An increase in temperature leads to a stronger overlap between excited singlets and triplets. The triplet states are eventually in thermal equilibrium with the singlet states. A unique DF quantum yield (Φ_{DF}) of ca. 8 % is shown by C_{70} at temperatures of around 150 °C and more, whilst at 20 °C Φ_{DF} is ≈ 1 % only.[9b] C_{70} also displays triplet-triplet absorption in the IR that is sensitive to oxygen.[10]

The highest O_2 permeabilities are displayed of silica-based polymers. But in all reports of sol-gels doped with unfunctionalized fullerenes, the fullerene was partially aggregated due to formation of small clusters.[11] These show largely reduced fluorescence intensities and lifetimes due to self-quenching.

We have observed a similar behavior of C_{70} in silica, both in plain and nanoparticle form, but were able to incorporate C_{70} into an organically modified silica without significant aggregation using a monomer where one alkoxy group is replaced by a phenyl ring.[11] Organosilica (OS) are less polar and thus more compatible with fullerenes.[12,13] Ethyl cellulose (EC) also is a highly permeable matrix for oxygen sensing.[14] C_{70} is compatible with this matrix. The absence of significant aggregation was demonstrated through fluorescence spectra at -30 °C (Fig. 2.2), phosphorescence spectra at 77 K (Fig. 2.3), singlet oxygen fluorescence spectra and lifetimes (Fig. 2.4-2.7), scanning electron microscopy (Fig. 2.8-2.9) and the obtained DF lifetimes (Fig. 2.10).

2.2.2. Fluorescence and phosphorescence spectra at low temperatures

The low-temperature fluorescence spectra and phosphorescence spectra correlate well with previous fullerene studies in different matrices and the features resemble a previous report of C70 in paraffin film.[9b] Phosphorescence lifetimes were determined at 77 K in the absence of oxygen and were found to be 48 and 49 ms for EC and OS, respectively. Both spectral and temporal features are in good agreement with C70 at low temperatures in inert matrices.[9a,15,16] Fullerene aggregates would show different spectra and phosphorescence lifetimes.

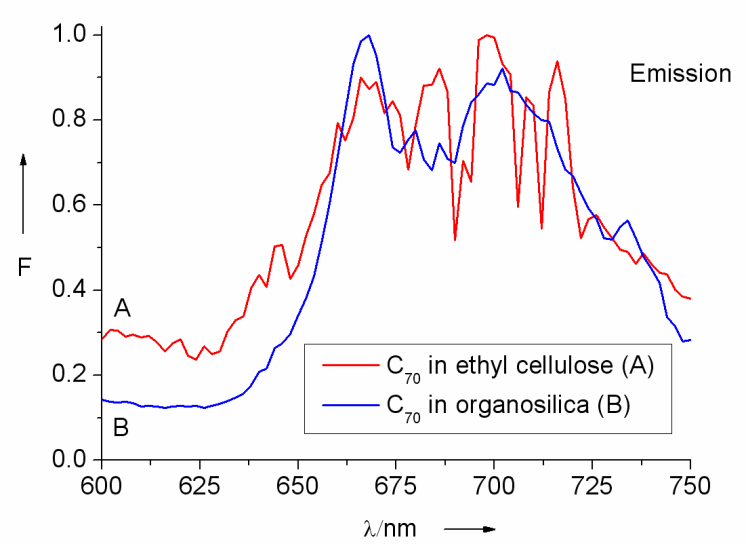

Fig. 2.2. High resolution fluorescence spectra of C_{70} in both matrices at – 30 °C.

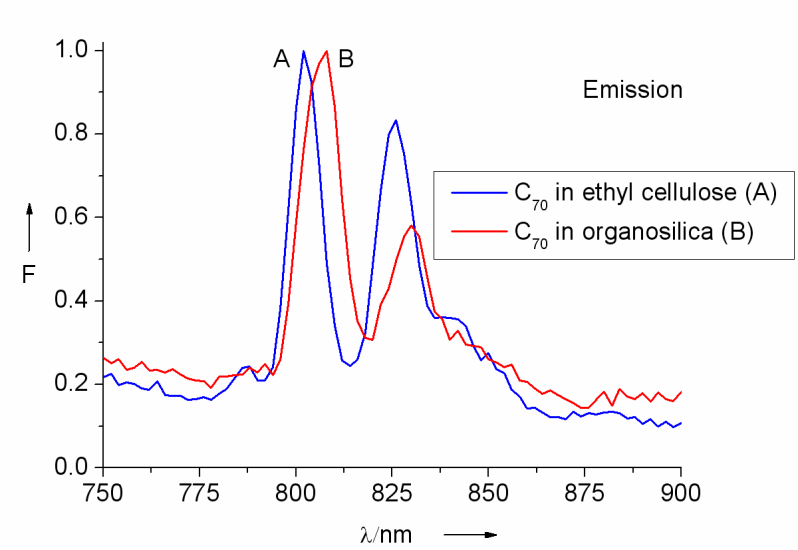

Fig. 2.3. Phosphorescence spectra of the degassed samples at 77 K.

2.2.3. Singlet oxygen luminescence spectra and lifetimes

The quenching mechanism was confirmed by direct detection of singlet oxygen emission at 1270 nm using the setup described in Ref. 17, 18. The signal was referenced against blank samples containing only the embedding polymer (OS, EC). Despite the very low quantum yield of singlet oxygen luminescence ($\Phi_F \approx 10^{-5}$ %) the peak of its emission was easily detectable at 1270 nm, and the membranes could clearly be discriminated against the blanks which showed no such peak at all. The observed decay times in the low µs range confirm the assignment of the signal to oxygen emission.

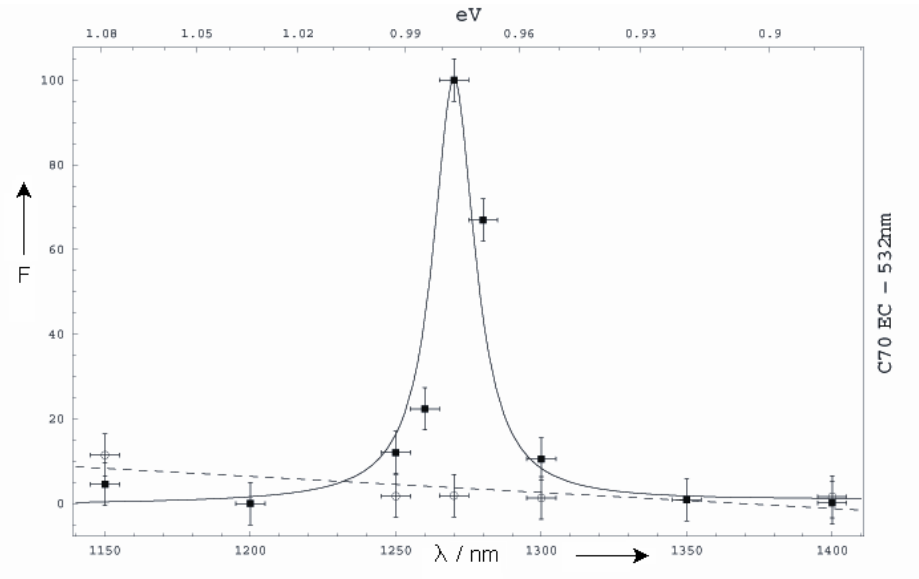

Fig. 2.4. IR emission spectra of C_{70}-EC (solid line) and EC alone (dashed line) at RT on air.

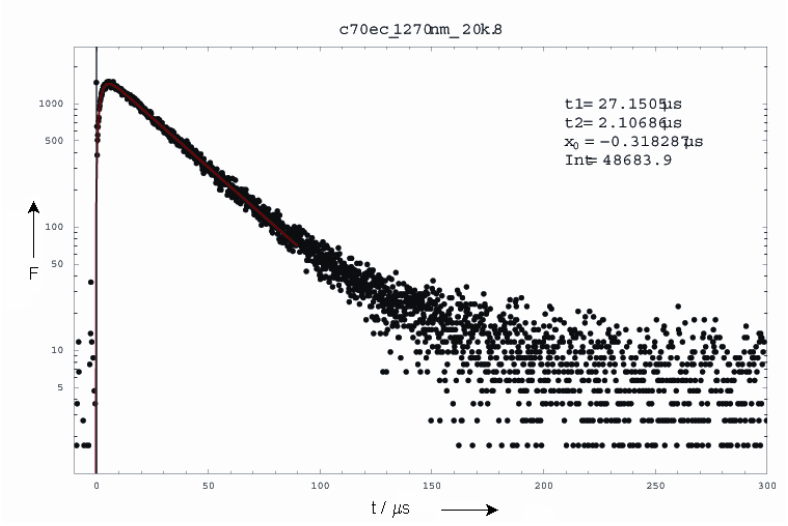

Fig. 2.5. Semi-log plot of the time profile of the singlet oxygen emission at 1270 nm of C_{70}-EC.

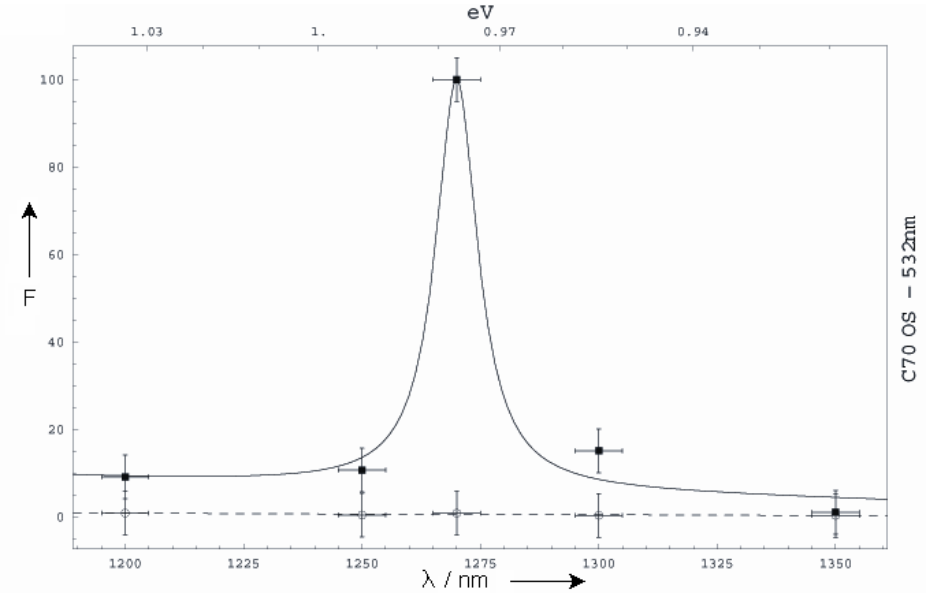

Fig. 2.6. IR emission spectra of C_{70}-OS (solid line) and OS alone (dashed line) at RT on air.

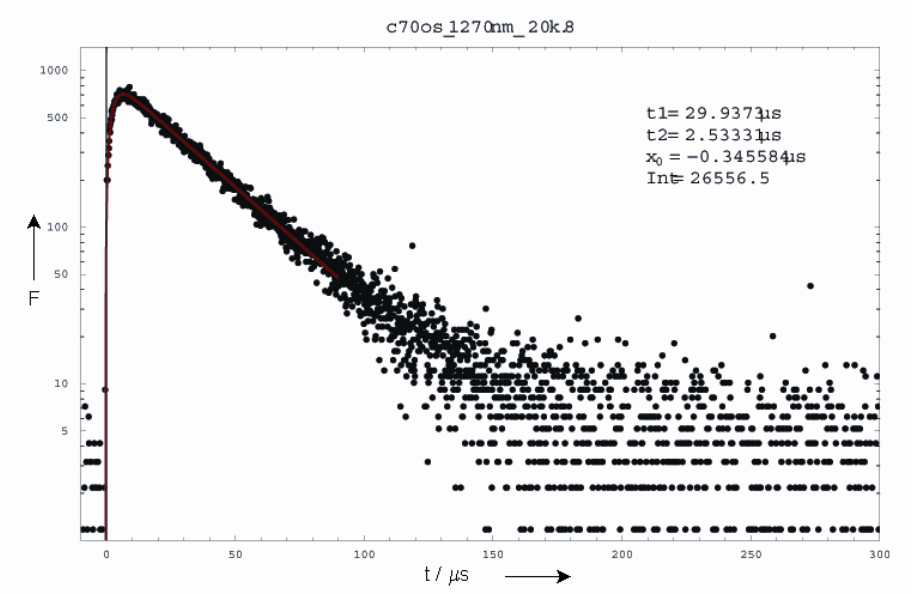

Fig. 2.7. Semi-log plot of the time profile of the singlet oxygen emission at 1270 nm of C_{70}-OS.

2.2.4. Scanning electron micrographs

The scanning electron micrographs show overall homogeneous polymer surfaces with a few defects, particularly in EC. As they are seen both on the samples and the blanks they are probably nanoparticles from the air or impurities in the polymer. The soft elastomer EC suffers from deterioration by the electron beam, as can already be seen in those initial images shown above. Organosilica, which features a strong silica backbone structure, appears to be stable.

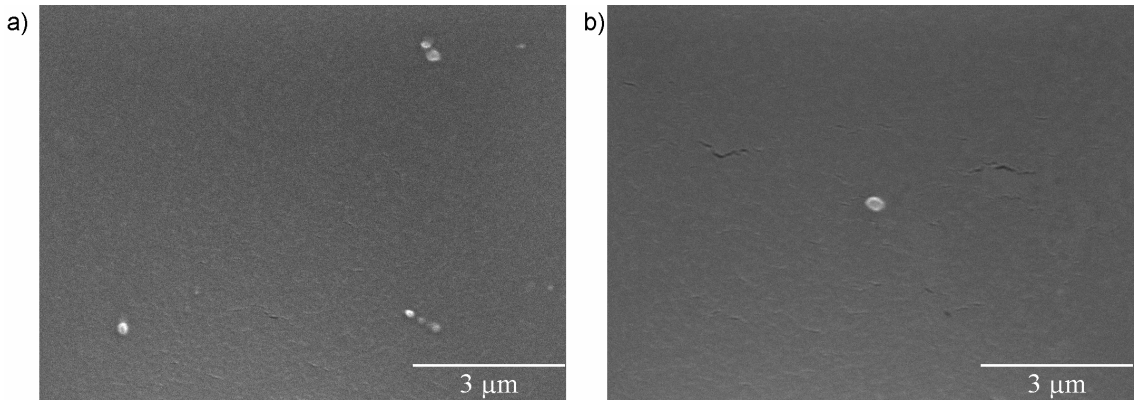

Fig. 2.8. Scanning electron micrograph of C_{70} in EC (a) and of plain EC (b).

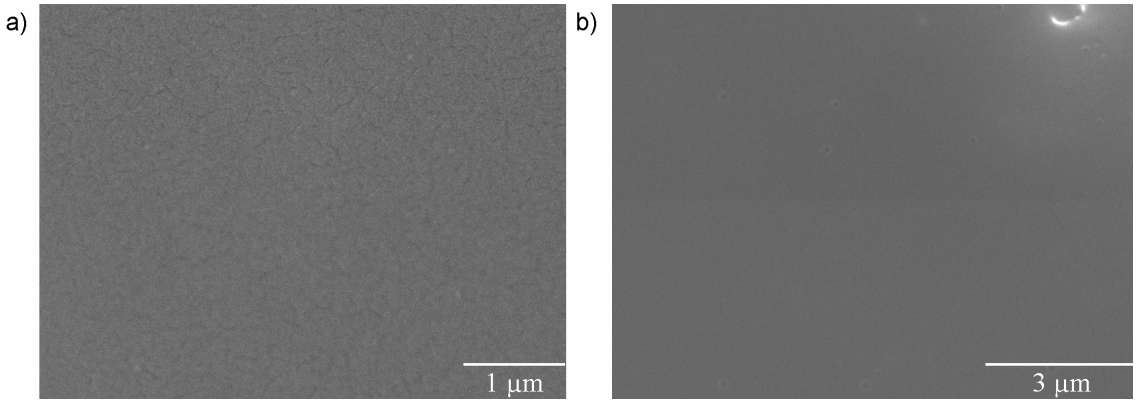

Fig. 2.9. Scanning electron micrograph of C_{70} in OS (a) and of plain OS (b).

2.2.5. Fluorescence lifetime imaging

The sensitivity to oxygen was investigated by time-domain fluorescence lifetime imaging[19] between 650 and 710 nm. A delay time of 1 μs was applied after the end of the excitation pulse, which did not only exclude scattered light, but also prompt fluorescence of C_{70} (which is not quenched by oxygen). To demonstrate the applicability towards spatially resolved detection, we placed a piece of the sensor strip in a custom flow chamber and calculated the DF lifetime for each pixel using a setup comparable to Ref. 20 (Fig. 2.10).

The DF lifetimes exceed 20 ms in the absence of oxygen at RT and below, and result in an extreme sensitivity to oxygen (Figs. 10, 11). The response is instantaneous (< 0.1 s). Best fits for the Stern-Volmer plots were obtained by applying the two-site quenching model.[21] The fluorescence is most pronounced at 120 °C, and C_{70} still shows DF lifetimes of > 5 ms. The temperature dependence of the sensitivity is therefore the result of the following three effects upon increasing temperature, a) increasing Φ_{DF}, b) decreasing DF lifetime, c) higher collision rate of O_2. The Stern-Volmer constants depend on temperature in a nonlinear way.

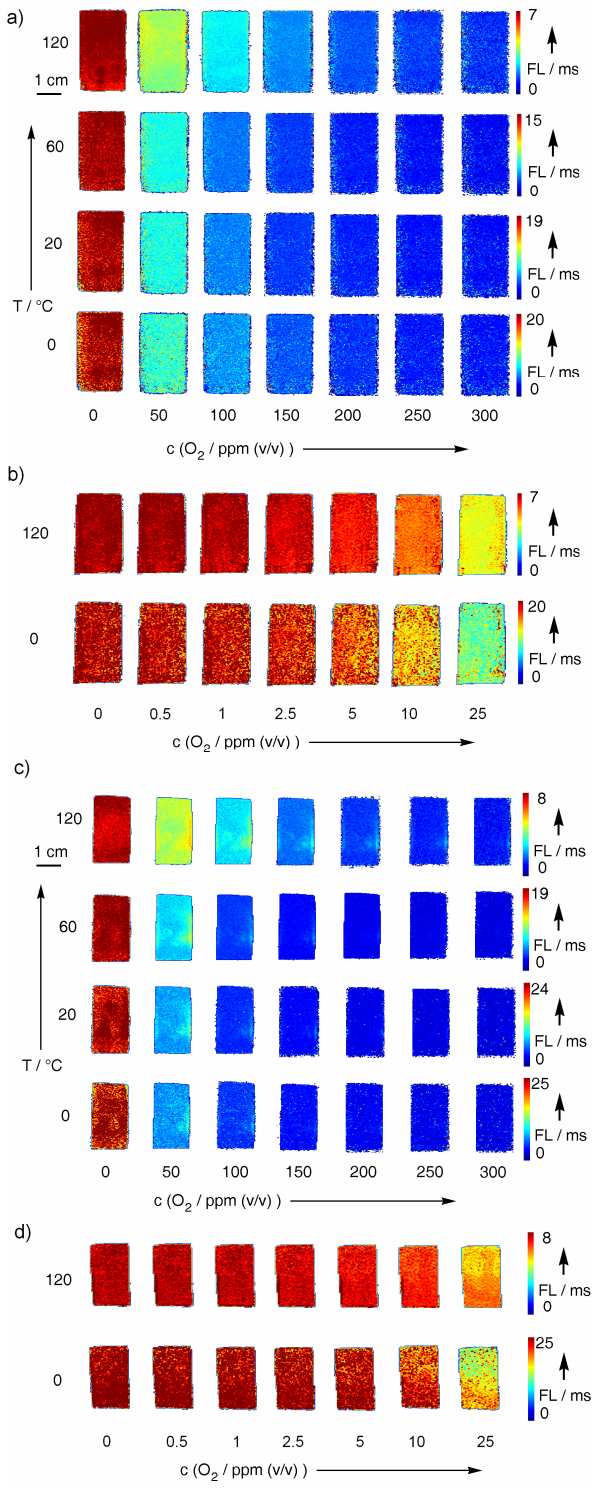

Fig. 2.10. Pseudo-colored (dark red: maximum, dark blue: zero) fluorescence lifetime (FL) images of a, b) C_{70} in organosilica and c, d) C_{70} in ethyl cellulose between 0 and 120 °C and O_2 concentrations from 0 to 300 ppm in nitrogen at atmospheric pressure. Fig. b) and d) are exemplary measurements at low ppm oxygen conc.

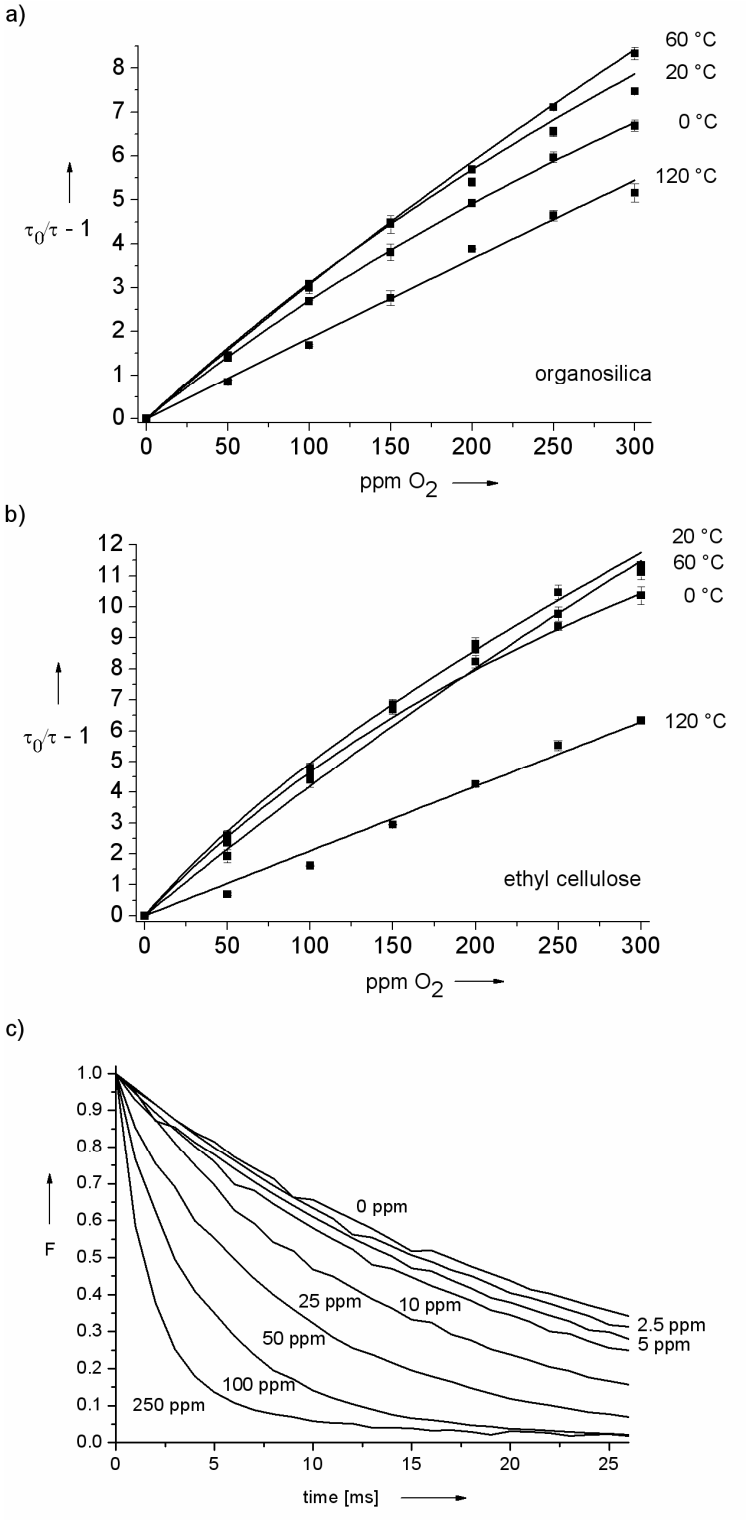

Fig. 2.11. Lifetime-based Stern-Volmer plots at various temperatures for both types of fullerene-doped membranes, a) OS, b) EC and c) exemplary time profile for EC at 20 °C (integrated values over the whole area.

2.2.6. Comparison of oxygen quenching efficiencies

Both systems display Stern-Volmer constants more than one order of magnitude better than state-of-the-art probes. The response of the matrices presented here is fully reversible many hundreds of times and showed no detectable degradation after three months of storage at RT in the dark on air. They are compared with literature data of related probes in Table 2.1. Stern-Volmer constants, fitted according to the two-site model, are given. These are material constants, independent of experimental conditions, and a function of temperature only. The detection limits were defined at 1 % quenching to ensure comparability and make them not subject to specific instrumental characteristics. The report of *Han et al.*[22] which features various commonly used probes in silica matrices, which are unmatched with respect to oxygen sensitivity, and the report of *Apostolidis et al.*[23] which is a very comprehensive and combinatorial investigation of commonly used probe-polymer combinations for oxygen sensing were selected. The PdOEP-silica membranes of *Han et al.* show the highest sensitivity using common probes. Higher sensitivities were only reported using the polytrimethylsilylpropyne (PTMSP) matrix, however this polymer suffers from very rapid aging of its oxygen permeability and therefore lack of stability (see Ref. 24 for a thorough investigation).

Table 2.1. Stern-Volmer constants and detection limits for O_2 sensing based on DF quenching of C_{70} in OS and EC, respectively, at various temperatures and a comparison with other common probes.

Probe	T [°C]	f_1	K_{SV1} / $[mg\ (O_2)\ /\ L]^{-1}$	f_2	K_{SV2} / $[mg\ (O_2)\ /\ L]^{-1}$	Detection limit / [µg (O_2) / L]	Reference
C_{70} - OS	0	0.96	25.1	0.04	$4.0 * 10^{-2}$	0.42	this work
	20	0.97	28.4	0.03	0	0.37	this work
	60	0.98	26.0	0.02	0	0.40	this work
	120	1.00	15.1	0.00	0	0.67	this work
C_{70} - EC*	0	0.96	47.0	0.04	0	0.22	this work
	20	0.95	52.9	0.05	1.45	0.20	this work
	60	0.99	36.1	0.01	0	0.28	this work
	120	1.00	16.9	0.00	-	0.60	this work
PdOEP - silica	20	0.89	3.74	0.11	$9.4 * 10^{-2}$	3.02	22
PtOEP - silica	20	0.87	0.37	0.13	$1.0 * 10^{-2}$	31.3	22
PtTFPP - silica	20	0.87	0.12	0.13	$3.5 * 10^{-3}$	96.5	22
PtTPP - silica	20	0.83	0.17	0.17	$7.0 * 10^{-3}$	71.1	22
$Ru(dpp)_3$ - silica	20	0.61	$3.2 * 10^{-2}$	0.39	$2.4 * 10^{-3}$	496	22
PdTFPP - PTBS	20	0.90	1.32	0.10	$4.78 * 10^{-3}$	8.51	23
PdTFPP - EC*	20	1.00	1.27	0.00	-	7.95	23
PdTFPP - EC#	20	0.99	1.12	0.01	0	9.11	23
PtTFPP - PTBS	20	0.81	0.13	0.19	$2.2 * 10^{-3}$	95.8	23
PtTFPP - EC*	20	0.89	0.18	0.11	$1.0 * 10^{-2}$	63.7	23
$Ru(dpp)_3$ - PTBS	20	0.75	$1.4 * 10^{-2}$	0.25	$1.3 * 10^{-4}$	962	23

*EC with 49% ethylation; #EC with 46% ethylation, PdOEP: Palladium octaethylporphyrin, PdTFPP: Palladium tetrakis-(pentafluorophenyl) porphyrin; PtOEP: Platinum ocatethylporphyrin, PTBS: Poly(4-tert.)butyl styrene, PtTFPP: Platinum tetrakis-(pentafluorophenyl)porphyrin; PtTPP: Platinum tetraphenylporphyrin, $Ru(dpp)_3$: Ruthenium tris-(4,7)-diphenylphenanthroline.

2.3. Conclusion

In conclusion, we introduce an optical oxygen sensor that is especially suited for sensing oxygen down to the ppb range and also at the elevated temperature range. It shows a response which is several factors greater than previous approaches. All of these properties can be explained by the atypical photophysics of E-type delayed fluorescence of the fullerene C_{70} dissolved in appropriate polymers. It enables, for the first time, ppb levels of oxygen at atm. pressure to be sensed and imaged by optical means, and thus has a large potential. The main backdraw is the only moderate brightness of the probe particularly at low temperatures (RT and below) where delayed fluorescence is weak. Metalloporphyrins are roughly two orders of magnitude brighter at these conditions. However, the brightness was still sufficient to use an imaging approach yielding high spatial resolution.

2.4. Experimental Section

C_{70} (> 98 %) was from Term USA (www.term-usa.com). Toluene (99.7 %) and EC (49 % ethylation) were from Sigma-Aldrich (www.sigmaaldrich.com). N_2 / O_2 mixtures were from Linde (www.linde-gas.com). OS was prepared according to [11].

C_{70}-OS was prepared by dissolving 0.5 mg C_{70} and 50 mg OS in 1 g toluene. The solution was ultrasonicated and heated to 40 °C for 15 min. C_{70}-EC was obtained by dissolving 0.5 mg C_{70} and 50 mg EC in 1 g toluene and stirring at RT for 15 min. The viscous solutions were spread as 120 µm thick films (using a coater from RK Print Coat Instruments, www.rkprint.com) onto a 100-µm polyester foil. The solvents were allowed to evaporate overnight to yield layers of around 6 µm thickness.

Luminescence was excited by four blue LEDs (Luxeon V Star, www.lumileds.com) using an interference filter centered at 470 nm. FL images were obtained using the Imagex TGi CCD camera system (www.prsbio.com). Three images were acquired and averaged for each oxygen concentration and temperature. For oxygen luminescence detection in the IR C_{70} was excited by the 532-nm frequency-doubled beam of a Q-switched Nd:YAG laser operating at 2 kHz (70 ns, 50 µJ pulse). Emission was detected through an IR-sensitive photomultiplier operating in single-photon counting mode, equipped with appropriate bandpass filters from 1150 to 1400 nm Emission.

Scanning electron micrographs were carried out on a Hitachi S-2400 scanning electron microscope.

2.5. References

[1] a) E. G. Nisbet, N. H. Sleep, *Nature* **2001**, *409*, 1083-1091. b) J. F. Kasting, *Science* **1993**, *259*, 920-926. c) N. Nathan, B.-S. Adam, *Nat. Rev. Mol. Cell. Biol.* **2004**, *5*, 971-982.

[2] C. Sagan, W. R. Thompson, R. Carlson, D. Gurnett, C. Hord, *Nature* **1993**, *365*, 715-721.

[3] C. Seife, *Science* **2003**, *299*, 1971.

[4] D. M. Denison, J. Ernsting, W. J. Tonkins, A. W. Cresswell, *Nature* **1968**, *218*, 1110-1113

[5] A. Mills, *Chem. Soc. Rev.* **2005**, *34*, 1003-1011.

[6] R. Ramamoothy, P. K. Dutta, S. A. Akbar, *J. Mat. Sci.* **2003**, 4271-4282.

[7] J. N. Demas, B. A. DeGraff, P. B. Coleman, *Anal. Chem.* **1999**, *71*, 793A-800A.

[8] F. Navarro-Villoslada, G. Orellana, M. C. Moreno-Bondi, T. Vick, M. Driver, G. Hildebrand, K. Liefeith, *Anal. Chem.* **2001**, *73*, 5150-5156.

[9] a) See G. Orlandi, F. Negri, *Photochem. Photobiol. Sci.* **2002**, *1*, 289-308, and references therein. b) M. N. Berberan-Santos, J. M. M. Garcia, *J. Am. Chem. Soc.* **1996**, *118*, 9391-9394.

[10] Y. Amao, K. Asai, I. Okura, *Chem. Lett.* **1999**, *28*, 183-184.

[11] G. Brusatin, P. Innocenzi, *J. Sol-Gel Sci. Technol.* **2001**, *22*, 189-204.

[12] I. Klimant, F. Ruckruh, G. Liebsch, A. Stangelmayer, O. S. Wolfbeis, *Mikrochim. Acta* **1999**, *131*, 35-46.

[13] M. Jaroniec, *Nature* **2006**, *442*, 638-640.

[14] A. Apostolidis, I. Klimant, D. Andrzejewski, O. S. Wolfbeis, *J. Comb. Chem.* **2004**, *6*, 325-331.

[15] J. Arbogast, C.S. Foote, J. Am. Chem. Soc. **1991**, *113*, 8886-8889.

[16] a) S. M. Argentine, A. H. Francis, C.-C. Chen, C. M. Lieber, J. S. Siegel, J. Phys. Chem. 1994, *98*, 7350-7354.

[17] J. Baier, M. Maier, R. Engl, M. Landthaler, W. Bäumler, J. Phys. Chem. B **2005**, *109*, 3041-3046.

[18] J. Baier, T. Maisch, M. Maier, E. Engel, M. Landthaler, W. Bäumler, Biophys. J. **2006**, *91*, 1452-1459.

[19] Z. Lin, M. Wu, M. Schäferling, O. S. Wolfbeis, *Angew. Chem.* **2004**, *116*, 1767-1770; *Angew. Chem. Int. Ed.* 2004, *43*, 1735-1738.

[20] G. Liebsch, I. Klimant, B. Frank, G. Holst, O. S. Wolfbeis, *Appl. Spectrosc.* **2000**, *54*, 548-559.

[21] J. N. Demas, B. A. DeGraff, *Anal. Chem.* **1995**, *67*, 1377-1380.

[22] B. H. Han, I. Manners, M. A. Winnik, Chem. Mater. **2005**, *17*, 3160-3171.

[23] a) A. Apostolidis, I. Klimant, D. Andrzejewski, O. S. Wolfbeis, J. Comb. Chem. **2004**, *6*, 325-331. b) A. Apostolidis, PhD Thesis, University of Regensburg, 2004.

[24] X.- Y. Wang, F. T. Willmore, R. D. Raharjo, X. Wang, B. D. Freeman, A. J. Hill, I. C. Sanchez, J. Phys. Chem. B **2006**, *110*, 16685-16693.

CHAPTER 3
A DUAL FLUORESCENCE SENSOR FOR TRACE OXYGEN AND TEMPERATURE WITH A LARGE TEMPERATURE RANGE AND UNMATCHED OXYGEN SENSITIVITY

3.1. Introduction

Oxygen, being essential for life, is an immensely important chemical species. Determination of oxygen levels is required in numerous areas including medicine, biotechnology, aerospace research, food packaged and in the chemical industry. After the discovery of the first optical, fluorescence-based sensor for oxygen 40 years ago,[1] it appeared hardly likely that optical sensors would rival the very successful and sensitive electrochemical oxygen measurement technique based on Clark electrodes. In the last decades, the potential offered by specific advantages of optical methods has been realized to a large extent. Among the many optical methods employed for sensing, fluorescence has attracted special attention because it is highly sensitive, versatile, non-invasive and of low toxicity.[2] Fluorescence-based sensors, in not requiring a physical contact with the medium during measurement, are advantageous compared to contact sensors in applications where electromagnetic noise is strong or it is physically difficult to connect a wire. Further advantages of sensors based on molecular fluorescence are the very fast response, the reversibility and the spatial resolution that can go from the macroscale (fluorescent paints) down to the nanoscale (fluorescence microscopy). These properties also overcome the limitations of electrochemical sensors which are difficult to miniaturize, invasive and limited to discrete points.[3]

All known fluorescence-based oxygen sensors and in fact almost any sensor, no matter what type, suffer from interference by temperature. This interference can be corrected for

using a second sensor to measure temperature. True multiple sensing methods are based on the use of a single sensor which provides analytical information on more than one physical or chemical parameter.[4] Up to date, several kinds of dual sensors have been described e.g. for CO_2/O_2,[5] CO_2/T,[5c] O_2/T[6] and pH/O_2.[7]

Pressure-sensitive paints (PSPs) and temperature-sensitive paints (TSPs) have been the subject of intense research which contributed to vast progresses in past years.[8] PSPs are oxygen sensors that take advantage of the fact the fraction of oxygen in air is constant, allowing the calculation of total pressure from the oxygen partial pressure.[9] With these materials, it is possible to record the entire pressure distribution on the surface of a large object (e.g. an aircraft in a wind tunnel), rather than just discrete points as with other sensors, e.g. mechanic pressure taps.[10] Sometimes, only trace concentrations of oxygen are employed in wind tunnels because sensor response is most sensitive under these conditions as a result of the Stern-Volmer equation.

Most of the food found in supermarkets is processed and stored in the absence of oxygen (modified atmosphere packaging (MAP)).[11] At the same time, food requires a specific range of temperatures during storage and transport so to maximize its shelf-life. Dual oxygen and temperature fluorescence sensors also have found application in this area, especially because it is a remote and non-invasive method, meaning that oxygen and temperature can be monitored without any contact to the sealing.[12]

Oxygen and temperature sensing also play a crucial role in the area of microbiology, namely in growth monitoring. Optical sensors are being increasingly used and a number of fluorescent dual sensors have been described recently.[5b,7c] It is challenging in this field to monitor organisms which grow under unusual conditions, e.g. hyperthermophilic organisms that require high temperatures,[13] and atmospheres of residual oxygen to anaerobic

conditions.[14] These organisms also are candidates for hydrogen production in a future hydrogen economy.[15] Another area of interest is chemical process and reaction monitoring. Many chemical reactions need to be carried out in the complete absence of oxygen, and at high temperatures. Optical sensors enable to observe the reaction parameters without disturbance, but at present they are limited to moderate temperatures and not applicable at trace oxygen levels.[6]

A variety of devices and sensors based on molecular optical properties has been developed to measure oxygen partial pressure.[16] For trace oxygen sensing, the choice of sensors is between palladium and platinum porphyrins or ruthenium complexes that most often are immobilized in oxygen permeable materials, with sensitivities in the ppmv range.[17] Another approach towards trace oxygen sensing is based on the thermally activated delayed fluorescence (TADF) effect displayed by C_{70}, leading to an extremely efficient quenching of the intensity and lifetime of TADF, and hence resulting in sensitivities in the ppbv range.[18]

Temperature sensing based on luminescence lifetime changes, using fiber optics in combination with phosphors, is a well established method.[19] More recently, several studies have been devoted to fluorescence-based molecular thermometry,[20] by exploiting the temperature dependence of either quantum yield or lifetime of hydrocarbons, the exciplex formation in anilines and perylenes, fluorescence quenching[21] and of the TADF[22] of fullerenes.

Most dual sensors of O_2/T reported so far[6] have in common a single excitation wavelength in the visible region, luminescence decay time as the analytical signal and a single matrix to disperse both temperature and oxygen probes. They exhibit working ranges from 0 to 70 ºC and O_2 concentrations in the range from 0 - 100 %. Detection limits in the best cases are at ppmv values. We describe here a dual sensor for simultaneous sensing of oxygen and

temperature based on luminescence lifetime measurements amd that we assume to be useful in the areas outlined above.

3.2. Experimental Section

3.2.1. Materials

C_{70} (> 99.9%), Ruthenium(II)-tris-1,10-phenanthroline chloride hydrate, titanium dioxide (TiO_2), hexane, toluene and ethyl cellulose 49 (EC) were purchased from Sigma-Aldrich (www.sigmaaldrich.com). Silicone RS 692-542 was obtained from RS Components (www.rs-components.com). Dimethyl formamide (Acros, www.acros.com) was used as received. Polyacrylonitrile (PAN, powder, M_w ~170,000) was purchased from Polysciences (www.polysciences.com). Ruthenium(II)-tris-1,10-phenanthroline-3-trimethylsilyl-1-propanesulfonate [$Ru(phen)_3$][24] and organosilica (OS)[25] were prepared according to the literature. Calibration gases (nitrogen and 50 ppm O_2 in nitrogen) were obtained from Linde (www.linde-gases.de). Polyester foil (125 µm, Poly(ethyleneterephtalate), Mylar) was from Goodfellow (www.goodfellow.com).

3.2.2. Methods

Preparation of the two-layer dual sensors: The sensor layers were prepared in two steps. First, a layer of $Ru(phen)_3$-PAN in dimethylformamide (DMF) was spread onto a polyester foil and after evaporation of the solvent, a second layer of C_{70}-OS or C_{70}-EC, both in toluene, was spread over the first layer. The $Ru(phen)_3$-PAN mixture was prepared by mixing $Ru(phen)_3$ (2 mg) and PAN (100 mg) in DMF (1.9 g) and stirring for 20 min at 50 ºC. The

mixture was spread as 120-µm-thick films (using a coater from RK Print-Coat Instruments Ltd., www.rkprint.com) onto a 125-µm polyester foil from Goodfellow (www.goodfellow.com). The solvent was allowed to evaporate to yield a layer of around 6 µm thickness. The C_{70}-OS layer was prepared by dissolving C_{70} (1 mg) and OS (100 mg) in toluene (0.9 g) and stirring at room temperature for 15 min. C_{70}-EC was obtained by dissolving C_{70} (1 mg) and EC (100 mg) in toluene (1.9 g), and the solution was ultrasonicated and heated at 40 ºC for 15 min. Both solutions were spread as 120-µm-thick films onto a 125-µm polyester foil to yield dry layers of around 12 µm (C_{70}-OS) and 6 µm (C_{70}-EC) thicknesses. The reflective layer was prepared by dissolving 1 g of one-component silicone RS692-542 and 0.3 g of TiO_2 in 0.7 g of hexane, and after 30 min stirring, it was knife-coated as 120-µm-thick films onto the 125-µm polyester foil and left for curing overnight.

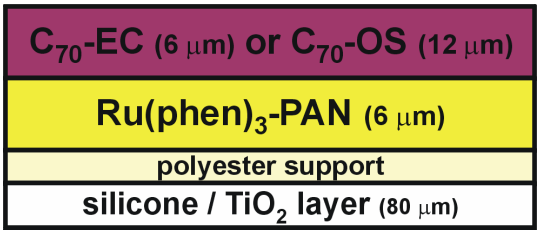

Fig. 3.1. Cross-section of the sensor layers for simultaneous optical sensing and imaging of oxygen and temperature. The luminescence of the compounds is excited from above, and emission is also collected there. The TiO_2 reflective layer acts as a scattering area to increase the intensity of the luminescence collected above.

Spectral characterization: Absorption and emission spectra were recorded on a Lambda 14 P UV-Vis spectrophotometer (www.perkinelmer.com) and Aminco AB 2 luminescence spectrometer (www.thermo.com) respectively.

Sensor calibration: The optical setup was identical to that in earlier studies.[18,22c] Briefly, The fluorescence of both dyes was excited using four 5 W 470 nm LEDs (Lumileds, www.lumileds.com) using PCX 18 x 18 MgF_2 TS lenses from Edmund Optics (www.edmundoptics.com). A strip of the sensing layer (approx. 4 x 2 cm) was placed in a custom-made calibration chamber. The preset gas composition was mixed by two PR 4000 pressure controllers from MKS Instruments (www.mks-instruments.com), which delivered a constant flow of the predetermined ratio of pure nitrogen and oxygen to the chamber at a total pressure of 0.8 bar. All measurements were carried out at ambient pressure. The temperature in the chamber was adjusted by a Lauda E-100 thermostat (www.lauda.de). The emission was recorded by an Imagex TGi gated CCD camera and software system from Photonic Research Systems (www.prsbio.com).

Excitation and emission detection of the luminescent compounds are detected from top. To increase the collection of exciting and the emitted light (backscatter luminescence), a reflective layer of TiO_2-silicone rubber composition was placed at the bottom of the sensor layer. Excitation light was filtered through an FITCA filter (Schott, www.schott.de). Emission was recorded through a Chroma 680 filter for the fullerene and a Chroma 580 filter for the Ru complex, both filters having a full width at half maximum (FWHM) of around 60 nm (AHF Analysentechnik, www.ahf.de). For calculation of luminescence lifetimes, the rapid lifetime determination (RLD) method was used.[26] Following a square-shaped light pulse, luminescence was detected quantitatively in two different gates. The first gate (G_1) was only opened after a delay period after switching off the LEDs. This enables short-lived background fluorescence almost quantitatively to be surpressed. Potential interferences caused by backscattered excitation light are also eliminated in this manner. The second gate (G_2) is opened immediately after the closure of G_1. In the case of $Ru(phen)_3$ the gates started 250 ns and 1250 ns after switching off the LEDs, they were 1 µs long each, and the LED was turned

on for 4 μs with a repetition rate of 100 kHz. For C_{70}, the gates started 100 μs and 5100 μs after switching off the LEDs, they were 5 ms long each, and the LED was turned on for 30 ms with a repetition rate of 10 Hz. The ratio G_1/G_2 is virtually independent of the overall signal intensity. Assuming a constant aperture time for each gate, the average decay time τ of each pixel can be calculated as $\tau = \Delta t / \ln(G_1 / G_2)$ where Δt is the integration time and G_1 and G_2 are the areas of each gate.

3.3. Results and Discussion

3.3.1. Composition of the dual sensors

The material contains two sensor layers, each with the luminescent probe dispersed in a polymer matrix, thus allowing simultaneous determination of oxygen partial pressure and temperature. The accurate sensing of oxygen and temperature is often affected by the mutual cross-sensitivities of the indicators, which have to be minimized. The cross-sensitivities can result from several effects: (i) overlap of the luminescence signals from both probes; (ii) temperature dependence of the lifetime and quenching kinetics of the oxygen probe; or (iii) quenching of the temperature probe by oxygen. To avoid the cross-sensitivities and to achieve optimal sensitivities, both probes and polymers must be carefully chosen.

The luminescences of ruthenium(II) polypyridyl complexes exhibit a strong temperature dependence.[20a] In particular, ruthenium(II) tris(phenanthroline) ($Ru(phen)_3$) is a common optical temperature probe that displays efficient temperature quenching and therefore high sensitivity.[24] Some $Ru(phen)_3$ complexes are commercially available and can be easily incorporated into solid matrices, such as sol–gels or polymers.[27] The photostability

of these complexes is rather high in the absence of oxygen, and they can be excited in the visible region, displaying a large Stokes shift with an emission centered at around 580 nm and a luminescence lifetime of several microseconds.[24] The luminescence of Ru(II) polypyridyl complexes is quenched by oxygen. In order to avoid this interference when sensing temperature, the $Ru(phen)_3$ complex was immobilized in poly(acrylonitrile) (PAN). The extremely low gas permeability of PAN ($P = 1.5 * 10^{-17}$ cm^2 Pa s^{-1})[23] in essence eliminates quenching by oxygen.

Fullerene C_{70} displays the TADF effect. In fact, there are two distinct unimolecular mechanisms for its fluorescence: prompt fluorescence (PF) and thermally activated delayed fluorescence (TADF).[28] In the PF mechanism, emission occurs after $S_n \leftarrow S_0$ absorption and excited state relaxation to S_1. The TADF mechanism takes place via the triplet manifold: after excitation to the S_1 state, intersystem crossing (ISC) to the triplet manifold (T_1 or a higher triplet) occurs, followed by a second ISC from T_1 back to S_1, and by fluorescence emission. The cycle $S_1 \rightarrow T_1 \rightarrow S_1$ may be repeated a number of times before fluorescence finally takes place.[29] TADF is significant only if both the quantum yield of triplet formation (Φ_T) and the quantum yield of singlet formation (Φ_S) are high.[22a] This in turn implies a small energy gap between S_1 and T_1 (ΔE_{ST}), a long T_1 lifetime, and temperature high enough for this process to take place.[22a] For most fluorophores, TADF is usually much weaker than is PF. Although known for many years, TADF continues to be a rare phenomenon, with a few observations in some xanthene dyes,[28b,30] aromatic ketones[31] and thiones,[32] metal porphyrins,[33] imidazole derivative[34] and aromatic hydrocarbons.[35]

The photophysical properties of fullerene C_{70} are remarkable in that the Φ_T is very close to one,[36] the ΔE_{ST} gap[37] is small, and the long intrinsic phosphorescence lifetime.[38] Such properties are required for the exceptionally strong TADF[22a] found in this molecule. C_{60}[39] and

some C_{60} derivatives,[40] as well as 1,2-$C_{70}H_2$,[41] also exhibit TADF, but weaker than that of C_{70}.

The outstanding TADF effect displayed by C_{70} with a maximum increase in quantum yield of by a factor ca. 100 times compared to PF, and the fact that TADF lifetimes fall in the ms range,[22c] are most useful features for the development of a trace oxygen sensor, because the longer the molecule resides in the triplet state the more efficient is the interaction with (triplet) oxygen. On the other hand only the unique TADF effect, based on a cycling of the molecule between singlet and a triplet excited states ensures that the molecule still has a quantum yield high enough to be practically useful.

3.3.2. Luminescence spectra

The absorption and emission of the luminescent compounds, the spectral data of the filters and the spectrum of the light source emission are shown in Figure 3.2. The $Ru(phen)_3$ complex and C_{70} in the polymer support exhibit similar absorption maxima in the visible. This is an advantage for the instrumental setup, as only a single excitation source is required to excite both probes. The excitation source used was a blue LED with a 470 nm peak wavelength. The emission spectra of the two compounds are quite different. While $Ru(phen)_3$ has an emission maximum around 580 nm, C_{70} shows its maximum in the region 670-700 nm. The luminescence signals are separated by appropriate emission filters, and the red part of the $Ru(phen)_3$ emission, which partially overlaps the emission window of C_{70}, was suppressed by using time-gated detection at a delay of 1ms after the end of the light pulse, where the emission of the Ru-complex has already decayed below measurable levels. The two layer

material described has the advantage of suppressing resonance energy transfer from $Ru(phen)_3$ to C_{70}, as a result of their spatial separation.

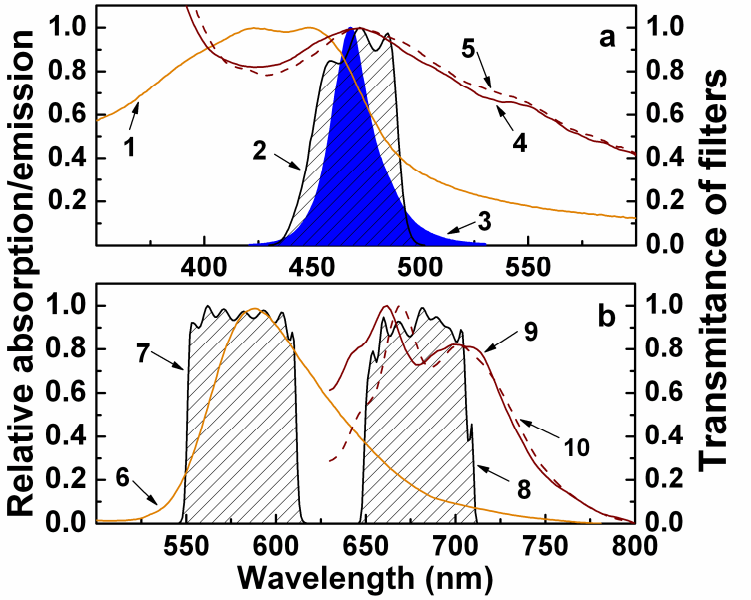

Fig. 3.2. Spectra of the materials and components used in the dual sensor system: (1) absorption of $Ru(phen)_3$ in PAN; (2) transmittance of the interference filter FITCA; (3) emission of the light source (LED 470); (4), (5) absorption of C_{70} (in EC and OS, respectively); (6) fluorescence of $Ru(phen)_3$ in PAN; (7) ,8) transmittance of the emission interference filters (Chroma 580 and Chroma 680, respectively); (9), (10) fluorescence of C_{70} (in EC and OS, respectively).

3.3.3. Calibration of the dual sensors

The calibration of the sensor was performed by time-domain fluorescence lifetime imaging,[42] with the determination of the lifetime of the indicators at several oxygen concentrations and temperatures, using the rapid lifetime determination (RLD) method.[26] The use of decay time is advantageous when compared to intensity-based methods in that interferences from drifts of the sensor and the optoelectonic system are minimized because lifetime is independent of the local dye concentration, turbidity of the sample, and scattering effects. The signal change caused by photobleaching is also usually much less significant when measuring lifetime rather than intensity. The RLD decay time sensing method enables the separation of the fluorescence signals from $Ru(phen)_3$ and C_{70} with relatively simple instrumentation.

The lifetimes of both layers were determined at different oxygen concentrations (0 to 50 ppmv in nitrogen at atmospheric pressure) and temperatures (0 to 120 ºC). The calibration plots for the temperature sensitive system ($Ru(phen)_3$-PAN) in the dual sensor are presented in Figure 3.3. The decay times are unaffected by increasing oxygen concentration (Figure 3.3a). In fact, when changing the oxygen concentration between 0 and 50 ppmv, all lifetimes are within 0.31% deviation for all temperatures measured. The PAN film shields oxygen and prevents quenching, and therefore the cross-sensitivity of the temperature indicator to oxygen is absent in our case.

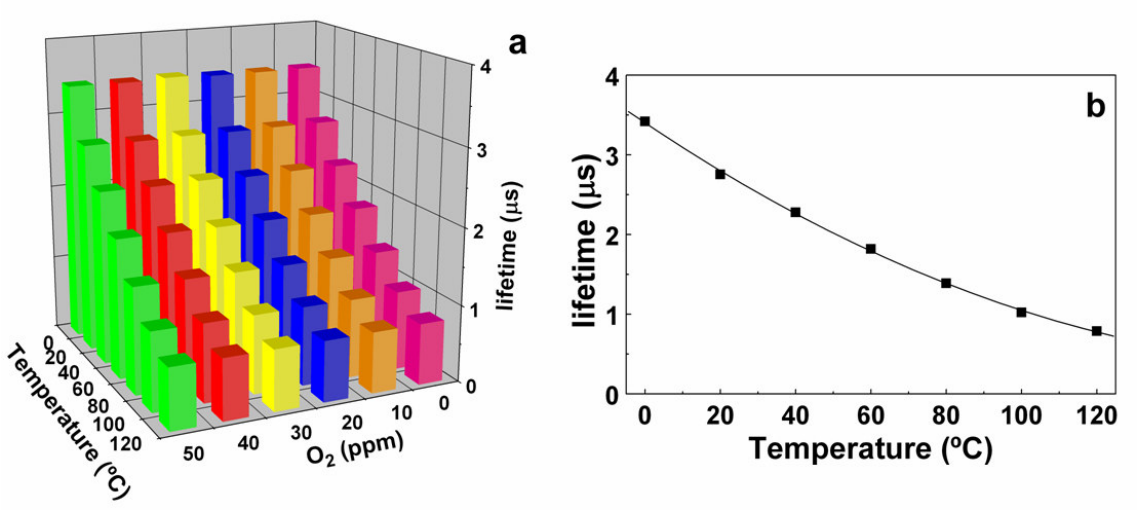

Fig. 3.3. Ru(phen)$_3$-PAN / C_{70}-EC dual sensor: (a) calibration plot for the temperature system Ru(phen)$_3$-PAN, and (b) temperature dependence of the average lifetimes of Ru(phen)$_3$-PAN shown as black squares with the solid line corresponding to the nonlinear fit. Oxygen concentrations are from 0 to 50 ppmv in nitrogen at atmospheric pressure.

The decay time of Ru(phen)$_3$-PAN is highly temperature dependent, decreasing with a temperature increase, as can be seen from Figure 3.3b. This dependence is attributed to a thermally activated nonradiative decay channel.[20a] The temperature dependence of the lifetime is well described by the following empirical equation (Fig. 3.3b) with τ in µs and T in ºC.

$$\tau = 8.2 * 10^{-5} * T^2 - 0.0318 * T + 3.4005 \qquad \text{(Eq. 3.1)}$$

For each temperature, the standard deviation of the average lifetime of the Ru(phen)$_3$-PAN system at several oxygen concentrations is lower than 9 ns. The lifetime of the Ru(phen)$_3$-PAN system is independent of oxygen concentration, so that one can use the measured lifetime to determine the temperature at any fraction (or partial pressure) of oxygen.

The RLD method was used to image the temperature dependence of the $Ru(phen)_3$ PAN system, allowing to determine the temperature at any point on the sensor's surface. Figure 3.4a shows the temperature dependence of the $Ru(phen)_3$ lifetime at different oxygen concentrations in pseudo-color code. The results allow the construction of the calibration plot shown in Figure 3.3a. The image profile displayed by the $Ru(phen)_3$-PAN layer is rather homogeneous at all temperatures.

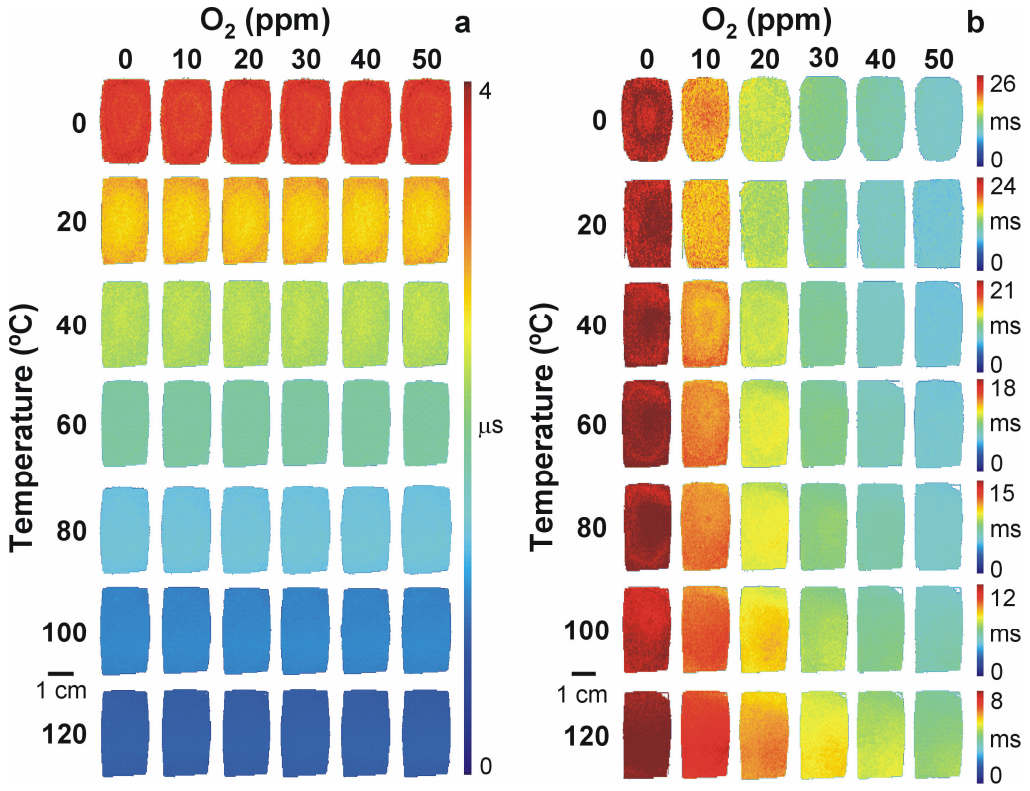

Fig. 3.4. Pseudocolored fluorescence lifetime images of $Ru(phen)_3$-PAN (a) and C_{70}-EC (b) in the double sensor $Ru(phen)_3$-PAN / C_{70}-EC, between 0 and 120 ºC and O_2 concentrations from 0 to 50 ppmv in nitrogen at atmospheric pressure.

The calibration plot for the oxygen sensitive system (C_{70}-EC) in the dual sensor was acquired by variation of the oxygen content in the flow cell from 0 to 50 ppm and is presented in Figure 3.5a. The lifetimes are highly temperature and oxygen dependent, as can be seen. In

the absence of oxygen, fluorescence lifetime (τ_0) is 25.1 ms at 0 °C and drops to 8.0 ms at 120 °C. The lifetime, as well as the sensitivity towards oxygen, decreases at elevated temperatures (Fig. 3.5b), because oxygen has less time to interact with C_{70}. However, because the lifetime is still much higher than those of common probes (which show the same effect, just on faster time scales) the sensitivity to oxygen is still very high at 120 °C and most likely at even higher temperatures. This effect is also compensated for, to some extent, by the higher collisional rate with oxygen at higher temperatures.[18] Because of the equilibrium of the singlet and triplet excited states, this lifetime decrease can be interpreted as a continuous decrease from the initial 49 ms phosphorescence lifetime at cryogenic temperatures.[22a]

Pseudo-color lifetime images of the oxygen sensitive probe in the dual sensor are shown in Figure 3.4b. The oxygen dependence of the C_{70} lifetime results in the calibration plot in Figure 3.5. The image profile displayed by the C_{70}-EC layer also is rather homogeneous.

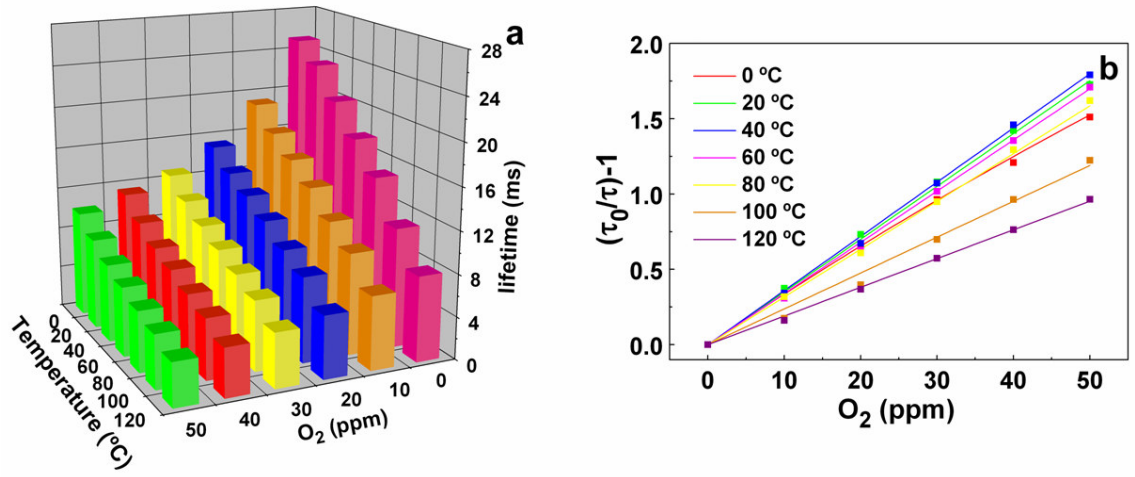

Fig. 3.5. $Ru(phen)_3$-PAN / C_{70}-EC dual sensor: a) calibration plot for the oxygen sensor C_{70}-EC, and b) lifetime-based Stern-Volmer plots at various temperatures for the oxygen sensor C_{70}-EC. O_2 concentrations from 0 to 50 ppmv in nitrogen at atmospheric pressure.

The quenching by oxygen is highly efficient for all temperatures, with the lifetime of C_{70} decreasing by 50 to 60% when the concentration of O_2 increases from 0 to 50 ppmv. As an example, the lifetime of C_{70} at 0 ºC decreases from 25.1 ms to 10.0 ms, and at 120 ºC from 8.0 ms to 4.1 ms. The Stern-Volmer plot ($[\tau_0/\tau\text{-}1]$ versus $[O_2]$) for quenching of C_{70} is presented in Figure 5b. The two-site model was used to fit the data.[43] It is an extension of the standard Stern-Volmer model and formally assigns the sensor molecules to two different microenvironments within the polymer, with dissimilar oxygen permeability. It is a very viable method to account for the non-ideal quenching behaviour found in many systems. Therefore, the quenching constants are different for these regions. The two-site model Stern-Volmer equation was used in the lifetime form reads

$$\frac{I}{I_0} = \frac{\tau}{\tau_0} = \frac{f_1}{1 + K_{SV}^1 [O_2]} + \frac{f_2}{1 + K_{SV}^2 [O_2]} \qquad \text{(Eq. 3.2)}$$

where K_{SV}^1 and K_{SV}^2 are the Stern-Volmer constants for each component, and f_1 and f_2 are the fractions of the total emission for each component, respectively (with $f_1 + f_2 = 1$).

The two-site model fits the experimental data very well (Fig. 3.5b), in that r^2 in all cases is better than 0.998. Table 3.1 compiles the Stern-Volmer constants extracted from the fitting along with the detection limits. These are a function of temperature.

The C_{70}-EC system exhibits an almost ideal ("one-site") behavior, with f_1 practically equal to unity (except for 0 ºC), meaning that EC is highly homogeneous with respect to oxygen diffusion. The limits of detection (LODs) are defined at the level at which 1% quenching occurs. The C_{70}-EC system displays LODs in the ppbv range (between 280 and 530 ppbv). As far as we know, this is one of the lowest LODs ever reported for gas phase oxygen sensors.[5]

Table 3.1. Stern-Volmer constants and detection limits for oxygen sensing using fullerene C_{70} in ethylcellulose or organosilica at various temperatures.

	C_{70}-EC		**C_{70}-OS**	
Temperature [ºC]	K_{SV}^{1} [a] **[mg (O_2)/L]**	**LOD[b,c] [µg (O_2)/L]**	K_{SV}^{1} [a] **[mg (O_2)/L]**	**LOD[b,c] [µg (O_2)/L]**
0	29.9 (0.93)	0.36 (0.29)	33.0 (0.88)	0.34 (0.27)
20	28.3 (1)	0.36 (0.29)	28.1 (0.94)	0.38 (0.31)
40	29.0 (1)	0.35 (0.28)	29.4 (0.95)	0.36 (0.29)
60	27.4 (1)	0.37 (0.28)	26.4 (0.99)	0.40 (0.33)
80	25.6 (1)	0.39 (0.32)	26.9 (0.93)	0.42 (0.34)
100	19.2 (1)	0.53 (0.42)	19.5 (1)	0.52 (0.42)
120	15.4 (1)	0.66 (0.53)	14.8 (1)	0.68 (0.55)

[a] in brackets, f_1 from the "two-site" quenching model, [b] at 1% quenching (τ/τ_0=0.99),[c] in brackets, the detection limits in ppmv of O_2. 1 µg of O_2 per liter corresponds to a concentration of 31.25 nmolL^{-1} or 807 ppbv at atmospheric pressure.

A second dual sensor material was evaluated for simultaneous sensing of oxygen and temperature. In this material, OS was used as the polymer for the oxygen system. The Ru(phen)$_3$-PAN / C_{70}-OS material was calibrated for temperatures between 0 and 120 ºC and oxygen concentrations from 0 to 50 ppmv in nitrogen at atmospheric pressure.[44] The temperature sensor is the same as the previous dual sensor material, and display identical behavior. The oxygen sensor is almost equally sensitive towards oxygen, with LODs in the ppbv range (see Table 1). The lifetime images of both systems are shown in Fig. 3.6. The C_{70}-OS system exhibit a high homogeneity over the entire range of conditions studied, favored by the high thermal stability of the silica-based materials.

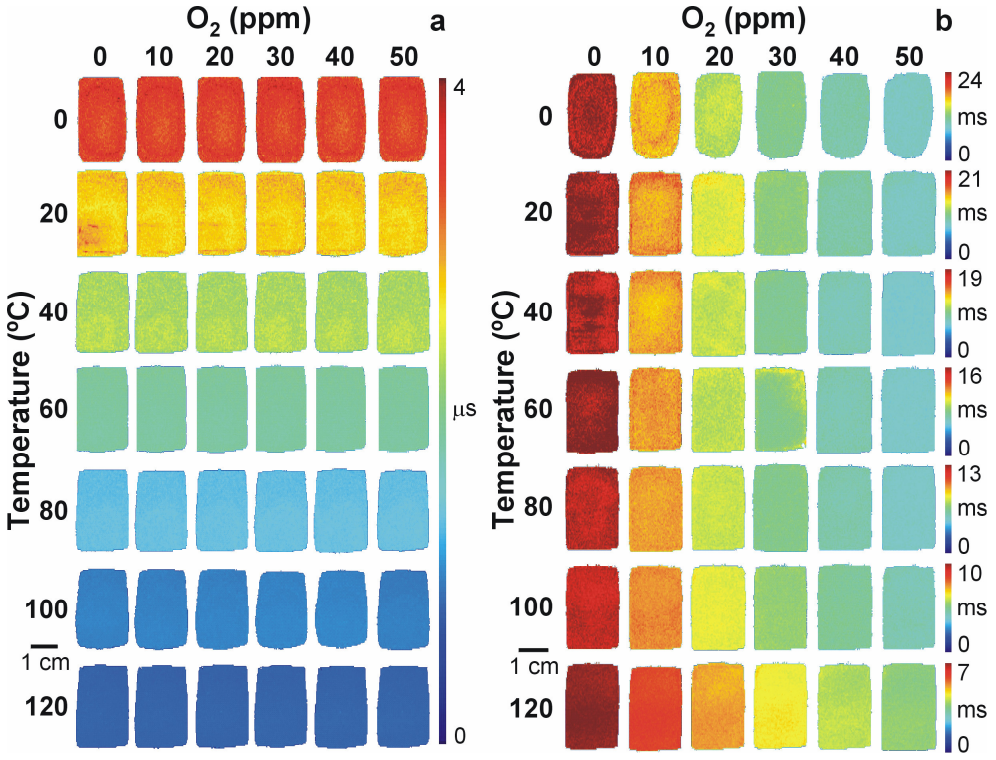

Fig. 3.6. Pseudo-colored fluorescence lifetime images of (a) Ru(phen)$_3$-PAN and (b) C_{70}-OS in the dual sensor Ru(phen)$_3$-PAN / C_{70}-OS, between 0 and 120 ºC and oxygen concentrations from 0 to 50 ppmv in nitrogen at atmospheric pressure.

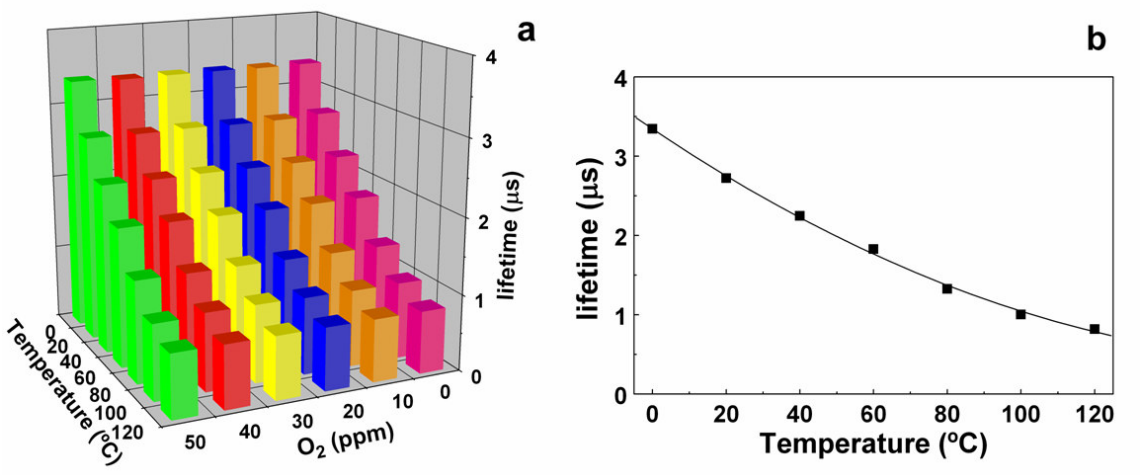

Fig. 3.7. Ru(phen)$_3$-PAN / C_{70}-OS dual sensor: a) calibration plot for the temperature sensor Ru(phen)$_3$-PAN, and b) temperature dependence of the average lifetimes of Ru(phen)$_3$-PAN shown as black squares with the solid line corresponding to the nonlinear fit to the data. O_2 concentrations from 0 to 50 ppmv in nitrogen at atmospheric pressure.

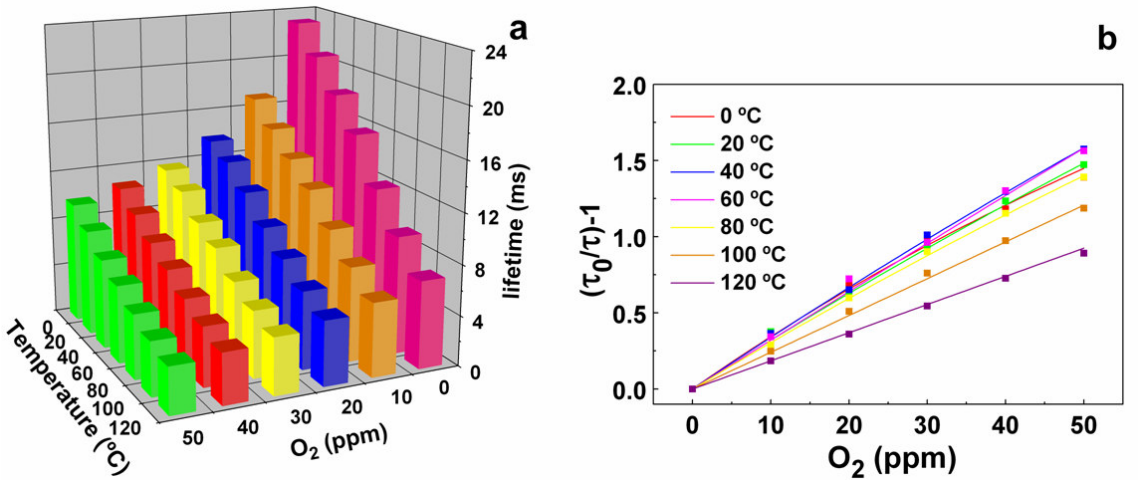

Fig. 3.8. Ru(phen)$_3$-PAN / C_{70}-OS dual sensor: a) calibration plot for the oxygen sensor C_{70}-OS, and b) lifetime-based Stern-Volmer plot at various temperatures for the oxygen sensor C_{70}-OS. O_2 concentrations from 0 to 50 ppmv in nitrogen at atmospheric pressure.

3.3.4. Response times of the dual sensors to oxygen

The response times to oxygen for both dual sensors were evaluated (Fig. 3.9 and 3.10). The plots are based on time-resolved fluorescence intensity, because of the possibility of faster data acquisition when using only a single gate instead of two for the lifetime data. With our experimental setup, we could acquire data each 2 s. The time-resolved fluorescence intensity drops by more than 50% on both systems (OS - 50% and EC - 60%) when going from pure nitrogen to 50 ppmv of oxygen in nitrogen (Fig. 3.9). The time for 95% of the total signal change to occur (t_{95}) is less than 2 s for the transition from pure nitrogen to 50 ppmv in both polymers, and most likely is limited by the time it takes for the gas to migrate from the mixing device to the flow chamber. The response can be regarded as practically instantaneous as would be expected for these highly permeable polymers. The response in the reverse direction is somewhat slower, as it takes more time for the nitrogen to replace all the oxygen left in the polymer, and is approx. 6 s (t_{95}) for both polymers.

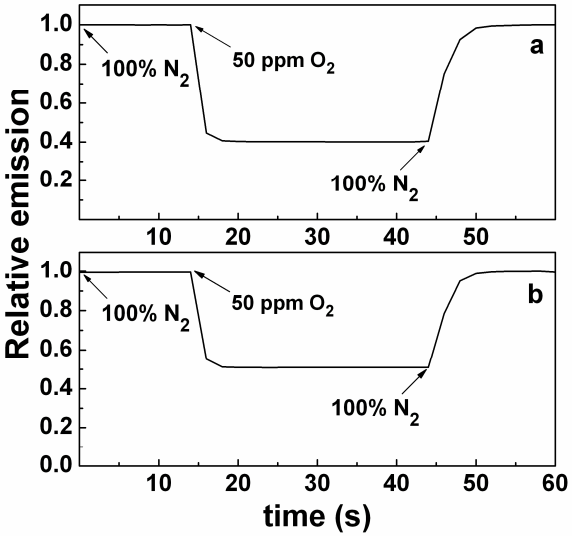

Fig. 3.9. Fluorescence intensity response time plots for a) C_{70}-EC and b) C_{70}-OS, at 20 ºC and for O_2 concentrations between 0 and 50 ppmv in nitrogen at atmospheric pressure.

The response time was also assessed when the concentration of oxygen changes from 0% to that of air. The corresponding plots are shown in Fig. 3.10, and the data was acquired every 10 s. The t_{95} for the reverse transition (air to pure nitrogen) was very slow (OS - 16 min and EC - 18 min). The C_{70}-OS sensor displays a lower t_{95} possibly because of its high porosity. The sensor is appropriate for trace oxygen concentrations, and when is flooded with approx. 20% of oxygen, the time to remove all oxygen from the system is substantial as can be seen from Fig. 3.10.

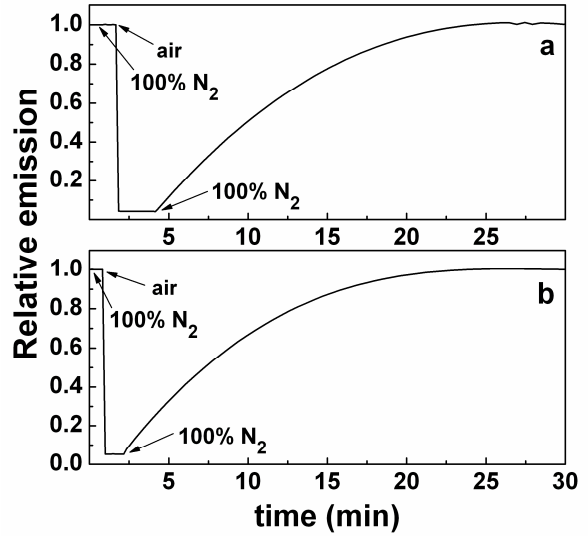

Fig. 3.10. Fluorescence intensity response time plots for a) C_{70}-EC and b) C_{70}-OS, at 20 ºC and for O_2 concentrations between 0 % in nitrogen and air at atmospheric pressure.

The materials exhibit full reversibility and the response time for oxygen variation in the low ppmv domain is extremely fast. The response of the materials is fully reversible many hundred times. The photostability is also high, no change in the fluorescence lifetimes being observed after several hours of continuous irradiation.

3.3.5. Derivation and validation of a bivariate calibration function for all temperatures and oxygen concentrations covered.

Here, we aimed to construct a relatively simple semiempirical calibration function which allows calculating the oxygen concentration at any temperature within the calibration range, rather than just the temperatures, where the calibration was performed. The temperature dependence, thermal stability and photostability, response times and sensitivity towards oxygen are very similar for both materials presented previously. However, the $Ru(phen)_3$-

PAN / C_{70}-EC dual sensor material was selected because of its almost linear ("one-site" behavior) Stern-Volmer fits (see Table 3.1). Thus, we assume only one Stern-Volmer constant in the subsequent calculations. The Stern-Volmer equation with one constant reads

$$\frac{\tau_0}{\tau_{(T)}} = 1 + K_{SV} \times [O_2] = 1 + k_{q(T)} \times \tau_{0(T)} \times [O_2] \qquad \text{(Eq. 3.3)}$$

where the τ_0 is the lifetime in the absence of oxygen, τ is the lifetime in the presence of a predetermined concentration of oxygen, and k_q is the quenching constant. It can be rearranged to give

$$[O_2] = \frac{\frac{1}{\tau_{(T)}} - \frac{1}{\tau_{0(T)}}}{k_{q(T)}} \qquad \text{(Eq. 3.4)}$$

and hence to compute the oxygen concentration. However, it is first necessary to determine τ_0 and k_q, which are temperature dependent. Fig. 3.11 shows the temperature dependence of τ_0 and k_q, and the nonlinear and linear fits to the data, respectively.

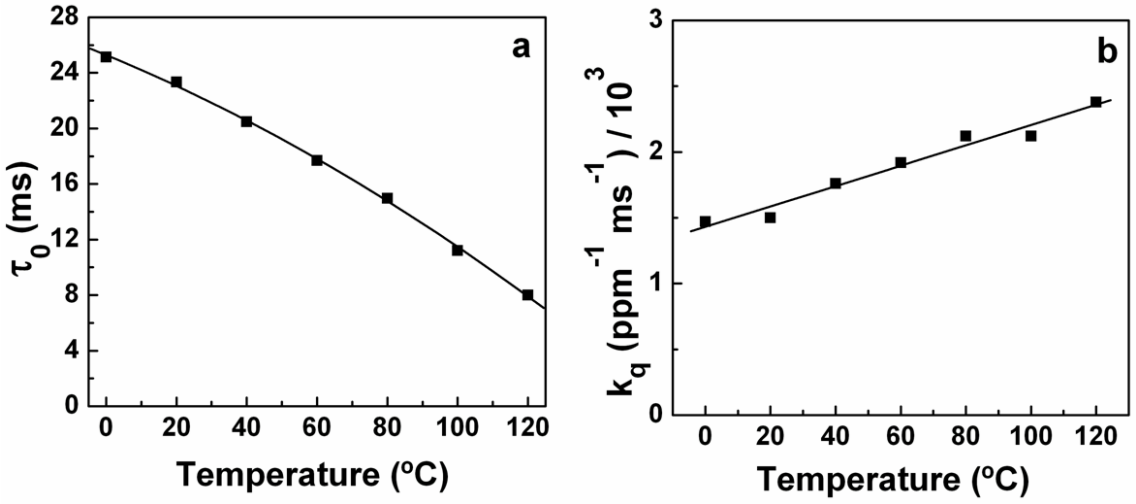

Fig. 3.11. Temperature dependence plots of (a) τ_0 and (b) k_q for C_{70}-EC shown as black squares, with the solid lines corresponding to the nonlinear and linear fit to the data, respectively.

By inserting the fits given in Fig. 3.11 into Eq. 3.4, we obtain

$$[O_2] = \frac{\frac{1}{\tau_{(T)}} - \frac{1}{25.3\text{-}0.0104\times T\text{-}3.38\times 10^{-4}\times T^2}}{1.43\times 10^{-3} + 7.71\times 10^{-6}\times T} \qquad \text{(Eq. 3.5)}$$

where T is the temperature in ºC. The temperature is determined from the lifetime of $Ru(phen)_3$-PAN using eq 1, and $\tau(T)$ is the lifetime of the oxygen probe (C_{70}-EC) measured at that same temperature.

The calibration functions were validated by using a set of experimental data points obtained at different temperatures and oxygen concentrations. The calculated values were determined using Eq. 3.1 for temperature and subsequently used in Eq. 3.5 as input for computing the oxygen concentration. Table 3.2 summarizes the experimental and calculated values. In order to check the reproducibility of the system, several measurements were made for each set of points.

Table 3.2. Experimental values from the $Ru(phen)_3$-PAN / C_{70}-EC dual sensor calibration function.

experimental settings		**calculated values**	
T (ºC)	O_2 (ppm) [a]	T (ºC) [b]	O_2 (ppm) [c]
28.0	7.0	28.0 ± 0.4	7.2 ± 0.2
37.0	0.5	36.5 ± 0.4	0.7 ± 0.5
73.0	23.0	73.1 ± 0.1	22.3 ± 1.4

[a] O_2 concentrations in nitrogen at atmospheric pressure,

[b] Calculated using Eq. 3.1, [c] Calculated using Eq. 3.5.

The calculated values are in good agreement with the experimental settings. Lifetime images were recorded for both systems, and are presented in Fig. 3.12. The images are in agreement with the results obtained from the calibration (see Fig. 3.3 and 3.5). For even higher accuracy, the calibration can of course be extended including more temperatures, and the calibration function for oxygen can be extended to account for the deviations from linearity in the oxygen sensor. However, we have shown that it is possible to obtain relatively accurate results using the procedure described above (Table 3.2).

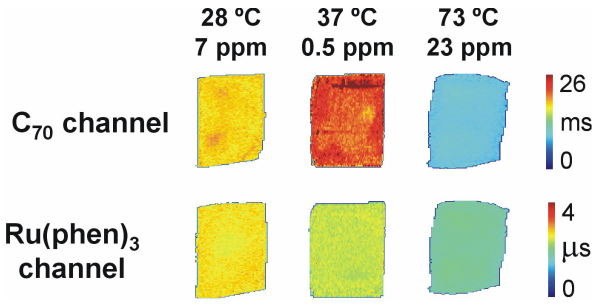

Fig. 3.12. Pseudocolored fluorescence lifetime images of the dual sensor Ru(phen)$_3$-PAN / C_{70}-EC, using the experimental points from Table 2.

A comparison between the fluorescence-based oxygen-temperature dual sensors reported so far and ours is presented in Table 3.3. The majority of the materials have common characteristics like a single excitation wavelength, luminescence decay time as the analytical information, an excitation wavelength in the visible region, and a single matrix to disperse both sensors. The materials reported so far use a single polymer to disperse both temperature and oxygen systems, while our materials use two polymers, one for each system. This is a disadvantage for large coatings. However, this strategy has the advantages to physically separate the two probes and therefore to avoid interferences such as energy transfer between the individual probes to a maximum extent. It also allows choosing an optimal environment

for each probe, rather than having to settle on compromise in order to account for the requirements of both probes. But the main distinctions of this dual sensor are the particular temperature and oxygen concentration operation ranges. The materials reported so far display operation temperatures between 0 - 70 ºC and 0 - 20 or 0 - 100% for oxygen concentrations, while our sensor is specifically suited for the determination of trace amounts of oxygen, and covers a very wide temperature range.

Table 3.3. Comparison between the materials used so far for dual sensing of temperature and oxygen.

Temperature probe	**Oxygen probe**	**Polymer**	**λ_{exc} (nm)[a]**	**Signal[b]**	**T range (ºC)**	**O_2 range (%)**	**Ref.**
$La_2O_2S:Eu_3^+$ phosphor	Pt–TFPP	FIB	337	DT , TD	0 - 50	0 - 20	6a
Magnesium fluoro-germanate	Ru–dpp	Sol-gel	470	DT , TD	25 - 65	0 - 100	6b
Eu-β-diketonate complex	Pt–TFPP lactone	FIB	390	DT, I, TD	5 - 45	0 - 20	6c
Ru–phen in PAN microbeads	Pt–TFPP	p-*t*BS-co-TFEM	465	I	10 - 50	0 - 20	6d
Eu complexes in PTBS or PVMK micro-beads	Pd–TFPP in PSAN microbeads	hydrogel for both particles	405	DT, FD	1 - 70	0 - 20	6e
Ru–phen in PAN microbeads	Pd–TFPP in PSAN microbeads	hydrogel for both particles	470 (Ru) 525 (Pd)	DT, FD	1 - 60	0 - 100	6f
$Eu(tta)_3dpbt$ in PVC microbeads	Pt-TFPP in PSAN microbeads	hydrogel for both particles	405	DT, TD	1 -50	1 - 40	6g
Ru–phen in PAN film	C_{70} in OS or EC-49 film	----------	470	DT, TD	0 - 120	0 - 0.005 (0 - 50 ppmv)	this work

[a] For both luminophores, except when mentioned otherwise, [b] Analytical Signal: DT - luminescence decay time; I - luminescence intensity; TD - time domain; FD - frequency domain.

All other optical dual sensors with oxygen sensing capabilities display less sensitivity and cannot be operated at such high temperatures because of their operating mechanism, which is mostly based on phosphorescence quenching. The $Ru(phen)_3$-PAN / C_{70}-EC and $Ru(phen)_3$-PAN / C_{70}-OS sensing materials cover a higher range of temperatures (between 0 and 120 ºC), and allow the measurement of oxygen concentrations between 0 and 50 ppmv with LODs in the ppbv range (see Table 3.1).

3.4. Conclusion

A dual sensor is presented for simultaneous sensing of temperature and oxygen, operating over a range of more than 100 °C, and specifically suited for detection of trace oxygen. The sensor takes advantage of the high temperature dependence of a Ru polypyridyl complex and of the strong thermally activated delayed fluorescence exhibited by fullerene C_{70} and its high sensitivity towards O_2. The luminescent compounds were incorporated in two polymers and can be excited at the same wavelength. The materials are photostable and display good storage stability. The signal of the temperature probe is independent of oxygen. The oxygen sensor exhibits sensitivities in the ppbv range, the highest ever reported. The response time of the oxygen sensor within the concentration range used is less than two seconds. A bivariate calibration function for the dual sensor was developed and validated, using a model that takes into account the effect of temperature on the oxygen sensor. The materials may find applications in areas as diverse as anaerobic (micro)biotechnological procedures, aerospace research, factory security and in the food packaging industry.

3.5. References

[1] I. Bergman, *Nature* **1968**, *218*, 396.

[2] (a) O. S. Wolfbeis, in Optical *Sensors for Industrial, Environmental and Clinical Application*s; R. Narayanaswamy, O. S. Wolfbeis, Eds; Springer: Berlin, 2004; pp 1-34. (b) O. S. Wolfbeis, *Anal. Chem.* **2006**, *78*, 3859-3874 and previous biannual reviews.

[3] (a) O. S. Wolfbeis, B. M. Weidgans pp. 17-44. (b) G. Orellana, pp. 99-116 in *Optical Chemical Sensors*, F. Baldini, A. N. Chester, J. Homola, S. Martellucci, Eds; Springer: Dordrecht, **2006**.

[4] S. Nagl, O. S. Wolfbeis, *Analyst* **2007**, *132*, 507-511.

[5] (a) O. S. Wolfbeis, L. J. Weis, M. J. P. Leiner, W. E. Ziegler, *Anal. Chem.* **1988**, *60*, 2028–2030. (b) S. M. Borisov, C. Krause, S. Arain, O. S. Wolfbeis, *Adv. Mater.* **2006**, *18*, 1511–1516. (c) S. M. Borisov, G. Neurauter, C. Schroeder, I. Klimant, O. S. Wolfbeis, *Appl. Spectrosc.* **2006**, *60*, 1167–1173. (d) C. R. Schroeder, G. Neurauter, I. Klimant, *Microchim. Acta* **2007**, *158*, 205-218.

[6] (a) L. M. Coyle, M. Gouterman, *Sens. Actuators B* **1999**, *61*, 92–99. (b) J. Hradil, C. Davis, K. Mongey, C. McDonagh, B. D. MacCraith, *Meas. Sci. Technol.* **2002**, *13*, 1552–1557. (c) B. Zelelow, G. E. Khalil, G. Phelan, B. Carlson, M. Gouterman, J. B. Callis, L. R. Dalton, *Sens. Actuators B* **2003**, *96*, 304–314. (d) M. E. Köse, B. F. Carroll, K. S. Schanze, *Langmuir* **2005**, *21*, 9121–9129. (e) S. M. Borisov, O. S. Wolfbeis, *Anal. Chem.* **2006**, *78*, 5094–5101. (f) S. M. Borisov, A. S. Vasylevska, C.

Krause, O. S. Wolfbeis, *Adv. Funct. Mater.* **2006**, *16*, 1536–1542. (g) M. I. J. Stich, S. Nagl, O. S. Wolfbeis, U. Henne, M. Schaeferling, *Adv. Funct. Mater.* **2008**, in press.

[7] (a) G. S. Vasylevska, S. M. Borisov, C. Krause, O. S. Wolfbeis, *Chem. Mater.* **2006**, *18*, 4609–4616. (b) C. R. Schröder, L. Polerecky, I. Klimant, *Anal. Chem.* **2007**, *79*, 60–70. (c) A. S. Kocincová, S. Nagl, S. Arain, C. Krause, S. M. Borisov, M. Arnold, O. S. Wolfbeis, *Biotechnol. Bioeng.* **2008**, in press.

[8] (a) *Pressure and Temperature Sensitive Paints*; T. Liu, J. P. Sullivan, Eds; Springer: New York, **2005**. (b) Y. Takeuchi, Y. Amao, pp. 303-322 in *Frontiers in Chemical Sensors*; G. Orellana, M. C. Moreno-Bondi, Eds; Springer: Berlin, **2005**.

[9] K. Mitsuo, K. Asai, A. Takahashi, H. Mizushima, *Meas. Sci. Technol.* **2006**, *17*, 1282-1291.

[10] (a) K. Kontis, *Aeronaut. J.* **2007**, *111*, 102 495-508. (b) J. W. Holmes, *Aeronaut. J.* **1998**, *102*, 189–194.

[11] (a) N. Church, *Trends Food Sci. Tech.* **1994**, *5*, 345-352. (b) A. Mills, *Chem. Soc. Rev.* **2005**, *34*, 1003-1011. (c) J. M. Valverde, F. Guillen, D. Martinez-Romero, S. Castillo, M. Serrano, D. Valero, *J. Agric. Food Chem.* **2005**, *53*, 7458-7464.

[12] (a) D. B. Papkovsky, N. Papkovskaia, A. Smyth, J. Kerry, V. I. Ogurtsov, *Anal. Lett.* **2000**, *33*, 1755-1777. (b) M. Fitzgerald, D. B. Papkovsky, M. Smiddy, J. P. Kerry, C. K. O'Sullivan, D. J. Buckley, G. G. Guilbault, *J. Food Sci.* **2001**, *66*, 105-110. (c) D. B. Papkovsky, M. A. Smiddy. N. Y. Papkovskaia, J. P. Kerry, *J. Food Sci.* **2002**, *67*, 3164-3169. (d) M. Smiddy, M. Fitzgerald, J. P. Kerry, D. B. Papkovsky, C. K. O'Sullivan, G. G.; Guilbault, *Meat Sci.* **2002**, *61*, 285-290.

[13] (a) S. Nakagawa, K. Takai, pp. 55-91. (b) A. Godfroy, A. Postec, N. Raven, pp. 93-108 in *Extremophiles*; F. A. Rainey, A., Oren, Eds; Academic Press: Amsterdam, **2006**.

[14] K. R. Sowers, E. M. J. Watts, pp. 757-782 *Extremophiles*; F. A. Rainey, A., Oren, Eds; Academic Press: Amsterdam, **2006**.

[15] T. de Vrije, A. E. Mars, M. A. W. Budde, M. H. Lai, C. Dijkema, P. de Waard, P. A. M. Claassen, *Appl. Microbiol. Biotechnol.* **2007**, *74*, 1358-1367.

[16] (a) R. Ramamoorthy, P. K. Dutta, S. A. Akbar. *J. Mater. Sci.* **2003**, *38*, 4271-4282. (b) B. A. DeGraff, J. N. Demas, pp. 125-150 in *Reviews in Fluorescence 2005*; C. D. Geddes, J. R. Lakowicz, Eds; Springer: New York, **2005**.

[17] (a) A. Apostolidis, I. Klimant, D. Andrzejewski, O. S. Wolfbeis, *J. Comb. Chem.* **2004**, *6*, 325-331. (b) B. H. Han, I.; Manners, M. A. Winnik, *Chem. Mater.* **2005**, *17*, 3160-3171

[18] S. Nagl, C. Baleizão, S. M. Borisov, M. Schäferling, M. N. Berberan-Santos, O. S. Wolfbeis, *Angew. Chem. Int. Ed.* **2007**, *46*, 2117-2119.

[19] *Fiber Optic Fluorescence Thermometry*; K. T. Grattan, Z. Y., Zhang, Eds; Chapman and Hall: London, **1995**.

[20] (a) J. N. Demas, B. A. DeGraff, *Coor. Chem Rev.* **2001**, *211*, 317-351. (b) N. Chandrasekharan, L. A. Kelly, pp. 21-40 in *Reviews in Fluorescence 2004*; C. D. Geddes J. R. Lakowicz, Eds; Kluwer Academic/Plenum: New York, **2004**. (c) S. Uchiyama, A. P. de Silva, K. Iwau, *J. Chem. Educ.* **2006**, *83*, 720-727.

[21] Y. Amao, I. Okura, *Bull. Chem. Soc. Jpn.* **2002**, *75*, 389-391.

[22] (a) M. N. Berberan-Santos, J. M. M.; Garcia, *J. Am. Chem. Soc.* **1996**, *118*, 9391-9394. (b) C. Baleizão, M. N. Berberan-Santos, *J. Fluoresc.* **2006**, *16*, 215-219. (c) C. Baleizão, S. Nagl, S. M. Borisov, M. Schäferling, O. S. Wolfbeis, M. N. Berberan-Santos, *Chem. Eur. J.* **2007**, *13*, 3643-3651.

[23] J. Brandrup, E. H. Immergut, E. A. Grulke, *Polymer Handbook*, Wiley: New York, **1999**.

[24] G. Liebsch, I. Klimant, O. S. Wolfbeis, *Adv. Mater.* **1999**, *11*, 1296-1299.

[25] G. Brusatin, P. Innocenzi, *J. Sol-Gel Sci. Technol.* **2001**, *22*, 189-204.

[26] G. Liebsch, I. Klimant, B. Frank, G. Holst, O. S. Wolfbeis, *Appl. Spectrosc.* **2000**, *54*, 548-559.

[27] (a) O. S. Wolfbeis, *J. Mater. Chem.* **2006**, *15*, 2657-2669. (b) H. Podbielska, A. Ulatowska-Jarza, G. Müller, H. J. Eichler, pp. 353-385. (c) G. J. Mohr, pp. 297-321 in *Optical Chemical Sensors*; F. Baldini A. N. Chester, J. Homola, S. Martellucci, Eds; Springer: Dordrecht, **2006**. (d) S. M. Borisov et al. pp. 431-463 in *Fluorescence of Supermolecules, Polymers, and Nanosystems*; M. N. Berberan-Santos, Ed; Springer: Berlin, **2008**.

[28] (a) B. Valeur, *Molecular Fluorescence: Principles and Applications*; Wiley, Weinheim, **2002**. (b) C. A. Parker, *Photoluminescence of Solutions;* Elsevier, Amsterdam, 1968.

[29] C. Baleizão, M. N. Berberan-Santos, *J. Chem. Phys.* **2007**, *126*, 204510.

[30] (a) S. K. Lam, D. Lo, *Chem. Phys. Lett.* **1997**, *281*, 35-43. (b) R. Duchowicz, M. L. Ferrer, A. U. Acuña, *Photochem. Photobiol.* **1998**, *68*, 494-501.

[31] (a) M. W. Wolf, K. D. Legg, R. E. Brown, L. A. Singer, J. H. Parks, *J. Am. Chem. Soc.* **1975**, *97*, 4490–4497. (b) A. M. Turek, G. Krishnammorthy, K. Phipps, J. Saltiel, *J. Phys. Chem. A* **2002**, *106*, 6044–6052.

[32] (a) A. Maciejewski, M. Szymanski, R. P. Steer, *J. Phys.Chem.* **1986**, *90*, 6314–6318. (b) H. Eisenberger, B. Nickel, *J. Chem. Soc., Faraday Trans.* **1996**, *92*, 733-740.

[33] S. Yusa, M. Kamachi, Y. Morishima, *Photochem. Photobiol.* **1998**, *67*, 519-525.

[34] S. Park, O. H. Kwon, Y. S. Lee, D. J. Jang, S. Y. Park, *J. Phys. Chem. A* **2007**, *111*, 9649-9653.

[35] (a) J. L. Kropp, W. R. Dawson, *J. Phys. Chem.* **1967**, *71*, 4499–4506. (b) B. Nickel, D. Klemp, *Chem. Phys.* **1993**, *174*, 297–318. (c) B. Nickel, D. Klemp, *Chem. Phys.* **1993**, *174*, 319–330.

[36] J. W. Arbogast, C. S. Foote, *J. Am. Chem. Soc.* **1991**, *113*, 8886–8889.

[37] S. M. Argentine, K. T. Kotz, A. H. Francis, *J. Am. Chem. Soc.* **1995**, *117*, 11762–11767.

[38] M. R. Wasielewski, M. P. O'Neil, K. R. Lykke, M. J. Pellin, D. M. Gruen, *J. Am. Chem. Soc.* **1991**, *113*, 2774–2776.

[39] F. A. Salazar, A. Fedorov, M. N. Berberan-Santos, *Chem. Phys. Lett.* **1997**, *271*, 361–366.

[40] (a) B. Gigante, C. Santos, T. Fonseca, M. J. M. Curto, H. Luftmann, K. Bergander, M. N. Berberan-Santos, *Tetrahedron* **1999**, *55*, 6175–6182. (b) S. M. Anthony, S. M. Bachilo, R. B. Weisman, *J. Phys. Chem. A* **2003**, *107*, 10674–10679.

[41] S. M. Bachilo, A. F. Benedetto, R. B. Weisman, J. R. Nossal, W. E. Billups, *J. Phys. Chem. A*, **2000**, *104*, 11265–11269.

[42] Z. Lin, M. Wu, M. Schäferling, O. S. Wolfbeis, *Angew. Chem. Int. Ed.* **2004**, *43*, 1735-1738.

[43] J. N. Demas, B. A. DeGraff, *Anal. Chem.* **1995**, *67*, 1377-1380.

CHAPTER 4
A METHOD FOR SIMULTANEOUS LUMINESCENCE SENSING AND IMAGING OF TWO SPECIES USING OPTICAL PROBES OF DIFFERENT LUMINESCENCE DECAY TIME

4.1. Introduction

Chemical sensing allows monitoring of concentrations and spatial distributions of molecules over time, either by making use of their intrinsic properties or by probes. Sensing schemes have been developed for a large number of analytes and employing many different detection methods.[1,2] A lot of research has been devoted to optical sensors, with fluorescence often being used for detection, due to its sensitivity, versatility, remote sensing capabilities, low toxicity, and the ability to detect in a spatially resolved manner.[3,4]

Fluorescence can be analyzed with respect to the number of photons (fluorescence intensity), their energy (fluorescence spectra), their temporal (fluorescence lifetime) or spatial (fluorescence anisotropy) distribution. By combining several sources of information, fluorescence-based sensors resolving more than one analyte can be realized as was demonstrated in several different approaches, mostly using a combination of intensity, spectral and lifetime discriminations.[5-12] Particularly useful in this respect proved to be the fluorescence lifetime as analytical parameter. Fluorescence lifetime measurements are not or less affected by many sources of noise in intensity measurements, such as inhomogeneities in the sensor layer, excitation or emission light path, scattering phenomena or photobleaching, and require less calibration due to their inherent self-referencing. Furthermore, when using

probes with a long fluorescence lifetime (here simply referred to as luminescence, covering all kinds of molecular light emission), short-lived fluorescent background can be surpressed in the time domain.

In recent years, there has been a lot of activity in the area of optical dual sensors, that can resolve two analytes at once, and thereby enable spatially resolved multianalyte detection.[13] One method to separate the two signals is via spectral distinction. There are a number of associated disadvantages with this method. As optical spectra are generally rather broad this discrimination is often incomplete, and requires use of a second excitation wavelength. It also makes it impossible to image both analytes at the same time from the same perspective. This is particularly troubling in cases where knowledge of the second analyte is needed in order to correct for the first such as in dual oxygen and temperature sensors, where a temperature correction for the oxygen sensor is generally needed. This is the case in all fluorescence-based oxygen sensors, because their signal depends strongly on temperature. In fact, most sensors regardless of the type show a temperature dependency. Another possible method of discrimination is with respect to the fluorescence lifetime. This appears promising, as due to the exponential decay of the fluorophores, a lifetime-based separation can be much more complete than a spectral one. Just as only two gates are needed for a calculation of the average fluorescence lifetime in the RLD method, only four gates are needed to obtain the parameters of a double exponential decay.[14]

Unfortunately, in practice the measurements are complicated by the fact that fluorescence decays within sensor matrices are hardly ever single exponential in the absence of a quencher, and even less so in the presence of a bimolecular quencher such as oxygen. One method of lifetime-based discrimination of an oxygen and temperature sensor has been shown that makes use of fluorophores with lifetimes that differ by several orders of

magnitude.[15] At such a lifetime difference, the background of the long-lived species in the detection window of the short-lived fluorophore is negligible. Although this approach seems attractive at first, there is a severe backdraw in this method, which is because the radiative rate of the long-lived species is several orders of magnitude smaller, so is the analytical signal (the collected photons), and therefore the signal-to-noise ratio. In order to collect good quality images resolving both analytes, lifetimes should be at a similar time scale but it should still be possible to decipher individual analytes in the time domain.

4.2. Results and Discussion

4.2.1. Experimental design

In order to understand the analytical signals that can be obtained from a time-domain fluorescence lifetime measurement it appears worthwhile to take a closer look first as to what introducing time resolution into a fluorescence intensity measurement can achieve. Although this separation is not strict, in principle, time-domain fluorescence lifetime methods can be categorized into two different groups, counting methods and gating methods. These are not based on separate methodologies, in fact, they can be regarded as mutual extremes of each other. (Fig. 4.1).

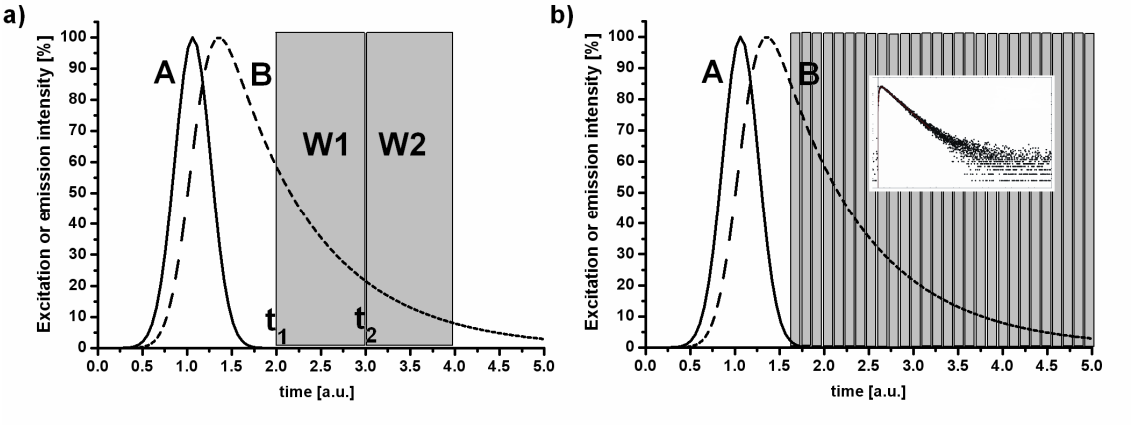

Fig. 4.1. a) The rapid lifetime determination (RLD) scheme, based on calculation of the lifetime from two time gates. b) A counting scheme based on many gates. The fluorescence lifetime is calculated from the decay curve. Solid lines A are an example excitation pulse, dashed lines B are simulated single exponential fluorescence decays with a lifetime of one time unit.

The average fluorescence lifetime can be calculated from only two equally long time gates by means of the popular Ashworth's rapid lifetime determination (RLD) method[16] (Fig. 4.1a) using the following formula,

$$\tau = \frac{t_2 - t_1}{\ln \frac{W_1}{W_2}} \qquad \text{(Eq. 4.1)}$$

where t_2-t_1 is the time difference between the gates, and W_1 and W_2 are the photon counts in each gate, respectively. In counting schemes (Fig. 4.1b), in contrast, the lifetime is being obtained by deconvolution from the obtained decay curve. The choice of method depends on a number of factors. In general, counting schemes give a lot of information, but gating schemes are often preferred in the analytical field because it is often not necessary to study detailed decay dynamics, but rather only the relative signal change. They also allow for a much better signal-to-noise ratio (due to the length of the gates), which is particularly important in the

field of macroscopic imaging where due to less favorable geometries, it is both difficult to achieve high excitation densities in an economical manner, and less emission light per space unit can be collected compared to point measurements or microscopic optics. Gating schemes also allow for shorter acquisition times and therefore faster read-out, which is important when studying fast dynamic processes, and consume less memory. Therefore, they were studied in detail with respect to their sensitivity, accuracy and application range in a number of reports[14, 17-20] and applied in many areas of research, e.g. for oxygen, temperature, pH, H_2O_2 or CO_2 imaging.[21]

In order to obtain data for two species, we show here a method that we termed "dual lifetime determination (DLD)" which is based on a double application of the RLD method at different delay times and does only require one individual lifetime to be resolved (Fig. 4.2).

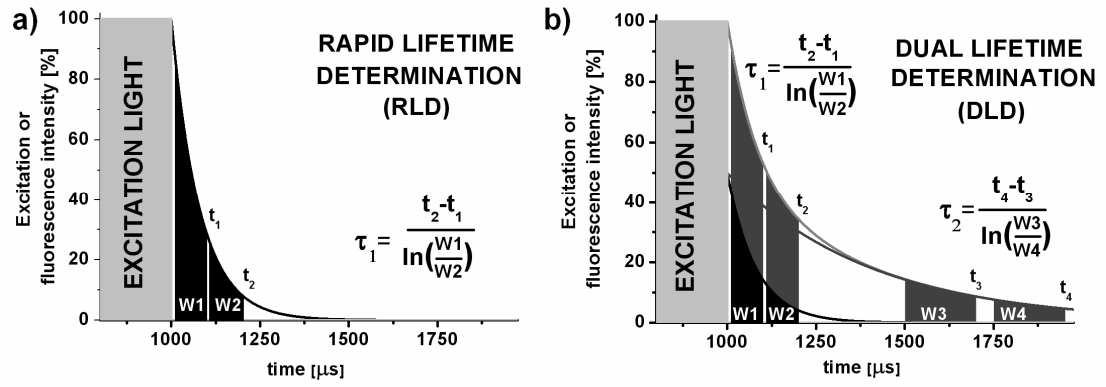

Fig. 4.2. a) The rapid lifetime determination (RLD) following a square-shaped excitation pulse typical for an LED (here 1 ms long) and b) a dual form termed dual lifetime determination (DLD) that calculates an average lifetime twice, in the first two gates (W1, W2) a mixed lifetime of both indicators, and in the second two gates (W3, W4) the pure lifetime of the longer-lived indicator. In the example above, idealized single exponential decays having lifetimes of 80 µs (red curve) and 400 µs (blue curve) were calculated.

The scheme is based on the idea that the lifetime of the longer-lived indicator (τ_2) can be calculated without interference from the shorter-lived one after a certain delay even if the lifetimes do not differ a lot because the exponential decay magnifies the emission differences the longer the delay after the end of the excitation is. If the second indicator is specific for one analyte (shown here for a temperature indicator), and if the right settings are chosen for a mixed lifetime calculation (τ_1) at a shorter delay, where both indicators are present (here one for temperature and oxygen, the oxygen indicator shows a temperature dependency), knowledge of the state of one analyte, and a signal responding to both analytes (τ_1) allows to calculate both analytes with good precision.

4.2.2. Material selection

The DLD scheme presented here works without spectral separation, but requires a sufficient overlap of the absorbance spectra of both compounds, so that both can be excited simultaneously. Furthermore, both emission spectra have to be sufficiently separated from both absorption spectra to avoid interferences by light reabsorption or energy transfer. Furthermore, in the case of a dual oxygen and temperature sensor, it is not possible to manufacture a oxygen sensor with emissive properties that are not affected by temperature, therefore the temperature sensitive component has to be a probe with a longer luminescence lifetime than the oxygen sensitive dye.

We have recently reported results on the properties of a number of europium complexes with an antenna chromophore, which allows their excitation in the visible at 405 nm.[8] These compounds possess a very high brightness (ε ($Eu(tta)_3dpbt$) > 70,000 $Lmol^{-1}cm^{-1}$, $\Phi \approx 0.4$ at 20 °C), and a luminescence lifetime of several hundred microseconds. They are

very temperature sensitive both in terms of luminescence intensity and lifetime, and only moderately cross-sensitive to oxygen. They are thus well suited as the long-lived component in the DLD scheme.

The oxygen sensitivity of temperature-sensitive probes in dual oxygen-temperature sensors can be generally reduced by two different strategies.[13] First, the compounds can be brought into polymer layers with little oxygen permeability, with an oxygen-sensitive polymer layer on top of it, and second, the dyes can be incorporated into microparticles using gasblocking materials, and dispersed alongside oxygen-sensitive micro- or nanoparticles into a common polymer. In this study the first approach was chosen. PVMK was selected as polymer matrix because of little oxygen permeability and good compatibility with Eu-complexes.

For the oxygen-sensitive layer, a common oxygen sensor material consisting of a platinum meso-tetrafluorophenylporphyrin (PtTFPP) immobilized in PS was selected.[22-24] It also has a very high brightness, particularly when excited at the Soretband near 400 nm, high photostability, a lifetime of approx. 70 µs at RT and it is very sensitive to oxygen. PS as a moderately high oxygen permeable polymer material allows achieving a dynamic range for oxygen detection between anoxic and standard atmospheric conditions. Like all common oxygen-sensitive dyes it also shows a rather substantial temperature dependency. When using the DLD scheme, a mixed lifetime of both dyes, is calculated from the average intensities in the first two windows (W1, W2). It is important to realize that the oxygen sensitivity therefore depends not only on the choice of probes and materials, but also on how much of each is present, and on the settings applied to the first two gates, as will be shown. This is true both for the dynamic range with respect to the oxygen conc. and to the temperature. Here the experimental settings were chosen to enable the sensing scheme to work at regimes typically

employed for enzymatic measurements, that is between the freezing point of water and physiological conditions (calibration from 1 - 40 °C) and between 0 and 25 % (slightly above the air content of 20.95 %) of oxygen at atmospheric pressure.

4.2.3. Calibration of the temperature sensitivity

Whereas the first two windows of the DLD scheme give a mixed response of both indicators, it is important to have a pure response of the longer-lived probe in the second two windows (W3 and W4) to be able to determine one analyte without interference from the shorter-lived dye. The necessary delay time after which the shorter-lived dye has decayed below measurable levels must be determined at the lowest temperature, because the lifetime of both indicators decreases with temperature, therefore the interference of the shorter-lived also decreases with temperature at fixed gate settings.

The interference of the shorter-lived indicator can be studied by observation of the luminescence lifetimes with respect to oxygen, as PtTFPP is strongly quenched by O_2 (Fig. 4.3a). The gates W3 and W4 were both of 300 µs length. W4 followed immediately after W3. The delay of W3 was varied in 200 µs steps from 200 to 800 µs. Both the recordings at 200 and 400 µs delay show an increase in lifetime upon addition of oxygen, because of decreasing contributions of PtTFPP. The effect is strongest at low O_2 concentrations because not only the intensity but also the lifetime of the shorter-lived “noise” decreases with increasing oxygen causing the measurement at 200 µs delay also to be almost free of interference at only about 10 % O_2. Both the measurements at 600 and 800 µs delay are virtually free of interference, therefore all measurements were carried out at 600 µs delay. Fig. 4.3b shows the calibration from 1 °C to 40 °C.

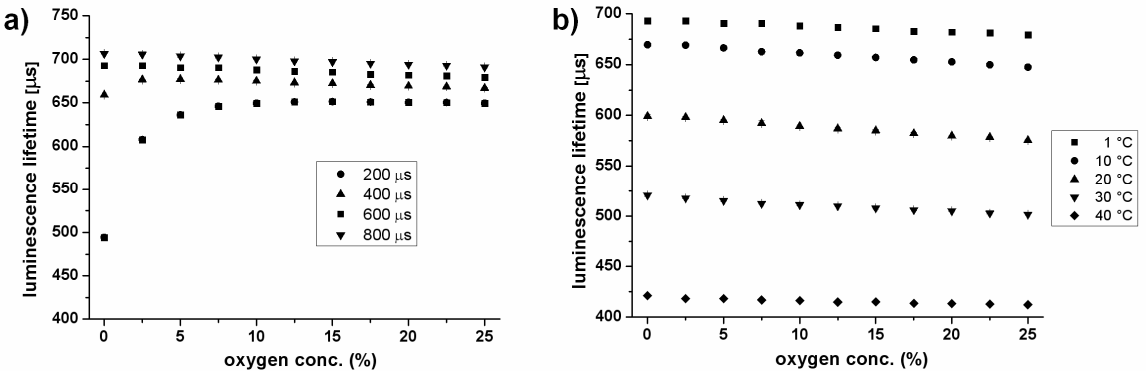

Fig. 4.3. a) Determination of the delay settings required for W3 and W4 of the DLD scheme. The luminescence lifetime is influenced by the shorter-lived oxygen indicator at 200 and 400 µs delay, the recordings at 600 and 800 µs delay are free of interference. b) Luminescence lifetimes of Eu(tta)$_3$dpbt in PVMK at 600 µs delay from 1 to 40 °C at various oxygen concentrations.

It can be seen that the probe shows a very strong temperature dependency within the calibration range. The oxygen dependency is very small. The luminescence lifetimes decrease by only about 2 % upon going from 0 % oxygen to 25 % at atmospheric pressure. The lifetime decreases by 40 % upon going from 1 °C to 40 °C allowing a rather precise determination of temperature. It has been shown previously that the temperature dependency of the lifetimes can be fitted with high precision for this probe,[8] just as for most fluorescence-based temperature sensors by an Arrhenius-type equation, which has the form of a single exponential decay (Fig. 4.4, see Ref. 5, 25 for details):

$$\tau^{-1} = k_0 + k_1 \cdot e^{\left(-\frac{\Delta E}{RT}\right)} \qquad \text{(Eq. 4.2)}$$

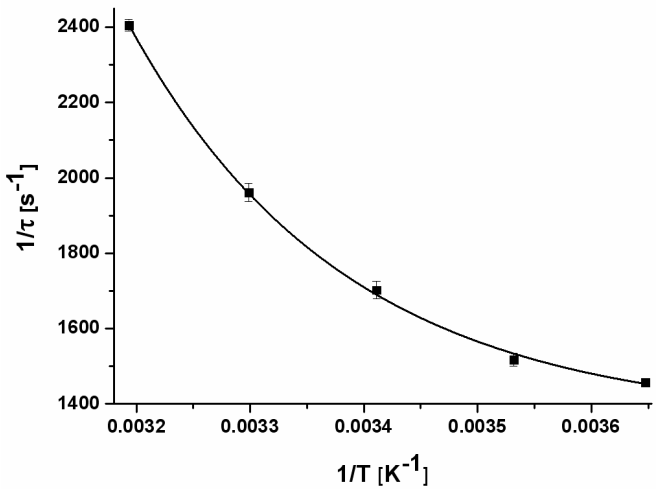

Fig. 4.4. Temperature calibration for Eu(tta)$_3$dpbt in PVMK using an Arrhenius-type fit.

Eq. 4.2 shows that the experimental parameters can be easily obtained when plotting 1/τ vs. 1/T. The curve fits the recorded calibration points very well. Table 4.1 summarizes the obtained parameters.

Table 4.1. Parameters for an Arrhenius-type fit of the temperature sensing component

Parameter	**k_0 [s^{-1}]**	**k_1[s^{-1}]**	**ΔE [kJ/mol]**	**R^2**
Value	$1.36 * 10^3$	$2.24 * 10^{10}$	43.9	0.999

4.2.4. Calibration of the oxygen sensitivity

The oxygen sensitivity in this measurement scheme is the result of the sensitivity of the oxygen-sensitive layer, the ratios of the oxygen and the temperature-sensitive dye and the settings applied to the first two windows. The first two windows should have maximum

oxygen sensitivity and therefore start right after the end of the excitation pulse, here a minimal delay of 1 µs was employed in order to exclude interferences from straylight and short-lived fluorescent background the sensing layers.

It is important to realize the effects that differing gatewidths have on the O_2 sensitivities. At very short gatewidths the emission of the oxygen-sensitive dye will be dominant, and the result will effectively be to have a quenching curve pretty similar to a single oxygen sensor, although with reduced sensitivity due to the constant background from the longer-lived dye, which is an undesirable situation. At longer gatewidths, a situation will result where the contribution of the short-lived dye (lifetime reduction due to quenching with increasing oxygen) and the longer-lived dye (average lifetime increase due to rising contribution of the unquenched, longer-lived emitter) are comparable in weight, and the result is an unsteady quenching curve with little sensitivity. This is clearly visible in Fig. 4.5 showing the curves with 50 and 100 µs gatewidths. The curves at 200 and 300 µs demonstrate the effects of a higher contribution of the long-lived component. The results are an effective increase in lifetime with good sensitivity due to rising contribution of the longer-lived, unquenched, temperature-sensitive dye with increasing oxygen concentration.

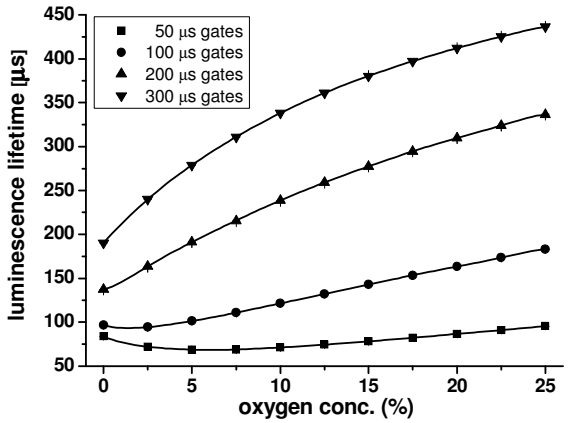

Fig. 4.5. The effect of gatewidth on the average luminescence lifetime in the first two windows of the DLD scheme at 1 °C.

However, increasing the gatewidths even more again results in a sensitivity decrease as the average lifetime will be more and more dominated by the longer-lived dye (which is insensitive to oxygen) with only a small background of the oxygen-sensitive short-lived dye (similar to the first situation). When observing the responses at more than one temperature though, there are additional aspects to consider. The contribution of the short-lived dye is again maximal at the lowest calibration temperature, both the lifetime decrease of the oxygen-sensitive and the temperature-sensitive dye causes an increase in the contribution of the latter at fixed gatewidths, which results in lower sensitivities. The average lifetimes at all calibration temperatures are shown in Fig. 4.6, along with polynomial fits (data not shown). Also, as the average lifetime decreases with increasing T, the emission ratios of W1/W2 increase. At 40 °C and zero oxygen, the combined lifetime τ_1 is approx. 89 µs meaning that with 200 µs gates there is almost 9.5 times as much fluorescence in the first gate compared to the second. Very high ratios result in poor signal-to-noise ratios due to little emission intensities in the second gate. Just as with single sensors, there is a trade-off between operating ranges and sensitivities, In the case of the DLD scheme, however, these ranges are not only selectable by the choice of materials but also by the choice of experimental settings.

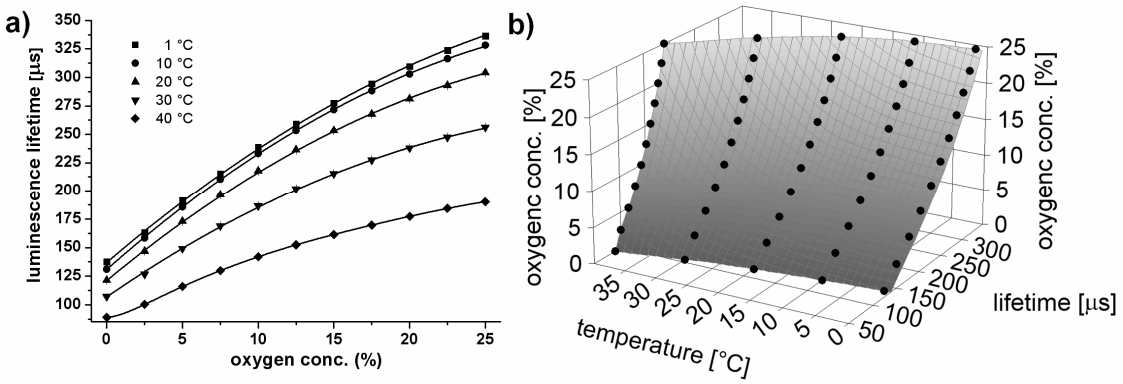

Fig. 4.6. a) Lifetime-based oxygen sensing calibration in the DLD scheme from 1 to 40 °C. b) 3D representation of the oxygen and temperature dependency of the lifetime τ_1 in the DLD scheme and surface fit according to Eq. 3.

One surface function which fits the experimental data points well is based on a polynomial function and shown in Eq. 4.3. The equation and the parameters were obtained using the Table Curve 3D software.

$$c(O_2) = \frac{a + b \cdot \ln(\tau) + c \cdot T + d \cdot T^2 + e \cdot T^3}{1 + f \cdot \ln(\tau) + g \cdot T + h \cdot T^2 + i \cdot T^3} \qquad \text{(Eq. 4.3)}$$

Table 4.2. The obtained oxygen calibration parameters for a calculation with the average lifetime in µs and the temperature in °C.

Parameter	**Value**	e	$9.89 * 10^{-6}$
a	-12.3	f	-0.156
b	2.51	g	$6.88 * 10^{-5}$
c	$6.48 * 10^{-3}$	h	$-1.29 * 10^{-5}$
d	$1.49 * 10^{-4}$	i	$-1.30 * 10^{-6}$

4.2.5. Measurement of oxygen consumption caused by enzymatic catalysis at varying temperatures

Having determined all the calibration parameters, we demonstrate a simple experiment to show that the proposed DLD scheme is able to simultaneously monitor oxygen and temperature without spectral separation. The dual sensing strip was fixed into a cuvette, which was then filled with 20 mL of a 100 mM phosphate buffer solution of pH 7.0 to which also contained 100 mM glucose. The cuvette was closed by a rubber seal, and 100 µL of glucose oxidase solution in PB were injected, causing a decrease in the oxygen conc. due to enzymatic

consumption of glucose. Oxygen and temperature were read out and after 20 minutes the system, which was inside a water bath, was cooled by addition of ice. After a further 20 min. the water bath was then heated to 40 °C (Fig. 4.7). The oxygen consumption is clearly detectable as well as the stable temperature signal over a wide range of oxygen concentrations. The detected temperature before the cooling and heating steps also correlated well with the 19.0 °C room temperature displayed by the contact thermometer in the experimental setup.

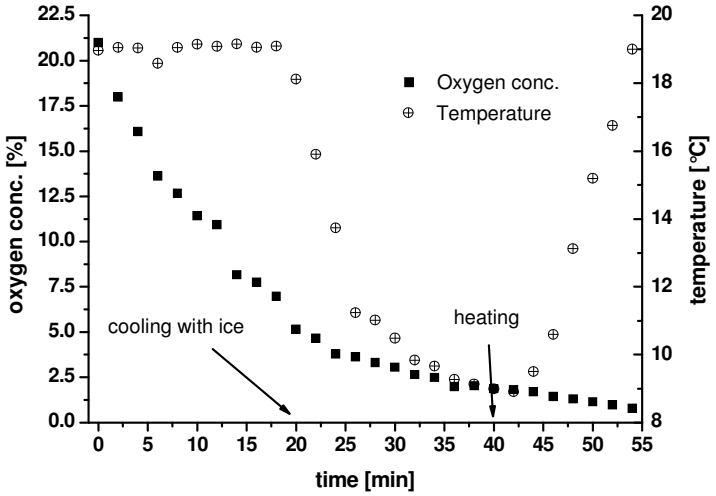

Fig. 4.7. Oxygen consumption of glucose oxidase monitored by the DLD scheme with varying ambient temperatures.

4.3. Conclusion

We have shown a new method termed dual lifetime determination, which is based on a double application of the RLD method, and which allows to follow signals from optical dual sensors without spectral separation in the time domain using only four time windows, and demonstrated it on a dual oxygen and temperature sensor operating between the freezing point of water and physiological conditions. By choice of materials and experimental parameters

analyte-specific responses can be extracted from multiexponential decay curves of fluorescent sensors with good sensitivity. The method also allows to tune the desired responses to some extent. Dual oxygen and temperature monitoring have a lot of applications such as in the field of biotechnology, microscopy, food monitoring and aerodynamics. Due to the readout-based on a single detector the two analytes can be recorded at the same geometry and almost simultaneously, and the scheme thus represents an advance to schemes demanding several detectors or filter changes. Other dual detection schemes can be realized according to this scheme if suitable indicators are available, e.g. a DLD dual glucose/temperature biosensor is readily realized by immobilizing glucose oxidase on an oxygen sensor such as presented, or entirely different sensors may be planned. One limitation of the scheme so far is still the availability of good materials though, the PVMK polymer still has a small oxygen dependency, and the Eu-complexes so far present the only suitable temperature-sensing compounds that work along with a long-lived oxygen indicator.

4.4. Experimental Section

4.4.1. Materials

Platinum(II)-5,10,15,20-tetrakis(2,3,4,5,6)-pentafluorophenylporphyrin (PtTFPP) was from Porphyrin Systems (www.porphyrin-systems.de), Europium(III)-tris(theonyltrifluoro-acetonato)-2-(4-diethylaminophenyl)-4,6-bis(3,5-dimethylpyrazol-1-yl)-1,3,5-triazine ($Eu(tta)_3(dpbt)$) was synthesized in our lab according to Refs. 8 and 26. Polystyrene (PS, average MW 280,000), toluene, glucose oxidase (type VII-S, from Asp. niger, 196,000 units/g) and natural rubber septa were obtained from Sigma-Aldrich (www.sigma-aldrich.com). Poly(vinylmethylketone) (PVMK, average MW 500,000) was purchased from

Acros Organics (www.acros.com). 1,2-Dichloroethane (DCE), glucose, $NaH_2PO_4*H_2O$ and 1 M NaOH solution were acquired from Merck (www.merck.de). Chemicals were of analytical purity and used as received. Polyester support was obtained from Goodfellow (www.goodfellow.com) and the calibration gases (nitrogen and oxygen, both of 99.999 % purity) were from Linde (www.linde-gase.de).

4.4.2. Preparation of the dual sensing film

3 mg $Eu(tta)_3(dpbt)$ and 300 mg PVMK were dissolved in 2 g DCE. 3 mg PtTFPP and 300 mg PS were dissolved in 3 g toluene. Both solutions were stirred at RT for several hours. The $Eu(tta)_3(dpbt)$/PVMK solution was spread as 120 µm thick films onto a 100 µm polyester support using a K Control Coater from RK Print Coat Instruments (www.rkprint.com). The solvent was allowed to evaporate for one hour and the PtTFPP/PS solution was cast on top of the $Eu(tta)_3(dpbt)$/PVMK layer as 100 µm thick film. The solvent was allowed to evaporate for several hours yielding a dual layer film of thicknesses of approx. 18 µm ($Eu(tta)_3(dpbt)$/PVMK) and 10 µm (PtTFPP/PS).

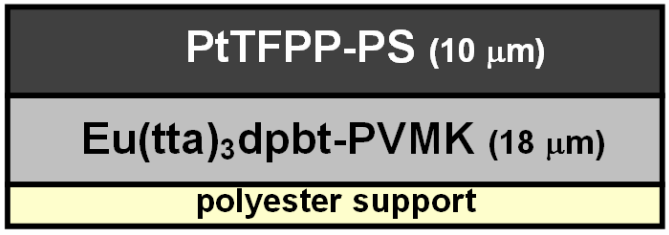

Fig. 4.8. Cross-section of the dual sensing layer. The temperature sensitive layer, consisting of a europium dye in PVMK, is sandwiched between the oxygen-sensitive polystsyrene layer and the inert polyester support.

4.4.3. Calibration of the dual sensor

Fluorescence of both dyes was excited using a multi-LED array emitting at 405 nm (LED405-66-60, 310 mW) of Roithner Lasertechnik (www.roithner-laser.com) equipped with a BG 12 excitation filter from Schott (www.schott.com) and a PCX 18 x 18 MgF_2 TS lens from Edmund Optics (www.edmundoptics.com). A strip of the sensing layer (approx. 4 x 2 cm) was placed in a custom-made calibration chamber which was similar to previous studies.[11,12,27] The preset gas composition was mixed by two PR 4000 pressure controllers from MKS Instruments (www.mks-instruments.com), which delivered a constant flow of the predetermined ratio of pure nitrogen and oxygen to the chamber at a total pressure of 0.4 bar. All measurements were carried out at ambient pressure. The temperature in the chamber was adjusted by a Lauda E-100 thermostat (www.lauda.de). The emission was collected through a Schott OG 590 filter and a Xenon 0.95/17 lens from Schneider (www.schneider-kreuznach.com) and recorded by an Imagex TGi gated CCD camera and software system from Photonic Research Systems (www.prsbio.com) (Fig. 4.9). All images were recorded using a frequency of 200 Hz, with a 2 ms long excitation of the sensing layer, and the rest reserved for detection of the decay and readout. The first two gates were integrated for 40 ms each, and the last two gates for 200 ms. Four images were recorded for each calibration point and the averages were used. Further evaluation was done using MS Excel 2003 (www.microsoft.com), Origin 8.0 (www.originlab.com) and TableCurve 3D v3.12 (www.systat.com).

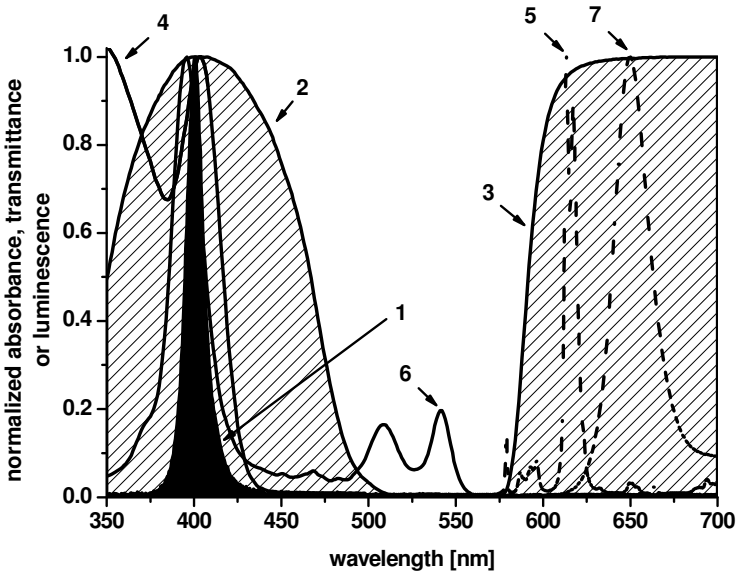

Fig. 4.9. The spectral setup. Luminescence of both indicators was excited by a 405 nm LED (1), using a BG 12 excitation filter (2) and the emission was collected through an OG 590 emission filter (3). The absorption (4) and emission (5) of Eu(tta)$_3$dpbt, and the absorption (6) and emission (7) of PtTFPP.

4.4.4. Enzymatic oxygen consumption measurements

100 mM phosphate buffer pH 7.0 (PB) was made by dissolving 13.8 g NaH_2PO_4*H_2O in ddH_2O and titrating with 1M NaOH solution until the desired pH. 4.5 g of glucose were added to 250 mL of PB to give a solution of 100 mM PB with 100 mM glucose. 0.51 mg glucose oxidase were dissolved in 10 mL PB to give a stock solution of 10 units/mL. The optical setup was identical to the calibration. The dual sensing layer was fixed into a home-made 20 mL cuvette, equipped with a magnetic stirbar. The cuvette was inside a water bath, the temperature could be controlled by a contact thermometer on a magnetic stirrer and heater. 20 mL of the PB/glucose solution were filled into the cuvette and the cuvette was closed by a septa and the measurement was started by injection of 100 µL of the PB/glucose oxidase

stock solution with a syringe to give a final conc. of 0.05 units/mL glucose oxidase in 100 mM PB with 100 mM glucose.

4.5. References

[1] O. S. Wolfbeis, (Series Ed) *Springer Series on Chemical Sensors and Biosensors*; Springer: Berlin, **2004-2006**; Vols. 1-4.

[2] B. R. Eggins, *Chemical Sensors and Biosensors*; Wiley: Chichester, **2002**.

[3] C. McDonagh, C. S. Burke, B. D. MacCraith, *Chem. Rev.* **2008**, *108*, 400-422.

[4] S. M. Borisov, O. S. Wolfbeis, *Chem. Rev.* **2008**, *108*, 423-461.

[5] L. M. Coyle, M. Gouterman, *Sens. Actuators B*, **1999**, *61*, 92-99.

[6] M. E. Köse, A. Omar, C. A. Virgin, B. F. Carroll, K. S. Schanze, *Langmuir* **2005**, *21*, 9110-9120.

[7] S. M. Borisov, C. Krause, S. Arain, O. S. Wolfbeis, *Adv. Mater.* **2006**, *18*, 1511-1516.

[8] S. M. Borisov, O. S. Wolfbeis, *Anal. Chem.* **2006**, *78*, 5094-5101.

[9] S. M. Borisov, A. S. Vasylevska, C. Krause, O. S. Wolfbeis, *Adv. Funct. Mater.* **2006**, *16*, 1536-1542.

[10] G. S. Vasylevska, S. M. Borisov, C. Krause, O. S. Wolfbeis, *Chem. Mater.* **2006**, *18*, 4609-4616.

[11] C. R. Schroeder, L. Polerecky, I. Klimant, *Anal. Chem.* **2007**, *79*, 60-70.

[12] C. R. Schroeder, G. Neurauter, I. Klimant, Microchim. Acta **2007**, 158, 205-218.

[13] S. Nagl, O. S. Wolfbeis, *Analyst* **2007**, *132*, 507-511.

[14] K. K. Sharman, A. Periasamy, H. Ashworth, J. N. Demas, N. H. Snow, *Anal. Chem.* **1999**, *71*, 947-952.

[15] J. Hradil, C. Davis, K. Mongey, C. McDonagh, B. D. MacCraith, *Meas. Sci. Technol.* **2002**, *13*, 1552-1557.

[16] R. J. Woods, S. Scypinski, L. J. C. Love, H. A. Ashworth, *Anal. Chem.* **1984**, *56*, 1395-1400.

[17] R. M. Ballew, J. N. Demas, *Anal. Chem.* **1989**, *61*, 30-33.

[18] S. P. Chan, Z. J. Fuller, J. N. Demas, B. A. DeGraff, *Anal. Chem.* **2001**, *73*, 4486-4490.

[19] S. P. Chan, Z. J. Fuller, J. N. Demas, F. Ding, B. A. DeGraff, *Appl. Spectrosc.* **2001**, *55*, 1245-1250.

[20] C. Moore, S. P. Chan, J. N. Demas, B. A. DeGraff, *Appl. Spectrosc.* **2004**, *58*, 603-607.

[21] G. Liebsch, I. Klimant, B. Frank, G. Holst, O. S. Wolfbeis, *Appl. Spectrosc.* **2000**, *54*, 548-559.

[22] A. Bizzarri, H. Koehler, M. Cajlakovic, A. Pasic, L. Schaupp, I. Klimant, V. Ribitsch, *Anal. Chim. Acta* **2006**, *573-574*, 48-56.

[23] S.-K. Lee, I. Okura, *Anal. Comm.* **1997**, *34*, 185-188.

[24] A. S. Kocincova, S. M. Borisov, C. Krause, O. S. Wolfbeis, *Anal. Chem.* **2007**, *79*, 8486-8493.

[25] G. Liebsch, I. Klimant, O. S. Wolfbeis, *Adv. Mater.* **1999**, *11*, 1296-1299.

[26] C. Yang, L. M. Fu, Y. Wang, J. P. Zhang, W. T. Wong, X. C. Ai, Y. F. Qiao, B. S. Zou, L. L. Gui, *Angew. Chem. Int. Ed.* **2004**, *43*, 5009-5013.

[27] S. Nagl, C. Baleizão, S. M. Borisov, M. Schaeferling, M. N. Berberan-Santos, O. S. Wolfbeis, *Angew. Chem. Int. Ed.* **2007**, *46*, 2317-2319.

CHAPTER 5
LUMINESCENT POLYMER NANOPARTICLES AS PROBES FOR PROTEIN, OXYGEN AND TEMPERATURE

5.1. Introduction

Permeation-selective micro- and nanobeads response to small molecules or changes in the environment can serve as probes for (bio)chemical species. They are particularly attractive in the field of multiple chemical sensing because they can be used along with other beads in order to achieve differential responsivities while maintaining macroscopic homogeneity within a matrix, such as a sensing layer.

There has also been much interest in the development of fluorescent nanoparticles which are completely inert over a wide range of conditions and therefore can serve as fluorescent labels in bioanalysis. Luminescent nanospheres can be divided into two categories: those where the nanoparticle itself is responsible for the emission of light, most prominently semiconductor nanocrystals ("quantum dots")[1], and those where dyes are incorporated into a nonluminescent carrier material, which itself forms tiny (nm-sized) beads. Among the latter category, most attention has been paid to silica beads[2] and organic polymer spheres.[3,4]

In order to be useful as a label, the particles need to fulfill several requirements in that they (a) are expected to be bioconjugatable, (b) are capable of incorporating and retaining fluorescent dyes, (c) display water solublility, (d) being resistant to non-specific binding, and

(e) not interfere with binding events occurring on the surface. Copolymers containing functionalities such as carboxy, amino, or hydroxy groups can be prepared by standard protocols for polymer synthesis or even be purchased. Polymers with carboxy groups are most often used because they are easier to activate than hydroxy groups, and also are more stable than particles containing amino groups. Fluorescent doping of the particles requires lipophilic dyes which will prefer to reside in the polymer matrix even in a mainly aqueous environment.

Most work on organic polymer particles has been performed with polystyrene ("latex") beads. The starting material is quite affordable and even nanospheres are comparatively easy to prepare in various sizes and stained with various fluorophores.[5,6] They are highly permeable to oxygen, and thus are not well suited for use as labels along with phosphorescent dyes displaying long luminescence lifetimes because of efficient quenching by oxygen. Polystyrene (PS) is also known for its strong hydrophobic interactions with proteins, this making selective protein binding rather difficult. They are, however, very well suited for oxygen sensing. Poly(acrylonitrile) (PAN) is a viable alternative for protein determination because of its low permeability for oxygen. PAN nanoparticles containing various fractions of carboxy groups can be obtained by copolymerization of acrylonitrile with acrylic acid. Such nanobeads can be easily stained with the phosphorescent ruthenium tris-(4,7-diphenyl-1,10-phenanthroline) complex (Ru-$(dpp)_3$). The particles were shown to be useful for biomolecular interaction screening.[7] Due to its specific chemical properties, PAN unfortunately is not suitable for some kinds of dyes. In looking for alternatives, we have investigated nanospheres made from the copolymer referred to as PD. It is obtained by copolymerization of methacrylonitrile, divinylbenzene and acrylic acid.

5.2. Experimental part

5.2.1. Materials

Platinum(II)-5,10,15,20-tetrakis-(2,3,4,5,6)-pentafluorophenylporphyrin (PtTFPP) and Palladium(II)-5,10,15,20-tetrakis-(2,3,4,5,6)-pentafluorophenylporphyrin (PdTFPP) were from Porphyrin Systems (www.porphyrin-systems.de). Europium(III)-tris(theonyltrifluoro-acetonate)-trihydrate ($Eu(tta)_3$) was from Acros Organics (www.acros.com). Meso-tetraphenyltetrabenzoporphine palladium(II) (PdTPTBP), glycine, N-hydroxysuccinimide (NHS), 1-ethyl-3-(3-dimethylaminopropyl) carbodiimide hydrochloride (EDC), 2-(N-morpholino)ethanesulfonic acid hydrate (MES), acrylonitrile, methacrylonitrile, NaN_3, and chloroform were from Sigma-Aldrich (www.sigmaaldrich.com), styrene, acrylic acid, ethanol, methanol, acetone, NaCl, KCl, $Na_2HPO_4*2H_2O$, KH_2PO_4, 1 M HCl, 1 NaOH, $NaHCO_3$, $K_2S_2O_8$, $(NH_4)_2S_2O_8$ and SDS were from Merck (www.merck.de). (+)Biotin-PEO3-amine was from Molecular Biosciences (www.molbio.com). Streptavidin was from Interchim (www.interchim.com). Cy5-mono-NHS-Ester and Sephadex G25 were from Amersham Biosciences (www.amersham.com). BCA assay kit was purchased from Pierce (www.piercenet.com). Doubly distilled (dd) water was purified in-house and used for all syntheses and preparations. Chemicals were of analytical purity and used as received. Polyester support was from Goodfellow (www.goodfellow.com) and the calibration gases (nitrogen and oxygen, both of 99.999 % purity) were from Linde (www.linde-gase.de). Cellulose membranes (Visking) were from Roth (www.carl-roth.de). 70 mm and 150 mm diameter cellulose filter paper (No. 595, 4 - 7 µm) and cellulose nitrate filters (100 nm, 25 mm diameter) were from Whatman (www.whatman.com). Presynthesized polymers (PD-Optosense, PMAN-3) were provided by C. Krause, PreSens GmbH (www.presens.de).

PBS buffer 150 mM, pH 7.4, 0.05 % NaN_3 (PBS) was made by adding 8 g NaCl, 400 mg KCl, 1.8 g $Na_2HPO_4*2H_2O$, 0.24 g KH_2PO_4 and 0.5g NaN_3 to 900 mL ddH_2O, titrating to pH 7.4 at RT and filling up to 1 L.

MES buffer 100 mM, pH 6.5, was made by adding 19.5 g MES to 900 mL ddH_2O, titrating to pH 6.5 at RT and filling up to 1 L.

Phosphate buffer 30 mM, pH 8.0, was made by adding 5.34 g $Na_2HPO_4*2H_2O$ to 900 mL ddH_2O, titrating to pH 8.0 at RT and filling up to 1 L.

Bicarbonate buffer 100 mM, pH 8.5, was made by adding 8.40 g $NaHCO_3$ to 900 mL ddH_2O, titrating to pH 8.5 at RT and filling up to 1 L.

Cy5-mono-NHS ester was conjugated conjugated to Streptavidin in bicarbonate buffer at room temperature (RT) for 1 h and separated from unreacted dye using size exclusion chromatography on Sephadex G25 eluting with PBS. Protein concentration was determined using the BCA assay.

40 mg of each of the polystyrene nanobeads were mixed with 100 mg of hydrogel D4 dissolved 2 g ethanol/water (9:1, v/v) and cast as 120 µm thick films onto a polyester foil to obtain a final thickness of about 8 µm for determination of the oxygen sensitivities for various nanoparticles.

5.2.2. Polymer syntheses

The syntheses were carried out according to Ref. 8. In a 500 mL flask equipped with a reflux condenser, large stirbar, gas inlet and temperature control 50 mL methacrylonitrile (for the polymethacrylonitrile (PMAN) polymer, 49 mL methacrylonitrile, 0.5 mL divinylbenzene and

0.5 mL acrylic acid for the PD polymer) were mixed with 400 mL ddH_2O, which had been saturated with N_2 and 4 g SDS and heated to 65 °C. A steady stream of N_2 was pouring through the gas inlet. 400 mg $(NH_4)_2S_2O_8$ were dissolved in 5 mL ddH_2O and immediately added to the mixture. The nitrogen stream was turned off immediately after the mixture turned slightly turbid (after approx. 5 min.) and the reaction was stirred at 70 °C for a further 16 h. After cooling to RT the emulsion was diluted to 1 L with ddH_2O and the pH was slowly adjusted to 3.5 using 1 M HCl. NaCl sat. was added until the polymer began to precipitate and the emulsion was allowed to complete the precipitation for several minutes. The product was collected by filtration using a 150 mm filter paper. It was resuspended in 1.5 L ddH_2O and filtrated five times and resuspended in 300 mL ethanol and filtrated twice to remove remaining SDS. The polymer was dried on air.

5.2.3. Nanoparticle syntheses

Polymethacrylonitrile nanoparticles

The particles were synthesized with modifications according to Ref. 9. 2mg $Eu(tta)_3$ and 200 mg PMAN were dissolved in 20 mL acetone. 40 mL ddH_2O were added dropwise via a dropping funnel. The dispersion was filtrated and the acetone was removed at a rotary evaporator. The particles were dialyzed for several days against ddH_2O and freeze dried.

Polymethacrylonitrile-co-divinylbenzene-co-acrylic acid (PD) nanoparticles

100 mg PD, 1 mg dye (PtTFPP or PdTPTBP for the experiments presented here) and 40 mg SDS were dissolved in 40 mL acetone and stirred for 1 h. Over the course of 3 h, 80 mL 1

mM NaOH was added dropwise via a pasteur pipette on a dropping funnel. The dispersion was slowly brought to pH 7 by addition of 100 mM HCl, filtrated and dialyzed against PBS for several days. It was further purified by size exclusion chromatography on Sephadex G 25 and sterile filtrated using a 100 nm cellulose nitrate filter.

Biotinylation of PD nanoparticles

1 mL of 0.4 % PD nanoparticle suspension stained with PtTFPP in PBS buffer were transferred to MES buffer, pH 6.5 by eluting on a Sephadex G25 column. 1 mg EDC and 2 mg NHS in 0.1 mL MES buffer are added, and the suspension is stirred for 8 min. The particles are transferred to phosphate buffer pH 8.0 and separated from free coupling agents by eluting on another G25 column. The eluate is dropped directly into a solution of 1.1 mg Biotin-PEO3-amine (a biotin containing a terminal amine and a spacer of three ethyleneoxide groups on the carboxylic acid end of the parent biotin molecule) in 500 µL phosphate buffer and stirred for 30 min. 1 mg glycine is added and stirred for another 30 min. The nanoparticle suspension is then transferred back into PBS buffer and separated from the reactants by another G25 column.

Polystyrene- and polystyrene-co-acrylic acid nanoparticle synthesis

The particles were synthesized and stained with modifications according to Ref. 10. In contrast to the polymethacrylonitrile-based particles, polystyrene-based nanoparticles are being synthesized directly from the monomers. 5 g styrene (or 4.75 g styrene and 0.25 g acrylic acid for the copolymer nanoparticles) are being mixed with 36 g dd H_2O in a 100 mL round flask equipped with reflux condenser and temperature control. 0.1 g $K_2S_2O_8$ is being

dissolved in 9 g dd H_2O and immediately added to the styrene/water mixture. It is then heated to 95 °C under reflux for 4 h. After cooling to RT, the synthesized particles are being dialyzed for several days against dd H_2O using cellulose membranes to remove traces of monomers, side products and impurities.

Staining of polystyrene- and polystyrene-co-acrylic acid nanoparticles

2 mL MeOH, 1mL ddH_2O and 500 µL of the 10 % nanoparticle emulsion in ddH_2O (synthesized in the previous step) are being stirred for several minutes. 25 µL chloroform are added and stirred for 10 minutes. The stirbar is removed to prevent aggregation of the particles onto it, and 1 mg dye dissolved in 500 µL chloroform is added and the emulsion is shaked for 4 h. Subsequently, a nitrogen stream is bubbled through the emulsion for 30 minutes, afterwards it is filtrated using glass wool. The filtrate is dialyzed against dd H_2O for several days in the dark using cellulose membranes and freeze dried.

5.2.4. Instruments

Excitation and emission spectra and decay curves were recorded on an SLM Aminco-Bowman 2 spectrometer (www.thermo.com). Dynamic light scattering experiments were performed on a Malvern Zetasizer 3000 HS (www.malvern.com). Transmission electron microscopy was carried out on a Zeiss 902 (www.zeiss.com) microscope.

Determination of the oxygen sensitivies of PS-based nanospheres was carried out using a setup similar to Chapters 2 - 4. PtTFPP- and PdTFPP-stained PS nanospheres were excited using a multi-LED array emitting at 405 nm (310 mW), PdTPTBP-stained PS

nanospheres were excited using a 450 nm LED (Luxeon V, 700 mW, royal blue, from Philipps Lumileds Lighting, www.lumileds.com). Emission was collected by a Chroma 650-60 filter (PtTFPP-PS), Chroma 680-60 filter (PdTFPP-PS) or Chroma 800-40 filter (PdTPTBP-PS), all from AHF Analysentechnik (www.ahf.de).

The microplate imaging setup is schematically depicted in Fig. 5.1. Luminescence was excited by 96 RLU405-9-30 LEDs (9 mW, from Roithner Lasertechnik, www.roithner-laser.com), one for each well, emitting at 405 nm. The excitation filter was a 125 x 85 mm BG 12 color glass filter from Schott (www.schott.com), the emission passed through a fiber optical adapter (3 mm optical fiber PG-R-FB3000, from Laser Components, www.lasercomponents.com) made in-house and was recorded through a RG 610 filter from Schott by an Imagex TGi camera from Photonic Research Systems (www.prsbio.com) equipped with a Xenon 0.95/17 lens from Schneider (www.schneider-kreuznach.com).

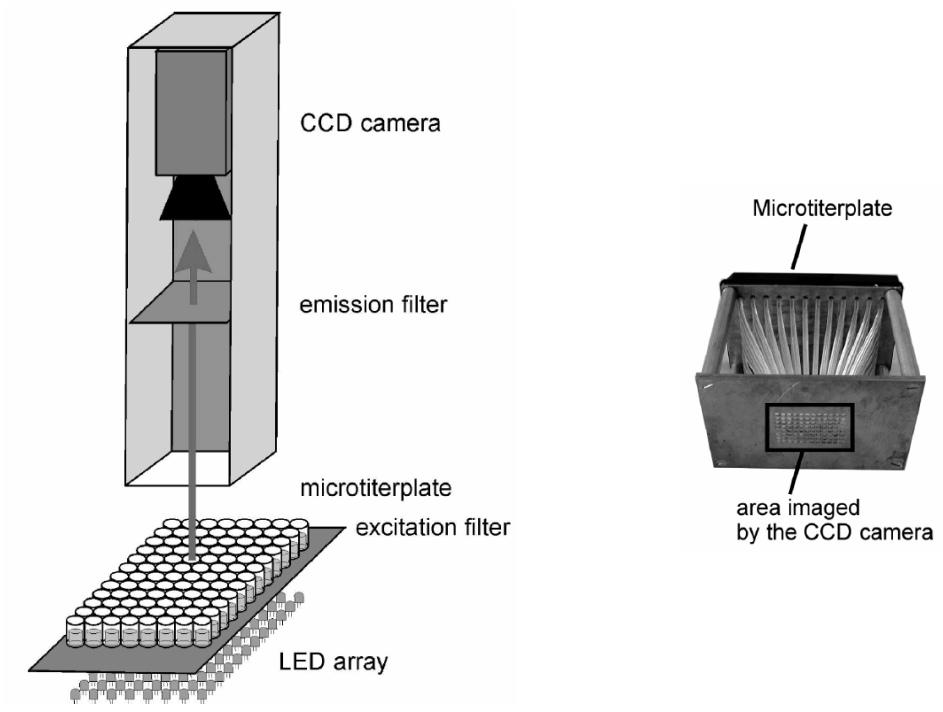

Fig. 5.1. Microwell plate optical imaging setup, from Ref. 11. All wells were excited simultaneously using 96 LEDs and a filter and the emission was recorded from the top of a fiberoptical adapter.

5.3. Metalloporphyrin-doped phosphorescent PD nanoparticles as optical probes

5.3.1. Platinum porphyrin-doped nanospheres displaying FRET to red-emitting cyanine dyes

In a previous work,[7] Polyacrylonitrile-co-acrylic acid nanoparticles were found to be applicable towards a biotin-streptavidin assay using time-resolved FRET. This assay used a Ruthenium complex as the FRET donor. The shortcomings of this assay were the only moderate brightness of the donor luminophore and the irregular shape of the PAN nanoparticles preventing their use in certain applications. Nanoparticles made from the PD polymer offer the advantage that they can be doped by metalloporphyrin dyes, that are much brighter, without aggregation, and that they are spherical in size. Fig. 5.2 shows the spectra of a platinum porphyrin dye in PD.

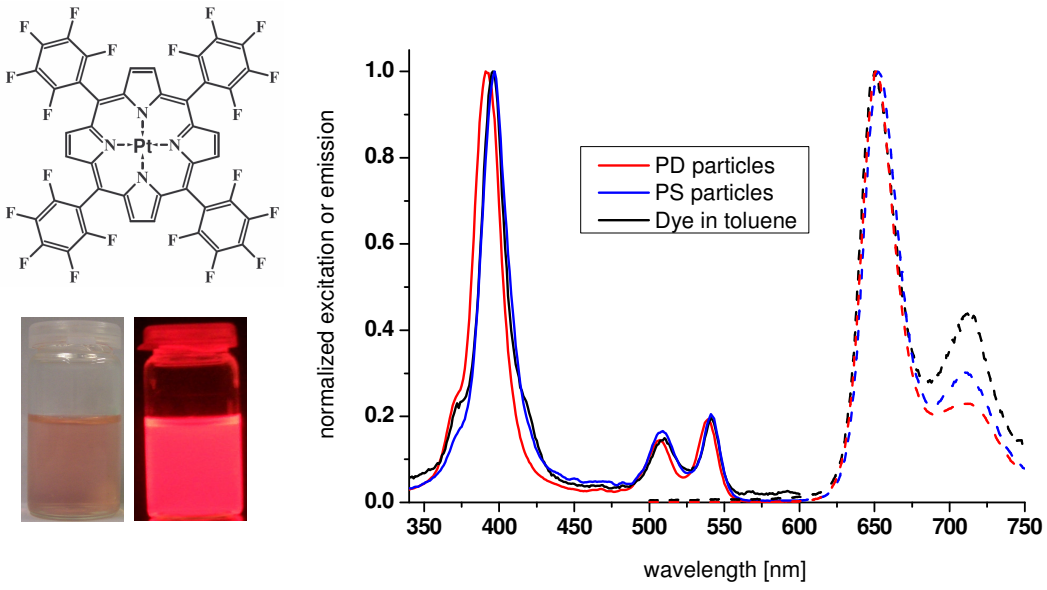

Fig. 5.2. Chemical structure of PtTFPP, brightfield and fluorescence color photographs (conc. approx. 0.1 %) and optical spectra of PtTFPP-PD nanoparticles (conc. 10 ppm in PBS) and comparison with PS nanoparticles and free dye.

The spectra closely resemble the free dye with a small blue shift in the excitation that can be attributed to the more polar environment in PD compared to toluene and polystyrene. Metalloporphyrin luminescence is strongly quenched by oxygen, however just as PAN, PD is rather oxygen impermeable and the particles did not display any detectable interference by oxygen (Fig. 5.3). The measured luminescence lifetime was 78 µs in both cases. Under the same experimental conditions, PS nanospheres stained with the same dye showed a luminescence decrease of over 50 % upon going from anaerobic conditions to ambient air (data not shown).

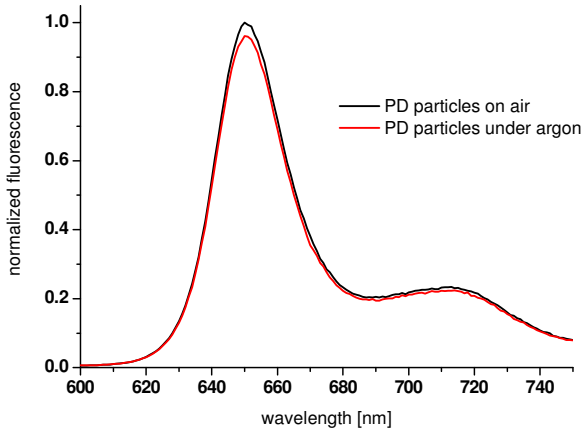

Fig. 5.3. Luminescence of PtTFPP-stained PD nanoparticles in PBS under argon and on ambient air at RT.

The particles are long-term stable (> one year) in all common buffers from pH 5-10. Acidic conditions cause precipitation of the particles due to protonation of the carboxylic acid groups and increased hydrophobicity. Strong bases disintegrate the particle shape and cause leaching of the dye. This is a much slower process, and basic conditions are possible for the particles on the time scale of hours to days.

For FRET-type applications the intermolecular distance is obviously very important, and so is therefore the nanoparticle size. We have optimized the nanoparticle synthesis, however we were not able reduce the average diameter to less than 100 nm using the PD polymer that we obtained. We have investigated the size of the beads obtained from several PD polymer batches using dynamic light scattering (DLS) and found that it is highly dependant upon the age of the parent PD polymer (Fig. 5.4). Obviously, the polymer shows an ageing effect that can possibly be attributed to incomplete deactivation of the reactive groups during polymer synthesis.

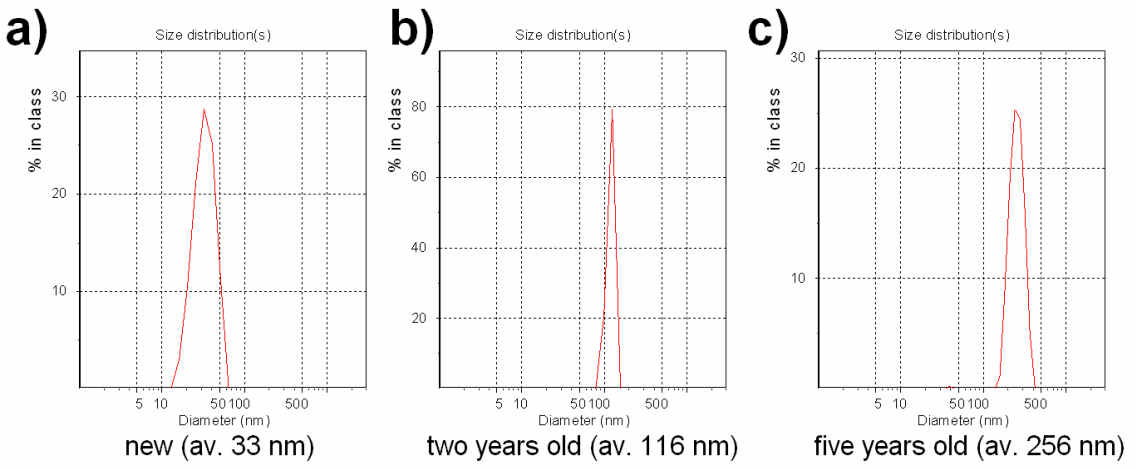

Fig. 5.4. PtTFPP-PD nanoparticle diameter obtained by dynamic light scattering depending on polymer age.

The diameter obtained from DLS and the proposed spherical shape of the beads was confirmed by electron microscopy of dried particles (Fig. 5.5).

The nanoparticles were conjugated to an amino-terminated biotin. A two-step procedure with carefully determined reaction times and conditions was elaborated as the

particles are very reactive towards cross-linking as soon as the coupling agents are added. The streptavidin assay is schematically depicted in Fig. 5.6.

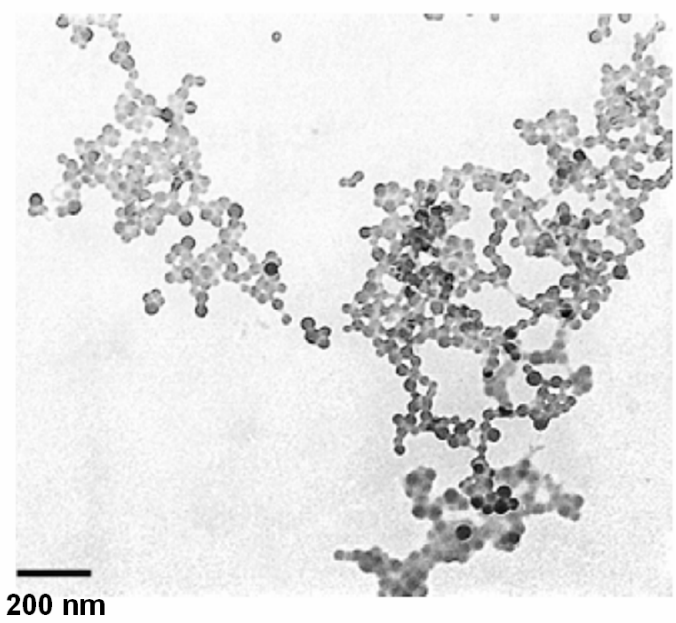

Fig. 5.5. Transmission electron micrograph of PtTFPP-PD nanoparticles.

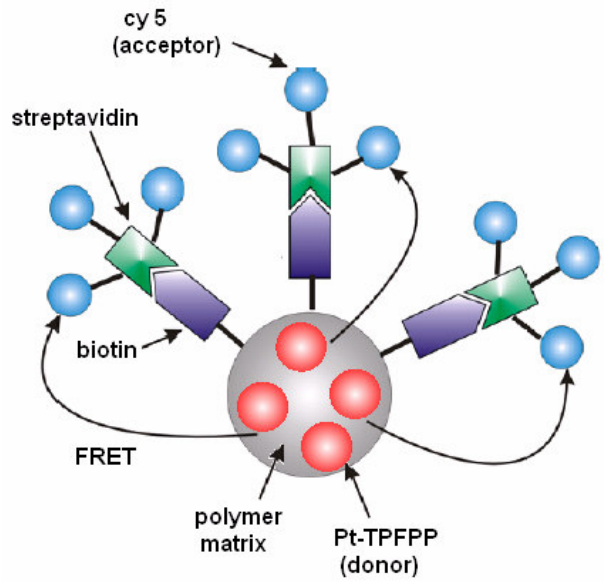

Fig. 5.6. The streptavidin assay based on PtTFPP-PD nanobeads. Modified from Ref. 9.

The biotinylated beads in PBS at 5 mg/L were subjected to differing amounts of Cy5 streptavidin, incubated for one hour, excited with a 405 nm LED in each well, and the luminescence lifetime was measured after a delay of 1 µs after the end of the light pulse. While the FRET donor emission overlaps well with the acceptor absorbance, donor and acceptor emission overlap almost completely and would be very hard to differentiate in an intensity-based approach (Fig. 5.7). However, because Pt-TFPP possesses a long lifetime in the µs domain, whereas the FRET acceptor Cy5 has a fluorescence lifetime of a few ns only a minimal delay ensured to measurement of donor emission only (time-resolved FRET approach). Furthermore, because the ratiometric RLD approach was used, the very inhomogeneous excitation intensity in each microwell was intrinsically referenced and homogenous lifetime images were obtained for each well (Fig. 5.8).

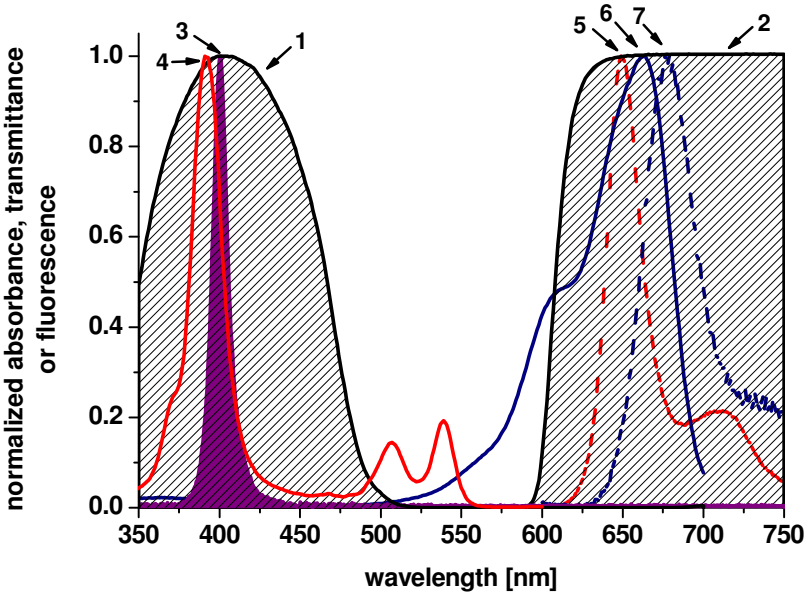

Fig. 5.7. Spectral setup of microplate FLIM-FRET detection. (1) and (2) are the transmittances of the excitation (BG 12) and emission filter (RG 610), respectively, (3) is the emission spectrum of the LED light source, (4) and (5) are the excitation and emission spectra of PtTFPP in PD beads, (6) and (7) are the absorbance and emission spectra of Cy5-streptavidin.

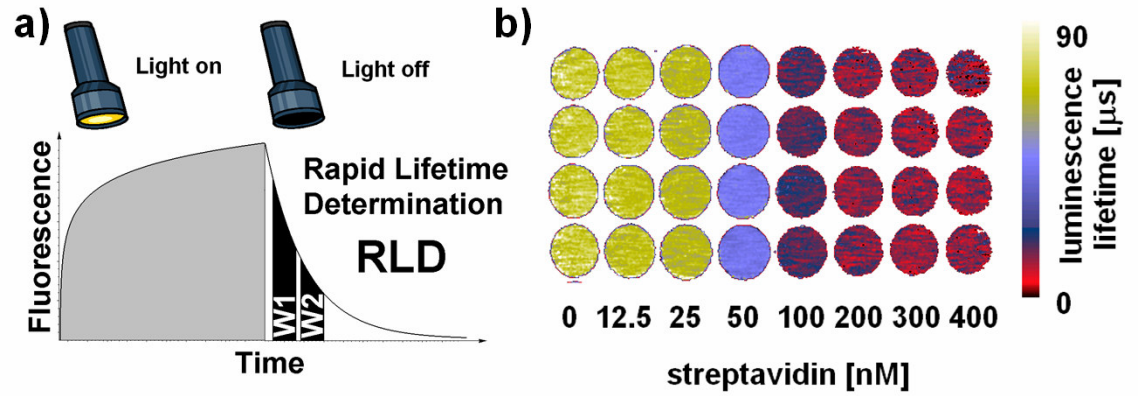

Fig. 5.8. a) The rapid lifetime determination scheme used for microplate evaluation. b) Luminescence lifetimes of microplate wells subjected to differing amounts of FRET acceptor dyed-streptavidin.

The results show a decrease of luminescence lifetime to about a third of the initial value (from 82 to 27 µs) upon saturation with Cy5-streptavidin when using the 33 nm-sized particles. The 116 nm nanobeads showed only a small FRET efficiency (Fig. 5.9), the 256 nm spheres practically none.

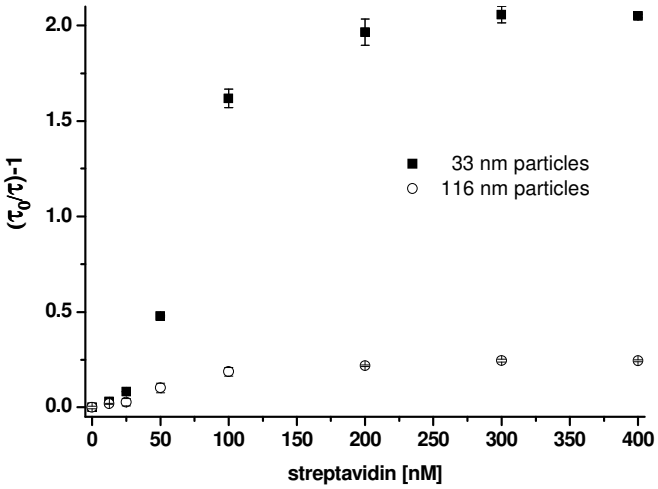

Fig. 5.9. Evaluation of lifetime decrease due to FRET on biotinylated PtTFPP-PD nanoparticles of differing diameter.

The interaction with streptavidin is specific, nonbiotinylated particles and particles coated with human serum albumin (HSA) instead of biotin did not show any measurable FRET (results not shown). However, there are still some interferants, e.g. polyclonal anti-HSA antibody labeled with Cy5 did adsorb efficiently and display efficient FRET on all of the PD particle surfaces that we produced (the parent carboxylated, biotinylated and HSA-coated ones).

5.3.2. Palladium benzoporphyrin-doped nanospheres for NIR applications

The PD nanobeads can be stained with a wide variety of dyes. Among the porphyrin compounds, there is a class of extended porphyrins with interesting spectral properties, metallobenzoporhyrins that have a benzene ring attached to each of the four pyrrole subunits of the porphyrin chromophore. Those compounds are known for around twenty years, and are especially interesting because they are highly luminescent with a redshift in absorbance and emission compared to the parent porphyrins.[12,13]

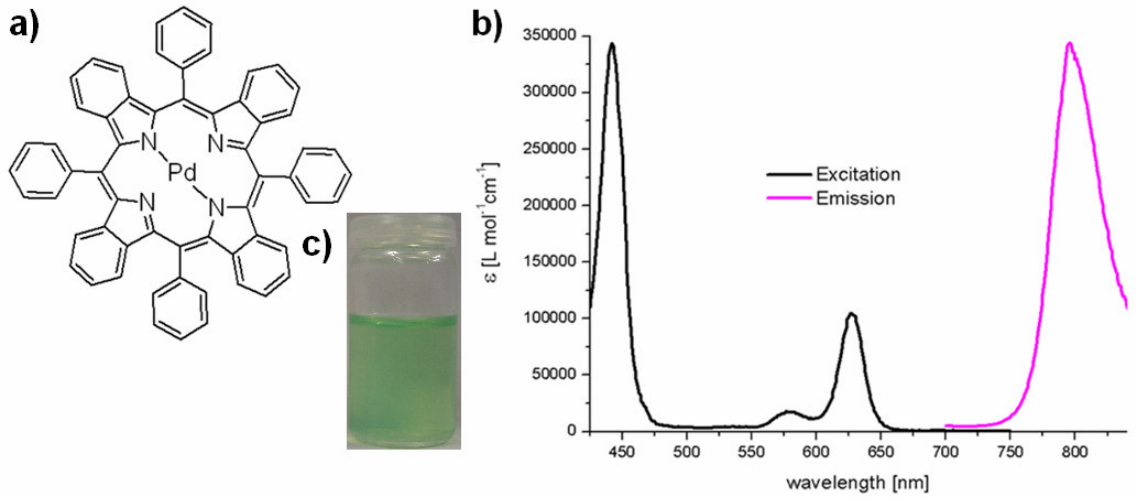

Fig. 5.10. a) Structure, b) spectral properties of PdTPTBP-stained PD nanoparticles (10 ppm in phosphate buffer 20 mM, pH 7.0), c) photograph (approx. 100 ppm in phosphate buffer).

However, they have only recently become more widely available because of their difficult and time-consuming synthesis. We have investigated the palladium-meso-tetraphenyl-tetrabenzoporphyrin (PdTPTBP) complex and found that it could be used for production of PD nanoparticles. The structure and the excitation and emission of PD nanoparticles are shown in Fig. 5.10. The spectra closely resemble the free dye in organic solvents. The Q-band in this compound is shifted to the red region of the visible spectrum with a maximum at 625 nm, and stronger with respect to the Soret band found around 450 nm. They can thus be used along with red lasers such as the He-Ne laser (635 nm) or red diode lasers. The emission is in the NIR with a maximum at 795 nm. The nanoparticle size, and the behavior of the decay time with respect to oxygen quenching were investigated as metallobenzoporphyrin luminescence is known to be very oxygen sensitive (Fig. 5.11).[14]

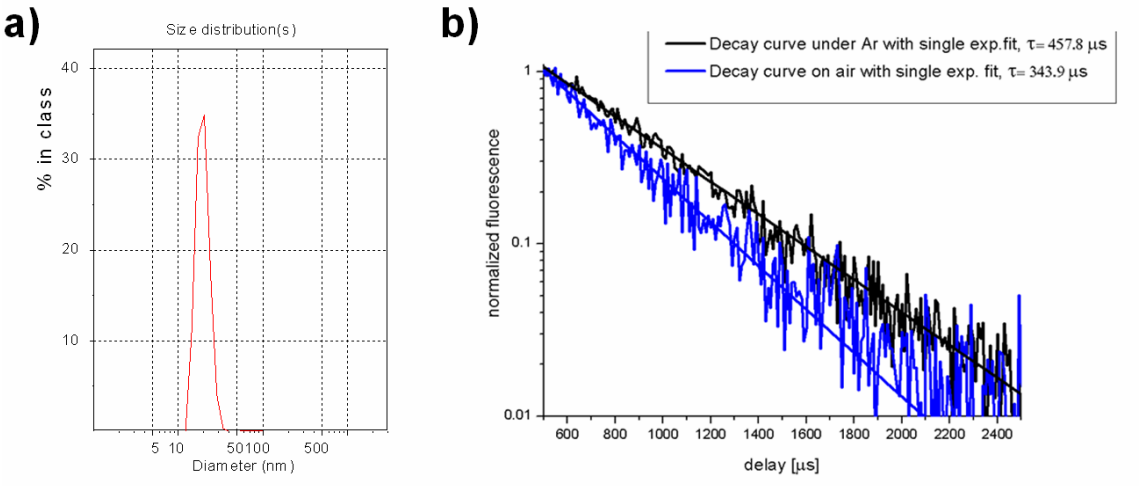

Fig. 5.11. a) Diameter determined by dynamic light scattering and b) decay curve of PdTPTBP-PD nanoparticles under argon and on ambient air.

The results show an average diameter of 27 nm for the particles, roughly the same size as for the PtTFPP-PD particles. Presumably mainly due to the small size there is still some degree of oxygen quenching. The lifetime decreases about 25 % upon going from anaerobic conditions

to ambient air. Notably, those luminescence lifetimes, which were confirmed by an independent measurement using the microplate imaging setup (results not shown), are significantly longer than those mentioned for the free dye in the literature (200-250 µs). This is a good indication of a high quantum yield (QY) of the PdTPTBP-PD nanoparticles. Unfortunately, due to the poor NIR sensitivity of the spectrometers available to us, neither the QY of the particles nor the lifetime of the free dye could be determined precisely, however, the estimated QY of this dye within PD particles is > 20 %, therefore the dye in the PD particles has a Brightness (Bs) of > 20,000 when excited in the red and > 60,000 when excited at the Soret-band at 450 nm. PdTPTBP-PD is the only bioconjugatable material so far that can be excited in the red, has a lifetime of over 1 µs and is usable in aqueous (buffer) solutions.

5.4. Temperature-sensitive doped PMAN nanospheres

The poly(methacrylonitrile) matrix is not restricted to metalloporphyrins and allows incorporation of many different classes of compounds. Because of the gas blocking capabilities of this polymer, they are interesting for nanospheres containing temperature-sensitive dyes in multiple sensing applications. The $Eu(tta)_3$-complex is among the most compounds with the highest temperature sensitivity of the luminescence.[15] It can not be incorporated into PD or PAN-based nanospheres, however we have found that nanobeads made of plain PMAN work well with this complex. Commercial PMAN (from Polysciences) is of insufficient quality to produce particles in the nm regime, however PMAN synthesized according to the experimental section, produces $Eu(tta)_3$-stained nanospheres.

5.4.1. Optical spectra and nanoparticle size

The optical spectra of the spheres in aqueous dispersion are shown in Fig. 5.12a. They are virtually identically with the free complex in organic solvents. DLS confirmed the nm size regime of the particles (147 nm average diameter, Fig. 5.12b).

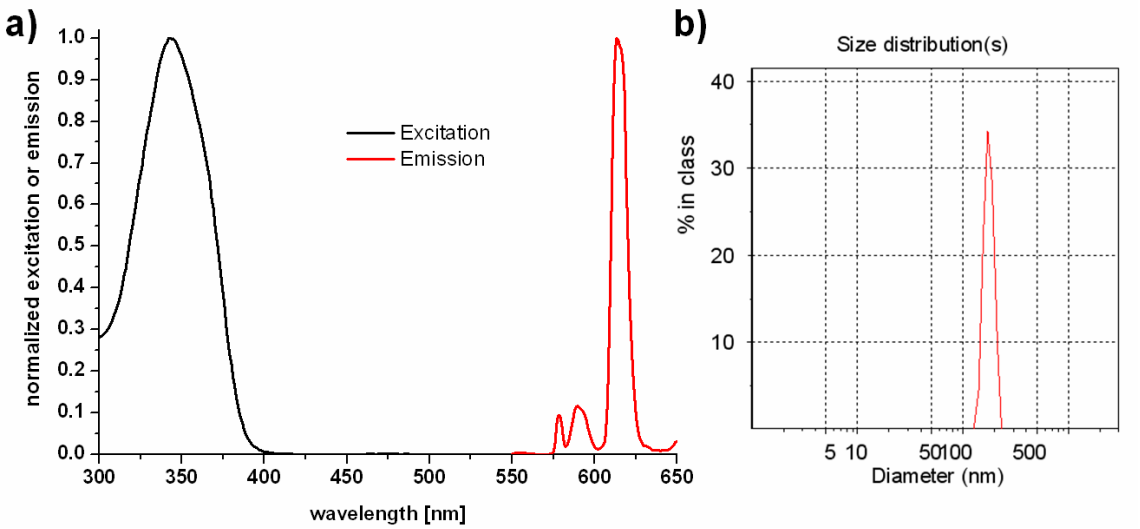

Fig. 5.12. a) Excitation and emission spectra of Eu(tta)$_3$-doped PMAN nanospheres. b) size determination by dynamic light scattering.

5.4.2. Temperature sensitivity

The dependence of luminescence intensities (Fig. 5.13a) and lifetimes (Fig. 5.13b) on temperature were investigated in aqueous solution. The luminescence intensities are highly temperature sensitive with a drop of about 90 % from 1 to 60 °C. The lifetimes are much less affected and only drop about 25 % in the same temperature range. In a one step dynamic quenching process changes in intensities and lifetimes should match. Eu-complexes often feature multistep processes of excited state deactivation. A discrepancy in intensity and lifetime quenching has been previously noted for this complex.[15] It is also present, although to a lesser extent, in the Eu(tta)$_3$dpbt complex used in Chapter 4.[16]

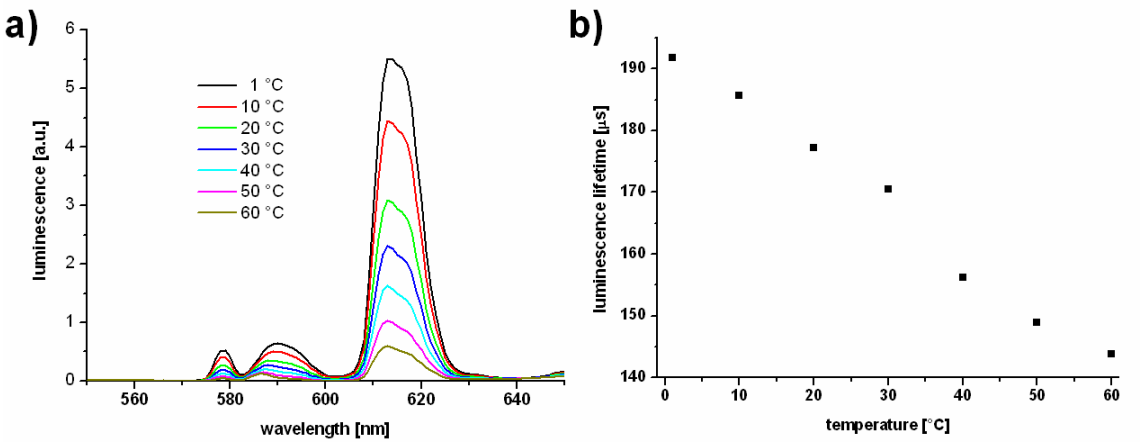

Fig. 5.13. a) Luminescence intensities and b) luminescence lifetimes of $Eu(tta)_3$-doped PMAN nanospheres from 1 to 60 °C.

5.5. Dye-doped polystyrene-based nanobeads for oxygen sensing

The polymethacrylonitrile-based nanobeads are attractive when shielding of the inherent oxygen sensitivity of long-lived luminescent dyes is desired. However, for oxygen sensing applications, polymers with higher oxygen permeabilities have to be used. Polystyrene is a common matrix for polymer nanospheres and PS-based nanospheres can be used as oxygen indicators along with nanoparticles for further analytes dispersed in a common matrix such as hydrogels. Below, oxygen sensitivities of polystyrene nanospheres that contain a carboxylic acid group for further functionalization are presented.

5.5.1. Optical spectra and nanoparticle size

The average diameter of the particles were determined by dynamic light scattering (266 nm av. diameter, Fig. 5.14) and the spectra were recorded for poly(styrene-co acrylic acid) nanoparticles stained with three different metalloporphyrin dyes (Fig. 5.15-17).

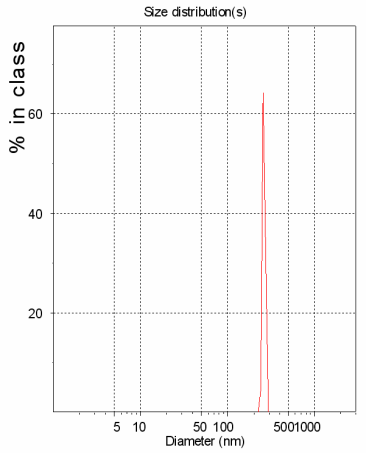

Fig. 5.14. Average diameter of PtTFPP-PS-co-AA particles determined by dynamic light scattering.

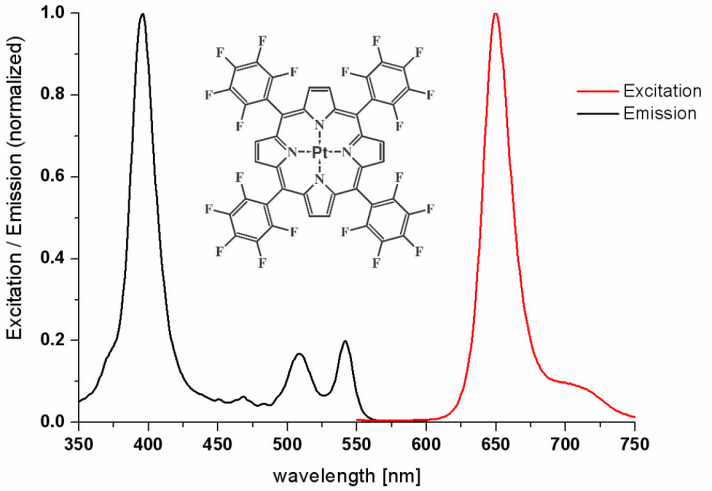

Fig. 5.15. Optical spectra of PtTFPP-PS-co-AA in PBS.

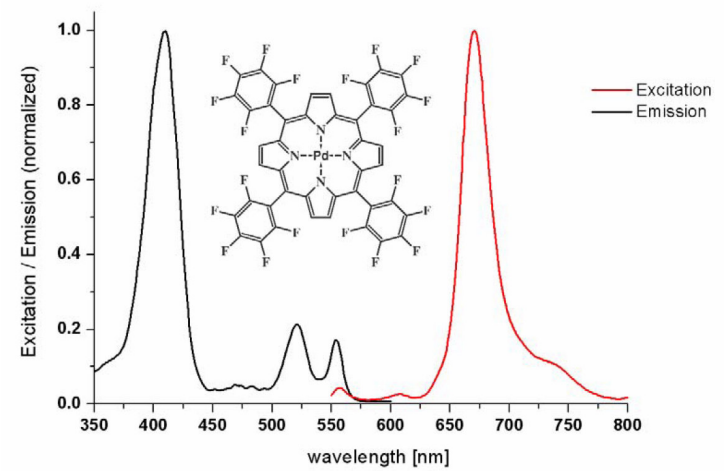

Fig. 5.16. Optical spectra of PdTFPP-PS-co-AA in PBS.

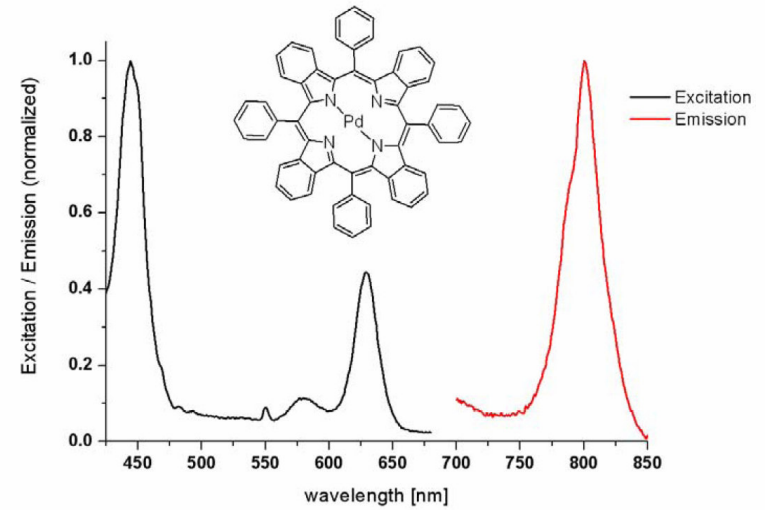

Fig. 5.17. Optical spectra of PdTPTBP-PS-co-AA in PBS.

5.5.2. Oxygen sensitivity

The oxygen sensitivities were investigated in a thin hydrogel layer at 20 °C, and the results were fitted using the two-site model[17] (Fig. 5.18 - 20) and summarized in Table 1.

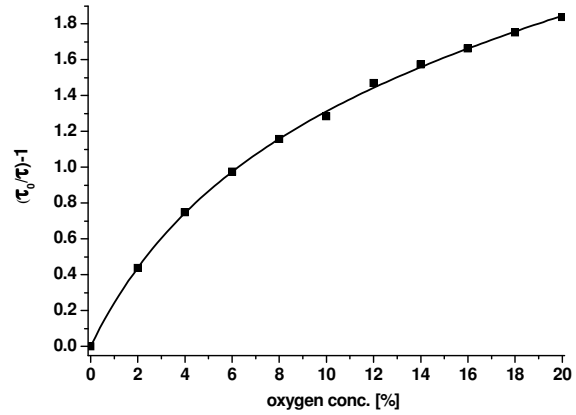

Fig. 5.18. Oxygen sensitivities of PtTFPP-PS-co-AA particles in hdyrogel D4 and two-site model fit.

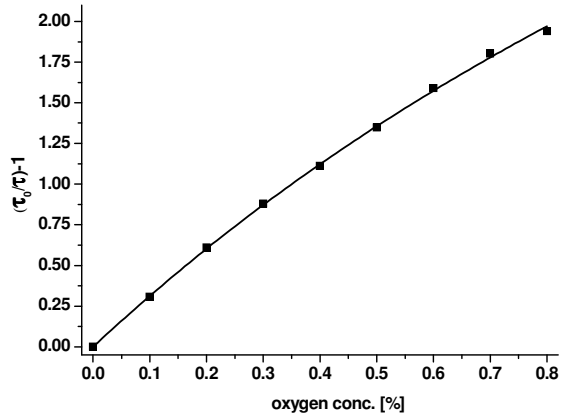

Fig. 5.19. Oxygen sensitivities of PdTFPP-PS-co-AA particles in hdyrogel D4 and two-site model fit.

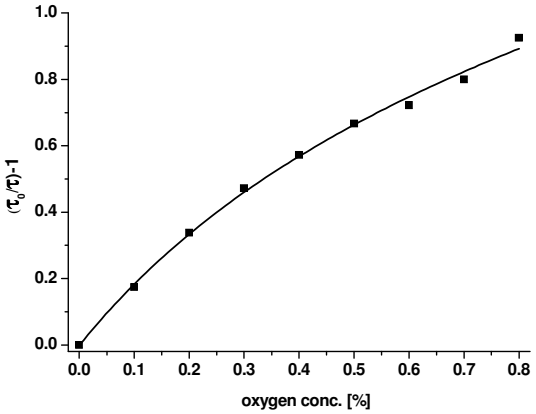

Fig. 5.20. Oxygen sensitivities of PdTPTBP-PS-co-AA particles in hdyrogel D4 and two-site model fit.

Table 5.1: Oxygen sensitivities of dyed PS-co-AA nanobeads in hydrogel D4 at 20 °C

Probe	k_1 [%(O_2)/L]	f_1	k_2 [%(O_2)/L]	f_2
PtTFPP	0.389	0.69	0.008	0.31
PdTFPP	3.68	0.89	0	0.11
PdTPTBP	3.32	0.61	0.10	0.39

PtTFPP-PS-co-AA particles give a sensitivity that covers the whole range from anerobic conditions to ambient air, whereas PdTFPP-PS-co-AA and PdTPTBP-PS-co-AA give a sensitivity that is about an order of magnitude higher. Those probes can be used for determination of lower oxygen amounts.

5.6. Conclusion

Dye-doped polymer nanospheres are a versatile platform that can be engineered to give desired sensitivities for different species, as shown here for oxygen, temperature and protein-sensitive nanobeads that work via an energy transfer mechanism. Because carboxylic acid functional groups can be integrated into the nanoparticles with relative ease, and the size can be manipulated to some extent via the polymer and nanoparticle synthesis, they can be manufactured to be long-term stable in aqueous buffer systems, and allow further surface manipulation. Their main advantages over simple molecular dyes are the increased brightness due to the presence of many dyes in a single particle, and the absence of interactions between the individual dyes in multiple sensing applications. Poly(methacrylonitrile) spheres are attractive for probes that show an unwanted interaction with oxygen, but can not be used with poly(acrylonitrile) because of lack of solubility or stability in the polymer itself or in the

solvents required for it, which is frequently the case for metalloporphyrins or lanthanide chelates. Polystyrene-based nanospheres, on the other hand are attractive for oxygen probes, because of the high oxygen permeability of these polymers.

5.7. References

[1] P. Alivisatos, *Nat. Biotechnol.* **2004** *22*, 47-52.

[2] A. Van Blaaderen, A. Vrij, *Langmuir* **1992**, 8, 2921-2931.

[3] L. B. Bangs, *Am. Biotechnol. Lab.* **1987**, *5*, 10-16.

[4] E. J. Park, M. Brasuel, C. Behrend, M. A. Philbert, R. Kopelman, *Anal Chem* 2003, *75*, 3784-3791.

[5] R. Meallet-Renault, P. Denjean, R. B. Pansu, *Sens. Actuators, B* **1999**, *59*, 108-112.

[6] E. P. Diamandis, *Clin. Chem.* **2001**, *47*, 380-381.

[7] J. Kuerner, O. S. Wolfbeis, I. Klimant, *Anal. Chem.* **2002,** *74*, 2151-2156.

[8] C. Krause, *Optosense PD synthesis instructions (internal document)*, Wörth a. d. Isar, **2004**.

[9] C. Krause, *Optosense PD dyeing instructions (internal document)*, Wörth a. d. Isar, **2004**.

[10] W. Römer, Immunochromatographischer Schwangerschaftstest, *Graduate Thesis, University of Regensburg*. Regensburg, **2000**.

[11] M. Schaeferling, M. Wu, J. Enderlein, H. Bauer, O. S. Wolfbeis, *Appl. Spectrosc.* **2003**, *57*, 1386-1392.

[12] J. E. Rogers, K. A. Nguyen, D. C. Hufnagle, D. G. McLean, W. Su, K. M. Gossett, A. R. Burke, S. A. Vinogradov, R. Pachter, P. A. Fleitz, J. Phys. Chem. **2003**, *107*, 11331-11339.

[13] S. A. Vinogradov, D. F. Wilson, *J. Chem. Soc. Perkin Trans. 2* **1995**, *1*, 103-111.

[14] S. A. Vinogradov, D. F. Wilson, *Adv. Exp. Med. Biol.* **1997**, *411*, 597-603.

[15] G. E. Khalil, K. Lau, G. D. Phelan, B. Carlson, M. C. Gouterman, Martin; J. B. Callis, L. R. Dalton, *Rev. Sci. Inst.* **2004**, *75*, 192-206.

[16] S. M. Borisov, O. S. Wolfbeis, *Anal. Chem.* **2006**, *78*, 5094-5101.

[17] J. N. Demas, B. A. DeGraff, W. Xu, *Anal. Chem.* **1995,** *67***,** 1377-1380.

CHAPTER 6

MICROARRAY ANALYSIS OF PROTEIN-PROTEIN INTERACTIONS BASED ON FRET USING SUBNANOSECOND-RESOLVED FLUORESCENCE LIFETIME IMAGING

6.1. Introduction

Microarrays are indispensable tools in modern biomedical research and allow large-scale investigations with minute amounts of sample.[1] DNA microarrays are an established technique used and commercialized in many different formats. The adaption of these successful formats onto other areas such as protein analysis[2,3] was a main focus in recent years. To this end, a lot of research has been devoted towards detection technologies, particularly as proteins show huge differences in natural abundancy, are structurally diverse and often unstable and therefore require highly reliable and reproducible analysis methods.[4] Many different kinds of protein- and antibody-based biosensors and assays on microarrays and other formats have been developed in recent years, using a variety of different recognition elements such as antibodies or antibody fragments, polynucleotides (e.g. peptide nucleic acids, aptamers), molecularly imprinted polymers, natural receptors and others (reviewed in Ref.s 5, 6).

Most of the detection methods in microarrays and other protein sensors and assays are based on fluorescence, due to its sensitivity, ease of use and the ability to obtain high spatial resolution. Another useful property is its versatility because various parameters can be employed for analysis, such as fluorescence intensity, anisotropy or lifetime.[7,8] The latter contains attractive information because it is largely independent of interferences that usually

cause noise in fluorescence measurements such local heterogeneities, photobleaching or scattering effects. Fluorescence lifetime has been used for detection of DNA microarrays using the lifetime differences of Cy3 and Cy 5[9] and with various near-infrared (NIR) dyes using the lifetime as additional dimension for multiplexing.[10]

In the field of protein arrays, the intrinsic UV fluorescence lifetime of the fluorescent aromatic amino acids of various proteins has been used for protein identification.[11,12] Those methods used only the difference between individual fluorescence lifetimes, we have sought a method that employs the change in fluorescence lifetime itself as the analytical signal. Used in this way, the fluorescence lifetime itself does become the dynamic signal, and can be used just as fluorescence intensity or any other signal for data evaluation. Because of the advantages discussed above is free of the shortcomings and artifacts of fluorescence intensity measurements.

An attractive means to achieve this is the use of FRET between two fluorescent dyes, which only occurs upon close molecular scale proximity between the dyes as in the case of a binding event. Binding leads to an increase in the emission of the acceptor dye, when the donor is excited, and a decrease in donor fluorescence intensity and lifetime due to resonance energy transfer that can be regarded as a dynamic quenching effect on the donor.[13] Because of the advantages discussed above, FRET is extensively used in the lifetime mode in fluorescence microscopy (Fluorescence Lifetime Imaging Microscopy (FLIM), [14-16]). This approach can also be multiplexed as shown in a tissue microarray.[17] FRET techniques were already used in various areas in microarrays e.g. in DNA microarrays in a molecular beacon-type approach[18,19] or in peptide-protein arrays[20] or PNA-based microarray libraries.[21]

In our approach, we have used the biotin-streptavidin model system employing biotinylated Bovine Serum Albumin as the protein interaction partner of streptavidin. This

system is widely used in bioanalysis and for model studies because it ensures a complete interaction between the binding partners due to its femtomolar dissociation constant.[22] A competitive assay was chosen (reviewed in Ref. 23). Competitive assays are preferred for quantitative protein array readout because they display a constant background in case of unspecific binding, better linearity, and the abilities to accommodate binding partners of different specificities (binding constants) as well as to adjust the desired dynamic ranges. They have been extensively used in the microarray field, e.g. for antibody affinity arrays of ovary and kidney samples,[24] in breast cancer protein antibody arrays[25] or pathogen arrays.[26]

6.2. Experimental part

6.2.1. Protein labeling

Alexa 555 and Alexa 647 (Molecular Probes, www.probes.com) were conjugated to biotinylated Bovine Serum Albumine (BSA-Bio, from Sigma, www.sigma-aldrich.com) and Straptavidin (from Interchim (www.interchim.com), respectively via their reactive NHS-Esters, in a solution of bicarbonate buffer 100 mM, pH 8.5, at room temperature (RT) for 1 h. Buffer exchange and removal of excess dye was accomplished by dialysis on Visking cellulose membranes (from Roth, www.carl-roth.de) for three days against PBS buffer 150 mM, pH 7.2, at 4 °C. Protein concentration was subsequently determined by the BCA assay (Pierce, www.piercenet.com).

6.2.2. Microarray production and incubation

Alexa 555-BSA-Biotin was spotted in a concentration of 1 µM in PBS buffer, 150 mM, pH 7.2, from Genetix (http://www.genetix.com) 384 well microplates at 50 % humidity overnight at 20 °C with an Omnigrid Arrayer (www.genomic-solutions.com), using an SMP3 pin. It produced spots of roughly 150 µm diameter (depending on the surface) and 400 µm spacing. The slides were subsequently kept in the fridge for 4 days. The surfaces used were a commercially available epoxy monolayer slides from Cel Associates (www.cel-1.com) and a 20 nm thick epoxy layer (ARChip Epoxy[27]) and a 250 nm hydrogel layer (ARChip Gel[28]), both provided by ARC. The microarrays were blocked with PBS-T (0.1 % Tween 20) and incubated for 1 h at RT with 100 µL of 100 nM Alexa 647-Streptavidin and washed with PBS-T for 5 min at RT and PBS overnight at 4 °C. The assay was performed in a competitive format. In this type of assay, the analyte does not need to be labeled, and is always present in excess and therefore binds quantitatively to the microarray surface because it competes for binding with a fluorescently labeled reference of itself that is added to the incubation solution. Therefore, binding always takes place, but the extent to which the fluorescently labeled reference binds, determines the analyte concentration. Here, an overall concentration of 100 nM Streptavidin was added to each slide, and the fraction of Alexa 647-streptavidin was increased from 0 % to 100 % in steps of 20 %.

6.2.3. Fluorescence excitation and detection

Fluorescence was excited using a Spectra Physics (www.spectraphysics.com) laser system composed of a mode-locked model 2020 argon-ion laser (80 MHz, 200 ps, 30 nJ) which was cavity-dumped by a model 344 S Cavity Dumper at a frequency of 80 kHz in order to

increase the pulse energy (120 nJ) and to adapt the repetition rate to the requirements of an intensified CCD camera (4 Picos, Stanford Computer Optics, www.stanfordcomputeroptics.com), which was used for fluorescence detection. Laser and camera were linked by custom-built electronics, whereby a Tektronix 7603 sampling oscilloscope (www.tektronix.com) was used for monitoring the excitation laser pulse (Fig. 6.1a). The laser light was channeled into a Zeiss Axiotech Vario microscope equipped with a 20x NA 0.5 objective (EC-Epiplan-Neofluar HD/DIC, www.zeiss.com) and a micropositioning system SCAN 225 x 75 from Maerzhaeuser-Wetzlar (www.marzhauser.com) using a custom mechanical slider built around a Filtercube (452888) equipped with a 514-10 laser excitation filter, a z532rdc dichroic mirror and a D580-60 emission filter, all from AHF Analysentechnik (www.ahf.de) (Fig. 6.1b and c). The temporal characteristics of the laser excitation pulse at the camera were quantified using an identical setup as in the microarray experiments but without emission filter and using a microscope slide covered with a 6 µm ethyl cellulose layer (which served as a non-fluorescent scattering sample, Fig. 6.1b).

6.2.4. Image acquisition and analysis

Two images were aquired for each spot at set delays of 2 and 3 ns (relative to the time scale in Fig. 6.1b) using the 4 Spec software of Stanford Computer Optics. Lifetime images were then calculated according to the Rapid Lifetime Determination scheme[29] and analyzed using a custom-built program written in IDL, Version 5.3.1 from ITT visual information solutions (http://www.ittvis.com). All lifetime images shown are unbiased raw data without noise reduction routines.

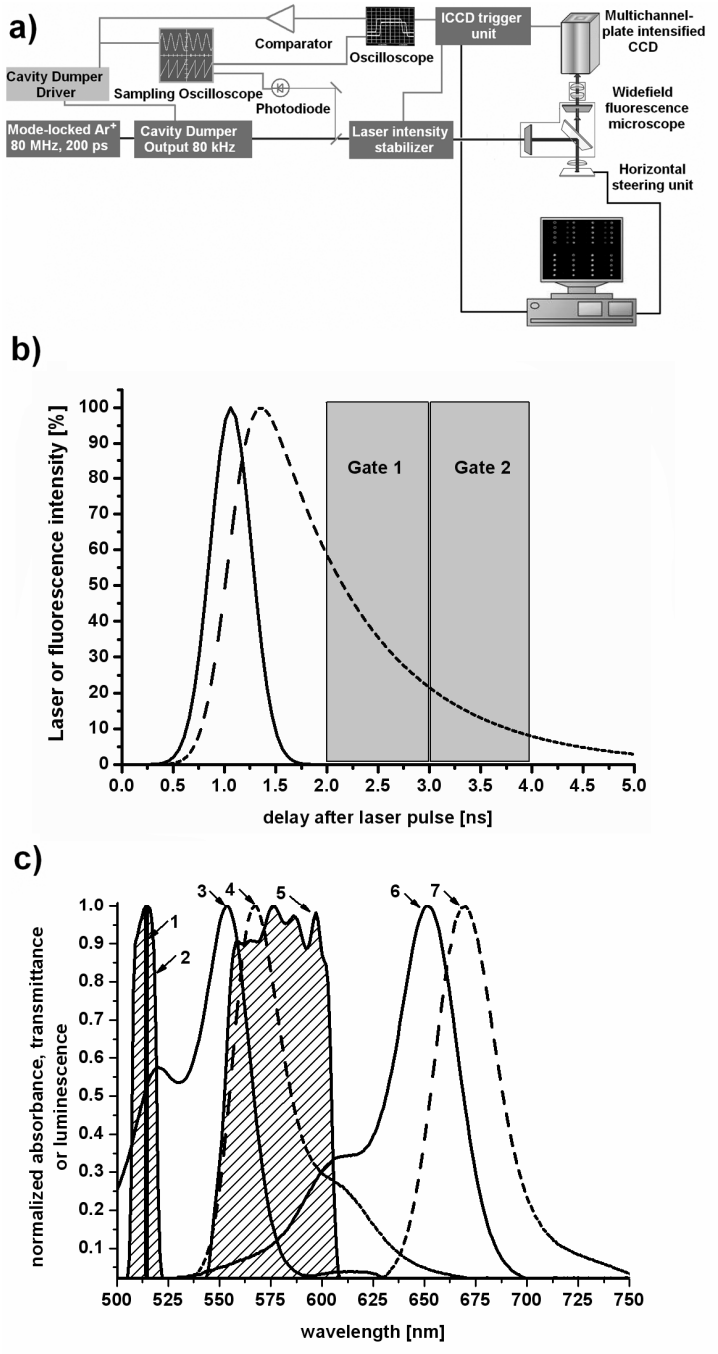

Fig. 6.1. a) Experimental setup of the fluorescence lifetime microarray imaging system based on a cavity dumping and mode-locking argon-ion laser system. b) time course of the laser intensity (Gauss fit, straight line) measured at the ICCD, a simulated single exponential fluorescence decay (τ = 1 ns, dashed line) and the image acquisition gates. c) The spectral setup. Laser pulse at 514.5 nm (1), 514-10 excitation filter (2), absorption (3) and emission spectrum (4) of Alexa 555-BSA-Biotin, combined transmittance spectrum of z532rdc dichroic mirror and D580-60 emission filter (5), Alexa 647-Streptavidin absorption (6) and emission spectrum (7).

6.3. Results and discussion

The microarrays were incubated in 100 µL of a 100 nM streptavidin solution in PBS buffer, in order to ensure complete binding and therefore being able to view the whole dynamic range of lifetime change possible. The competitive nature of the assay ensured that no artifacts entered the calibration, as the binding of a second protein alone can cause a change in intensity and lifetime (usually an increase) due to the rigidization of the local dye environment. The obtained Alexa 555-BSA-Bio lifetimes upon streptavidin binding in absence of acceptor dye were nearly identical at almost 1.7 ns for all three surfaces (Table 6.1), which is higher than for non-incubated microarrays with Alexa 555-BSA-Bio alone which were all around 1.3 ns (not shown) and mostly reported for protein conjugates of this dye. This can be explained by the binding of the second protein.

The fact that recording was only started about 1 ns after the peak of the laser pulse also gives a bias towards longer lifetimes components, as the fluorescence lifetimes of such complex protein conjugates is highly multiexponential due to the different microenvironments where the dyes are located. The RLD method was chosen because it allows fast construction of average lifetime maps and gives reliable information about the relative extent of lifetime change. Due to its origin in just two images at different delay times it is not very accurate in calculating absolute lifetimes in the event of multiexponential fluorescence decays. [30]

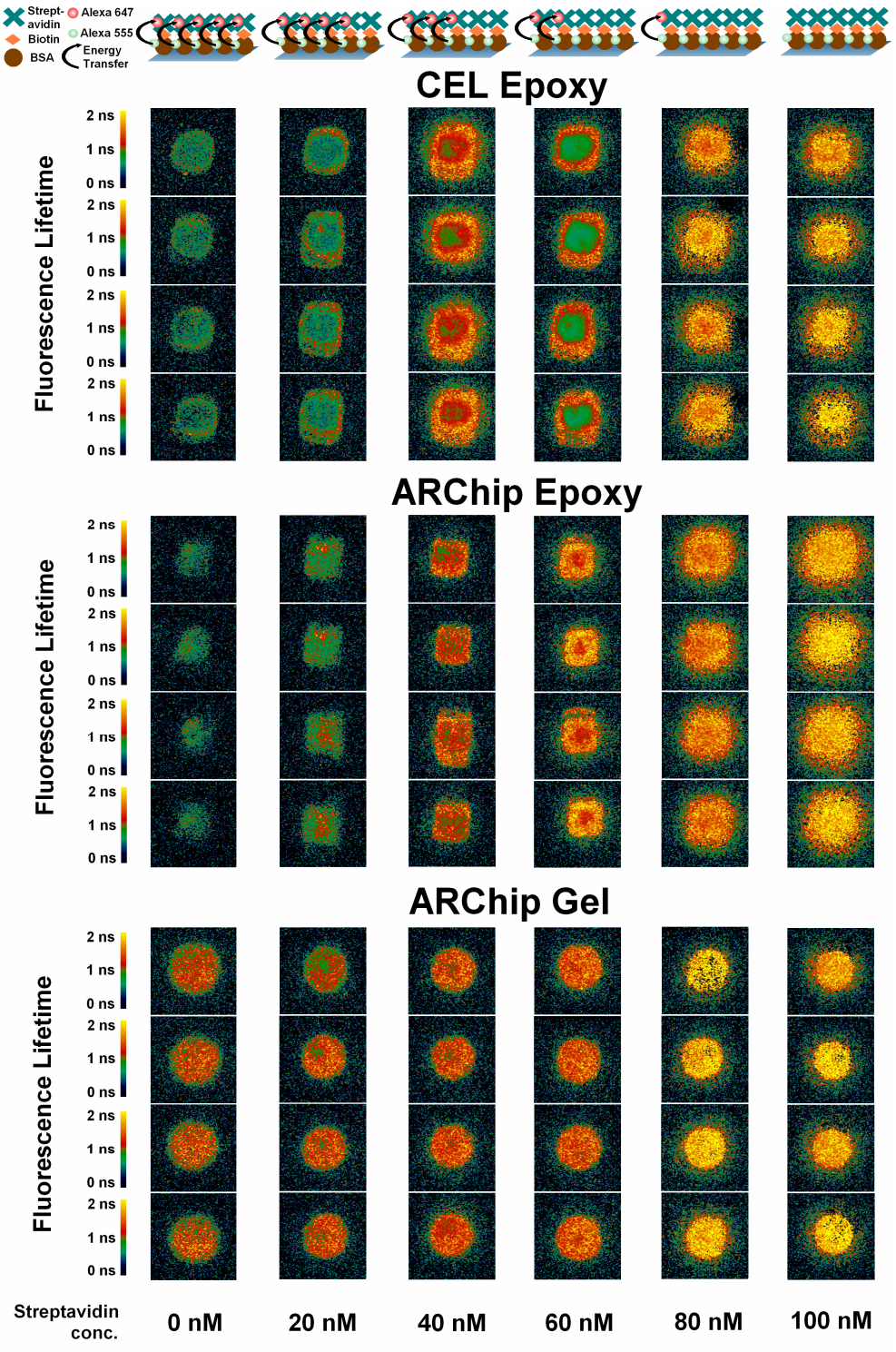

Fig. 6.2. Lifetime maps of Alexa 555-BSA-Biotin spots incubated with various amounts of Streptavidin on three different surfaces. Shown on top is a schematic of the competitive assay (for simplicity, single FRET interactions are shown, in reality each protein carried approx. two fluorophores and the BSA was conjugated to approx. 9 biotins, on average).

A very pronounced change in fluorescence lifetime could be observed upon addition of acceptor-labeled streptavidin (Fig. 6.2) on all surfaces. In the case of the epoxy-surfaces almost complete quenching could be observed at 100 nM acceptor dye concentration showing that the proteins bind very closely and their interaction can be monitored via lifetime change. In fact, at 100 nM Alexa 647-Streptavidin the fluorescence intensity of Alexa 555-BSA-Bio on the epoxy slides is too low for achieving an accurate signal-to noise ratio for fluorescence lifetime calculation. For this reason, those data points were ignored (Fig. 6.3). The remaining data points, however, show a good linearity and therefore allow an easy construction of the calibration curve using a simple linear fit. A broad linearity of the assay, usually over more than two orders of magnitude is another advantage of the competitive approach. [23]

The fluorescence intensity and lifetime quenching on the hydrogel slides is less pronounced than on the epoxy slides, and whereas the curve initially also shows a good degree of linearity the quenching appears to be already saturated at around 60 % of labeled streptavidin. The reason for this behavior might be a partially inhibited diffusion of the streptavidin within the hydrogel matrix after the spotting and blocking step. The CEL epoxy slides appeared to be best suited to the experimental protocol that we have chosen. Distinct lifetime changes can be observed on all surfaces, and can certainly be optimized with respect to the requirements of individual surfaces. The method does not depend on specific surface properties, and all microarray surfaces that allow for specific protein binding can be applied, in principle.

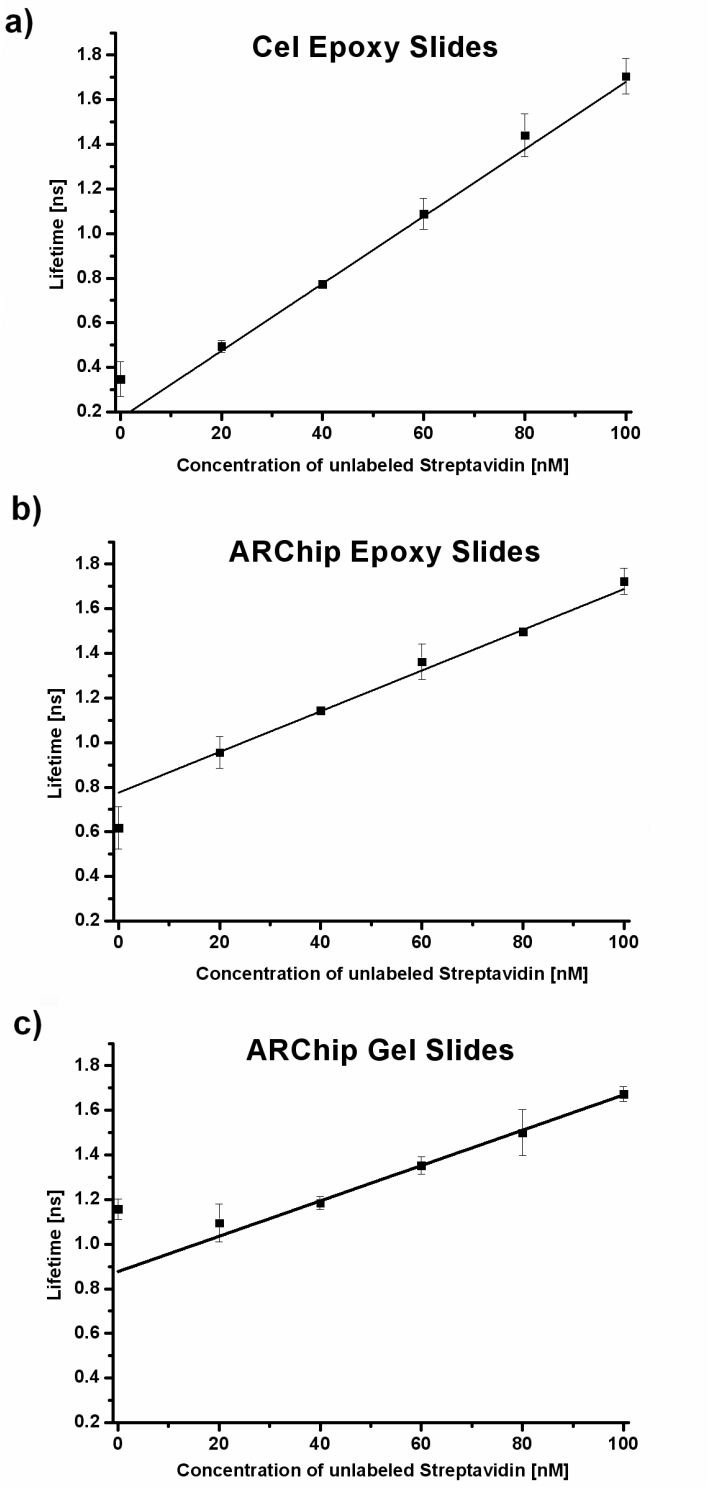

Fig. 6.3. Average lifetimes of Alexa 555-BSA-Biotin after incubation with Streptavidin on a) Cel epoxy slides, b) ARChip Epoxy slides, and c) ARChip Gel slides and linear fits. Error bars show deviations between individual spots.

Table 6.1. Parameters of FRET-FLIM detection of streptavidin binding on different surfaces.

Slide Surface	Cel Epoxy	ARChip Epoxy	ARChip Gel
Alexa555-BSA-Biotin-Lifetime in the absence of Alexa 647-Streptavidin [ns]	1.70 ± 0.07	1.72 ± 0.06	1.67 ± 0.03
Alexa555-BSA-Biotin-Lifetime with excess of Alexa 647-Streptavidin [ns]	0.35 ± 0.08	0.62 ± 0.10	1.16 ± 0.05
Relative Standard Deviation [% RSD]	7.83	6.32	4.35
R^2 of the linear fit (Fig. 6.3)	0.995	0.991	0.994
Detection Limit [nM]*	1.11	1.85	2.11

*: Defined as 1 % signal change.

6.4. Conclusion

The determination of FRET by fluorescence lifetime imaging was shown as an advanced combined method for the analysis of protein-protein interactions on microarrays. Binding of a labeled FRET acceptor protein conjugate could be monitored via lifetime change and the method displays the common advantages of lifetime-based schemes having good precision, sensitivity and little susceptibility for interferences. The method is especially suited for use in the competitive assay format, as applied here, because a strong, adjustable signal change and a good linearity of the lifetime curve can be achieved upon the displacement of labeled reference with unlabeled analyte.

Our setup was capable of achieving precise and reliable results, and it also shows a high degree of flexibility. Many lasers of different design, emission wavelengths and repetition rates can be integrated into it without major difficulties. Concerning the optical setup there is still potential for further noise reduction and greater accuracy. The improved contrast and therewith signal-to-noise ratio compared to fluorescence intensity imaging indicates good potential for further development. The lifetime-based evaluation can also complement intensity-based protein microarray imaging and is therefore able to introduce an additional dimension for evaluation. Finally, although two common microarray dyes were used here, the method is applicable with other FRET donor/acceptor pairs applied to protein microarrays, such as Cy3/Cy5 or fluorescent proteins.

6.5. References

[1] C. M. Niemayer, D. Blohm, *Angew. Chem. Int. Ed.* **1999**, *38*, 2865-2869.

[2] D. N. Howbrook, A. M. van der Valk, M. C. O'Shaughnessy, D. K. Sarker, S.C. Baker, A. W. Llyod, *Drug Discovery Today,* **2003**, *8*, 642-651.

[3] M. F. Templin, D. Stoll, J. M. Schwenk, O. Pötz, S. Kramer, T. O. Joos, *Proteomics* **2003**, *3*, 2155-2166.

[4] V. Espina, E. C. Woodhouse, J. Wulfkuhle, H. D. Asmussen, E. F. III Petricoin, L. A. Liotta, *J. Immunol. Methods* **2004**, *290*, 121-133.

[5] H. Nakamura, I. Karube, *Anal. Bioanal. Chem.* **2003**, *377*, 446-468.

[6] D. Altschuh, S. Oncul, A. P. Demchenko, *J. Mol. Recognit.* **2006**, *19*, 459-477.

[7] S. Nagl, M. Schaeferling, O. S. Wolfbeis, *Microchim. Acta* **2005**, *151*, 1-21.

[8] M. Schaeferling, S. Nagl, *Anal. Bioanal. Chem.* **2006**, *385*, 500-517.

[9] G. Valentini, C. D'Andrea, D. Comelli, A. Pifferi, P. Taroni, A. Torricelli, R. Cubeddu, C. Battaglia, C. Consolandi, G. Salani, L. Rossi-Bernardi, G. De Bellis, *Opt. Lett.* **2000**, *25*, 1648-1650.

[10] E. Waddell, Y. Wang, W. Stryjewski, S. McWhorter, A. C. Henry, D. Evans, R. L. McCarley, S. A. Soper, *Anal. Chem.* **2000**, *72*, 5907-5917.

[11] H.-M. Striebel, P. Schellenberg, P. Grigaravicius, K. O. Greulich, *Proteomics* **2004**, *4*, 1703-1711.

[12] M. Schüttpelz, C. Müller, H. Neuweiler, M. Sauer, *Anal. Chem.* **2006**, *78*, 663-669.

[13] K. E. Sapsford, L. Berti, I. L. Medintz, *Angew. Chem. Int. Ed.* **2006**, *45*, 4562-4588.

[14] K. Suhling, P. M. W. French, D. Phillips, *Photochem. Photobiol. Sci.* **2005**, *4*, 13-22.

[15] Y. Gu, D. Zicha, in Encyclopedia of Genetics, Genomics, Proteomics and Bioinformatics, Wiley, New York, **2006**.

[16] W. Zhong, M. Wu, C.-W. Chang, K. A. Merrick, S. D. Merajver, M.-A. Mycek, *Opt. Express* **2008**, *15*, 18220-18235.

[17] A. Kong, P. Leboucher, R. Leek, V. Calleja, S. Winter, A. Harris, P. J. Parker, B. Larijani, *Cancer Res.* **2006**, *66*, 2834-2843.

[18] A. G. Frutos, S. Pal, M. Quesada, J. Lahiri, *J. Am. Chem. Soc.* **2002**, *124*, 2396-2397.

[19] H. Kim, M. D. Kane, S. Kim, W. Dominguez, B. M. Applegate, S. Savikhin, *Biosens. Bioelectron.* **2007**, *22*, 1041-1047.

[20] K. Usui, M. Takahashi, K. Nokihara, H. Mihara, *Mol. Diversity* **2004**, *8*, 209-218.

[21] J. J. Díaz-Mochón, L. Bialy, M. Bradley, *Chem. Commun.* **2006**, *38*, 3984-3986.

[22] M. Wilchek, E. A. Bayer, *Methods Enzymol.* **1990**, *184*, 5-13.

[23] R. Barry, M. Soloviev, *Proteomics* **2004**, *4*, 3717-3726.

[24] R. Barry, T. Diggle, J. Terrett, M. Soloviev, *J. Biomol. Screen.* **2003**, *8*, 257-263.

[25] G. Yeretssian, M. Lecocq, G. Lebon, H. C. Hurst, V. Sakanyan, *Mol. Cell. Proteomics* **2004**, *4*, 605-617.

[26] T. Kostić, A. Weilharter, S. Rubino, G. Delogu, S. Uzzau, K. Rudi, A. Sessitsch, L. Bodrossy, *Anal. Biochem.* **2007**, *360*, 244-254.

[27] K. Derwinska, L. A. Gheber, C. Preininger, *Anal. Chim. Acta* **2007**, *592*, 132-138.

[28] K. Derwinska, L. A. Gheber, U. Sauer, L. Schorn, C. Preininger, *Langmuir* **2007**, *23*, 10551-10558.

[29] R. J. Woods, S. Scypinski, L. J. C. Love, H. A. Ashworth, *Anal. Chem.* **1984**, *56*, 1395-1400.

[30] K. K. Sharman, A. Periasamy, H. Ashworth, J. N. Demas, N. H. Snow, *Anal. Chem.* **1999**, *71*, 947-952.

7. Summary

This thesis describes applications of fluorescence lifetime imaging in multiple chemical sensing approaches. Using fluorescence lifetime as an analytical parameter allows extracting more information out of probes than fluorescence intensity measurements and it is therefore attractive in order to quantitate multiple species. It leads to better data quality as fluorescence lifetime measurements are not or less affected by many sources of noise in fluorescence signals such as straylight and other scattering phenomena, background fluorescence, inhomogeneous fluorophore concentration in the sensing layer, excitation light intensity, or filter transmissions, and photobleaching. It is also superior for FRET measurements as no errors due to background excitation of the acceptor molecule are monitored when observing lifetime decrease of the donor molecule.

Chapter 2 introduced a novel oxygen probe, the fullerene compound C_{70}, which displays the unusual phenomenon of thermally activated, delayed fluorescence (TADF) with a lifetime in the ms domain. Due to the long lifetime of this process, which involves repeated cycles of this molecule between the singlet and the triplet state, it is exceptionally sensitive to oxygen. We embedded C_{70} into highly oxygen permeable polymeric matrices, a phenyl-substituted organosilica, and an ethyl cellulose and observed ppb (v/v) sensitivities of the delayed fluorescence lifetime in the temperature range of 0 to 120 °C. These properties make the fullerene layers superior both in terms of oxygen sensitivities and usable temperature range compared to fluorescent oxygen probes known to date.

Those materials, sensitive to trace oxygen amounts, were then used in chapter 3 along with a highly temperature sensitive probe, the Ruthenium-tris-phenanthroline complex in a dual sensing layer that is able to measure both temperature and trace oxygen amounts simultaneously. In order to avoid interference of oxygen to the Ru-complex it was embedded

into a poly(acrylonitrile) matrix. Because of differing solubilities of the polymers the oxygen permeable matrix containing C_{70} in organosilica or ethyl cellulose can be applied on top of the temperature sensitive layer containg the Ru-complex and both analytes can be monitored in the range of 0 - 50 ppm oxygen and 0 - 120 °C. The lifetime of both probes in response to the analytes was recorded and the separation of the signals was achieved by spectral as well as luminescence lifetime discrimination, as the emission of the Ru-complex was monitored between 550 and 610 nm, and in the µs domain, and the fullerene was monitored between 650 and 710 nm and in the ms domain.

In chapter 4, a method that allows for discrimination of two species purely based on luminescence lifetimes without spectral separation was introduced. A scheme was described, based on a dual application of the Rapid Lifetime Determination (RLD) method, that records four time gates within the emission period whereby the last two are used for measuring the analyte sensed by the longer-lived probe and this information was used to decipher the second species from the first two windows that gives a mixed signal of both analytes. By appropriate choice of the experimental conditions both sensitivity and operating range could be adjusted as desired for the application. The scheme was demonstrated in a dual oxygen and temperature sensor using a platinum porphyrin compound as the oxygen sensitive probe and a europium chelate as the temperature probe.

In chapter 5 uses of luminescent nanoparticles in multiple sensing applications were pointed out. Novel poly(methacrylonitrile)-based copolymer nanobeads were presented with diameters down to less than 30 nm that can be used as biological labels as demonstrated on a homogeneous FRET-based protein assay using a platinum porphyrin inside biotinylated nanoparticles as donors and the red-emitting cyanine dye Cy5 coupled to streptavidin as FRET acceptors. When stained with a palladium benzoporphyrin compound those nanoparticles can be used as red-excitable, long lifetime, high brightness probes favorable for

applications with a high biological background absorbance. Poly(methacrylonitrile)-based nanospheres stained with a europium compound, on the other hand, were found to be efficient temperature-sensitive components for multiple sensors. For oxygen-sensing applications polystyrene-based beads are preferred for its high oxygen permeability. Syntheses, staining, and determination of oxygen sensitivities of metalloporphyrins in these beads were shown. The spheres do also possess a carboxylic acid group that allows further manipulation.

In chapter 6 miniaturized multiple protein sensing based on fluorescence lifetime imaging with subnanosecond resolution on microarrays was presented in a model assay. Alexa 555-stained biotinylated bovine serum albumin was immobilized on various surfaces and FRET to Alexa 647-dyed streptavidin was observed in a competitive assay approach using the fluorescence lifetime decrease in the donor channel. Excitation was carried out using a mode-locked cavity-dumped picosecond Ar^+-laser operating at 514.5 nm at 80 kHz and the temporal characteristics of the emission were recorded using a microchannelplate intensified CCD camera. The maximum lifetime decrease on an epoxysilane-based surface was found to be almost 90 % meaning that the method has is able to monitor minute concentration changes.

8. Abbreviations, Acronyms and Symbols

atm.	atmospheric
BCA	bicinchoninic acid
Bs	brightness
BSA	bovine serum albumine
BSA-Bio	biotinylated bovine serum albumine
CCD	charge-coupled device
Cy3	3H-Indolium, 2-[3-[1-[6-[(2,5-dioxo-1-pyrrolidinyl)oxy]-6-oxohexyl]-1,3-dihydro-3,3-dimethyl-5-sulfo-2H-indol-2-ylidene]-1-propen-1-yl]-1-ethyl-3,3-dimethyl-5-sulfo-, inner salt.
Cy5	3H-Indolium, 2-[5-[1-[6-[(2,5-dioxo-1-pyrrolidinyl)oxy]-6-oxohexyl]-1,3-dihydro-3,3-dimethyl-5-sulfo-2H-indol-2-ylidene]-1,3-pentadien-1-yl]-1-ethyl-3,3-dimethyl-5-sulfo-, inner salt.
DCE	1,2-dichloroethane
DF	delayed fluorescence
DLD	dual lifetime determination
DLS	dynamic light scattering
DNA	desoxyribonucleic acid
EC	ethyl cellulose
EDC	1-ethyl-3-(3-dimethylaminopropyl) carbodiimide hydrochloride
$Eu(tta)_3$	europium(III)-tris(theonyltrifluoro-acetonate)-trihydrate
$Eu(tta)_3dpbt$	europium(III)-tris(theonyltrifluoro-acetonato)-2-(4-diethylamino-phenyl)-4,6-bis(3,5-dimethylpyrazol-1-yl)-1,3,5-triazine)
f_1, f_2	molar fractions in the two-site Stern-Volmer model
FAD	flavin adenine dinucleotide (oxidized form)
$FADH_2$	flavin adenine dinucleotide (reduced form)

FL	fluorescence lifetime
FLIM	fluorescence lifetime imaging microscopy
FRET	förster resonance energy transfer
ICCD	intensified charge-coupled device
IR	infrared
ISC	intersystem crossing
IUPAC	international union of pure and applied chemistry
K_{SV}^1 , K_{SV}^2	quenching constants in the two-site Stern-Volmer model
k_q	quenching constant in the Stern-Volmer model
LED	light emitting diode
LOD	limit of detection
MAP	modified atmosphere packaging
MES	2-(N-morpholino)ethanesulfonic acid hydrate
MIP	molecularly imprinted polymer
MS	mass spectrometry
ms	milliseconds
NAD^+	nicotine adenine dinucleotide (oxidized form)
NADH	nicotine adenine dinucleotide (reduced form)
NHS	N-hydroxysuccinimide
NIR	near-infrared
nm	nanometer
ns	nanoseconds
OS	organosilica
PAN	poly(acrylonitrile)
PB	phosphate buffer

PBS	phosphate buffered saline
PBS-T	phosphate buffered saline containing Tween 20
PCR	polymerase chain reaction
PD	polymer derivative (poly(methacrylonitrile co- acrylic acid co-divinylstyrene)
PdOEP	palladium octaethylporphyrin
PdTFPP	palladium meso-tetrapentafluorophenylporphyrin
PdTPTBP	meso-tetraphenyltetrabenzoporphine palladium(II)-complex
PF	prompt fluorescence
PMAN	poly(methacrylonitrile)
PNA	peptide nucleic acid
ppbv	parts per billion (volume/volume)
ppm	parts per million
ps	picoseconds
PS	polystyrene
PS-co-AA	poly(styrene-co-acrylic acid)
PSP	pressure sensitive paint
PTBS	poly(4-tert.butylstyrene)
PTMSP	poly(trimethylsilylpropyne)
PtTFPP	platinum meso-tetrapentafluorophenylporphyrin
PVMK	poly(vinylmethylketone)
QY	quantum yield
r^2	correlation coefficient
RLD	rapid lifetime determination
RNA	ribonucleic acid
RSD	relative standard deviation

RT	room temperature
$Ru(dpp)_3$	Ruthenium(II)-tris-(4,7-diphenylphenathroline)- trimethylsilyl-1-propanesulfonate
$Ru(phen)_3$	Ruthenium(II)-tris-1,10-phenanthroline-3-trimethylsilyl-1-propanesulfonate
SDS	sodium dodecyl sulfate
SNP	single nucleotide polymorphism
SPR	surface plsamon resonance
t_{95}	time for 95% of the total signal change to occur
TADF	thermally activated delayed fluorescence
TCSPC	time-correlated single photon counting
TSP	temperature sensitive paint
UV	ultraviolet
UV-Vis	ultraviolet and visible region
µs	microseconds
ΔE_{ST}	energy gap between singlet and triplet state
ε	molar absorbance coefficient
λ_{exc}	excitation wavelength
τ	fluorescence (or luminescence, phosphorescence) lifetime
τ_0	luminescence lifetime in the absence of quencher
Φ_{DF}	delayed fluorescence quantum yield
Φ_F	fluorescence quantum yield
Φ_s	quantum yield of singlet formation
Φ_T	quantum yield of triplet formation

9. Curriculum Vitae

CONTACT INFORMATION

Name: Nagl, Stefan

Address: Rotteneckstr. 25, 93053 Regensburg

Cell Phone: +49-177-4102058

E-mail: st.nagl@web.de

EDUCATION

2004 - present **Graduate Student**

Institute of Analytical Chemistry, Chemo- and Biosensors, University of Regensburg, Supervisor: Prof. Otto S. Wolfbeis.

1997 - 2000, 2001 - 2004 **Diploma in Chemistry**

University of Regensburg, Intermediate Diploma: February 2000, Diploma exams: June 2003, Diploma Thesis (Supervisor Prof. Otto S. Wolfbeis) April 2004, Title: Quantitative Determination of Proteins on Microarrays by Time-Resolved Luminescent Imaging.

2000 - 2001 **Chemistry Erasmus**

Undergraduate Exchange Program in Chemistry, University of Leeds, United Kingdom. Erasmus Certificate June 2001.

1987- 1996 **Grammar School**

Comenius Gymnasium Deggendorf, Majors: English, Chemistry, University Entrance Diploma, June 1996.

EMPLOYMENT HISTORY

2004 - present **Scientific Associate**

Institute of Analytical Chemistry, Chemo- and Biosensors, University of Regensburg.

2003 - 2004 **Student Assistant**

Chemistry Department, University of Regensburg.

1996 - 1997 **Alternative National Service**

Kreiskrankenhaus Deggendorf.

PUBLICATIONS

(12) Carlos Baleizão, Stefan Nagl, Michael Schaeferling, Mário N. Berberan-Santos, Otto S. Wolfbeis, A Dual Fluorescence Sensor for Trace Oxygen and Temperature with a Large Temperature Range and Unmatched Oxygen Sensitivity, *submitted.*

(11) Stefan Nagl, Matthias I. J. Stich, Michael Schaeferling, Otto S. Wolfbeis, A method for simultaneous luminescence sensing and imaging of two species using optical probes of different luminescence decay time, *submitted.*

(10) Stefan Nagl, Reinhard Bauer, Ursula Sauer, Claudia Preininger, Udo Bogner, Michael Schaeferling, Microarray Analysis of Protein-Protein Interactions Based on FRET Using Subnanosecond-resolved Fluorescence Lifetime Imaging, *Biosens. Bioelectron.* **2008**, *in press*.

(9) Anna S. Kocincová, Stefan Nagl, Sarina Arain, Christian Krause, Sergey M. Borisov, Matthias Arnold, Otto S. Wolfbeis, Multiplex bacterial growth monitoring in 24-well microplates using a dual optical sensor for dissolved oxygen and pH, *Biotechnol. Bioeng.* **2008**, *100*, 430-438. http://dx.doi.org/10.1002/bit.21793.

(8) Matthias I. J. Stich, Stefan Nagl, Otto S. Wolfbeis, Ulrich Henne, Michael Schäferling, Dual Fluorescent Sensor Material for Simultaneous Imaging of Pressure and Temperature on Surfaces, *Adv. Funct. Mater.* **2008**, *18*, 1399-1406. http://dx.doi.org/10.1002/adfm.200701199

(7) Stefan Nagl, Otto S. Wolfbeis, Classification of Chemical Sensors and Biosensors Based on Fluorescence and Phosphorescence (Review), Springer Series on Fluorescence 5 - Standardization and Quality Assurance in Fluorescence Measurements, U. Resch-Genger (ed.) Springer, Berlin, **2008**, *in press.*

(6) Sergey M. Borisov, Torsten Mayr, Alexander A. Karasyov, Ingo Klimant, Pawel Chojnacki, Christoph Moser, Stefan Nagl, Michael Schäferling, Matthias I. Stich, Ganna S. Vasilevskaya, Otto S. Wolfbeis, New Plastic Microparticles and Nanoparticles for Fluorescent Sensing and Encoding, Springer Series on Fluorescence 4, Mário Nuno Berberan-Santos (ed.) Springer, Berlin, **2008**. http://dx.doi.org/10.1007/4243_2007_013.

(5) Stefan Nagl, Otto S. Wolfbeis, Optical Multiple Chemical Sensing - Status and Current Challenges (Review), *Analyst* **2007**, *132*, 507-511. http://dx.doi.org/10.1039/b702753b.

(4) Stefan Nagl, Carlos Baleizão, Sergey M. Borisov, Michael Schaeferling, Mário N. Berberan-Santos, Otto S. Wolfbeis, Optical Sensing and Imaging of Trace Oxygen with Record Response, *Angew. Chem. Int. Ed.* **2007**, *46*, 2317-2319. http://dx.doi.org/10.1002/anie.200603754.
Optische Sauerstoffsensorik und -bildgebung im Spurenbereich und mit Rekordansprechverhalten, *Angew. Chem.* **2007**, *119*, 2368-2371. http://dx.doi.org/10.1002/ange.200603754.

(3) Carlos Baleizão, Stefan Nagl, Sergey M. Borisov, Michael Schäferling, Otto S. Wolfbeis, Mário N. Berberan-Santos, An Optical Thermometer Based on the Delayed Fluorescence of C70, *Chem. Eur. J.* **2007**, *13*, 3643-3651. http://dx.doi.org/10.1002/chem.200601580.

(2) Michael Schäferling, Stefan Nagl, Optical Technologies for the Read Out and Quality Control of DNA and Protein Microarrays (Review), *Anal. Bioanal. Chem.* **2006**, *385*, 500-517. http://dx.doi.org/10.1007/s00216-006-0317-5.

(1) Stefan Nagl, Michael Schäferling, Otto S. Wolfbeis, Fluorescence Analysis in Microarray Technology (Review), *Microchim. Acta* **2005**, *151*, 1-21. http://dx.doi.org/10.1007/s00604-005-0393-9.

ORAL PRESENTATIONS

(3) *Fluorescence Lifetime Imaging*, **University of Leipzig** (invited lecture), Leipzig, Germany, 2008.

(2) *Fluoreszente Dualsensoren für Sauerstoff und Temperatur*, **Zweites Doktoranden-Seminar der GDCh, Fachgruppe Analytische Chemie, Arbeitskreise Chemometrik und Labordatenverarbeitung**, **Chemo- und Biosensoren**, **Prozessanalytik** und **Elektroanalytische Chemie**, Attendorn, Germany, 2008.

(1) *Fluorescent chemosensors for oxygen, pH and temperature monitoring: Materials, methods and applications*, **6th International Colloquium on Process Related Analytical Chemistry (PREACH 2007)**, Dortmund, Germany, 2007.

ABSTRACTS AND PRESENTATIONS

(9) *Analysis of Biomolecular Interactions on Micorarray Formats by Time-resolved FRET*, Stefan Nagl, Reinhard Bauer, Ursula Sauer, Claudia Preininger, Udo Bogner, Michael Schäferling, **9th European Conference on Optical Chemical Sensors and Biosensors, Europtrode IX**, Dublin, Ireland, 2008.

(8) *Trace oxygen sensing (ppb range) using fullerene C_{70} in polymeric materials as an optical sensor*, Stefan Nagl, Carlos Baleizão, Sergey M. Borisov, Michael Schäferling, Mário N. Berberan-Santos, Otto S. Wolfbeis, **06º Encontro da Divisão de Química Analítica, SPQ-Analítica '07**, Lisbon, Portugal, 2007

(7) *C70 in Polymer Films as a Temperature Optical Sensor*, Carlos Baleizão, Stefan Nagl, Sergey M. Borisov, Michael Schäferling, Otto S. Wolfbeis, Mário Nuno Berberan-Santos, **210th ECS Meeting**, Cancun, Mexico, 2006.

(6) *Monitoring protein binding on microarrays by fluorescence lifetime imaging using multiple total internal reflection chip assemblies,* Stefan Nagl, Michael Schäferling, Otto S. Wolfbeis, Gerd Sulz, Albrecht Brandenburg, **8th European Conference on Optical Chemical Sensors and Biosensors, Europtrode VIII**, Tübingen, Germany, 2006.

(5) *Luminescence Lifetime Based Simultaneous Imaging of Pressure and Temperature,* Matthias I. Stich, Stefan Nagl, Michael Schäferling, Otto S. Wolfbeis, **8th European Conference on Optical Chemical Sensors and Biosensors, Europtrode VIII**, Tübingen, Germany, 2006.

(4) *Novel Time-Resolved Fluorescence Based Assays and Detection Schemes on Microplates and Microarrays,* Stefan Nagl, Michael Schäferling, Otto S. Wolfbeis, **9th Conference on Methods and Applications of Fluorescence (MAF 9): Spectroscopy, Imaging and Probes**, Lisbon, Portugal, 2005.

(3) *Calibration of Dual Pressure and Temperature-Sensitive Paints Using Luminescence Lifetime Imaging,* Matthias I. Stich, Stefan Nagl, Otto S. Wolfbeis, Michael Schäferling, Ulrich Henne, Rolf H. Engler, Christian Klein, **9th Conference on Methods and Applications of Fluorescence: Spectroscopy, Imaging and Probes (MAF 9)**, Lisbon, Portugal, 2005.

(2) *Intrinsically Referenced Expression Profiling on Microarrays Using Time-Resolved Fluorescent Imaging,* Stefan Nagl, Michael Schäferling, Josef Riedl, **4. Deutsches Biosensor Symposium**, Regensburg, Germany, 2005.

(1) *Time-Resolved Fluorescent Imaging of Oligonucleotide and Protein Microarrays,* Stefan Nagl, Michael Schäferling, Otto S. Wolfbeis, **7th European Conference on Optical Chemical Sensors and Biosensors, Europtrode VII**, Madrid, Spain, 2004

Acknowledgements

I want to thank **Prof. Dr. Otto S. Wolfbeis** for giving me the opportunity to work on this thesis, and for his inspiring leadership and all the assistance throughout.

No less, I thank our group leader **Dr. Michael Schäferling** for all the help throughout this work.

I also want to thank **all present and former colleagues at the institute** for the good atmosphere and lots of mutual help during the course of this work**.**

Our secretary **Edeltraud Schmid** and our present and former technicians **Karl-Heinz Berghausen, Barbara Goricnik, Nadja Hinterreiter** and **Angelika Stoiber** also helped in the years in very many respects.

For all the work on oxygen and temperature sensing, I want to thank for a very good cooperation **Dr. Carlos Baleizão** and **Prof. Mário N. Berberan-Santos** (Instituto Superior Técnico, Lisbon) as well as former and current members of the Institute **Dr. Sergey Borisov and Dipl.-Chem. Matthias Stich**. I am also grateful to **Dr. Jürgen Baier** (Institute of Dermatology) and **Dr. Edith Schnell** (Institute of Physical Chemistry) of the University of Regensburg.

Concerning the work on nanoparticles, I want to express my gratitudes to **Dr. Christian Krause** (Presens GmbH, Regensburg), **Dr. Miriam Breunig** and **Prof. Achim Göpferich** (Institute of Pharmaceutical Technology) and **Prof. Ralph Witzgall** (Institute of Molecular and Cellular Anatomy, University of Regensburg)

For all the work on the microarray project, I want to thank **Dr. Reinhard Bauer** and **Dr. Udo Bogner** (Institute of Experimental and Applied Physics, University of Regensburg) as well as **Ursula Sauer** and **Prof. Claudia Preininger** (Austrian Research Centers, ARCS, Seibersdorf) for very good cooperation.

I also appreciate the work that my research students **Stefanie Obermaier, Josef Riedl, Bernhard Schwanitz** and **Mark-Steven Steiner** contributed to this thesis.

Lastly, I also want to thank the guest scientists of our institute that I was working with, particularly **Dr. Clara Cano-Raya** and **M.Sc. Lidia Siemieniako.**

Erklärung

Hiermit erkläre ich, dass ich die vorliegende Arbeit selbst verfasst, und keine anderen als die angegebenen Hilfsmittel verwendet habe.

Regensburg, den 15.05.08

Stefan Nagl